Solids Transport Models Comparison and Fine-Tuning for Horizontal, Low Concentration Flow in Single-Phase Carrier Fluid

Frits Byron Soepyan and Selen Cremaschi
Dept. of Chemical Engineering, The University of Tulsa, Tulsa, OK 74104

Cem Sarica
McDougall School of Petroleum Engineering, The University of Tulsa, Tulsa, OK 74104

Hariprasad J. Subramani
Flow Assurance, Chevron Energy Technology Company, Houston, TX 77002

Gene E. Kouba
Production Systems & Flow Assurance, Chevron Energy Technology Company, Houston, TX 77002

DOI 10.1002/aic.14255
Published online December 2, 2013 in Wiley Online Library (wileyonlinelibrary.com)

We determined and fine-tuned the solids transport models appropriate for predicting the single-phase carrier fluid velocity to transport solid particles in conduits for horizontal, low concentration flow. A database with 538 experimental data points was compiled. A literature review was performed to determine the data ranges, forces, and mechanisms used to develop 44 models, and their velocity predictions were compared against the database using statistics. Using the dimensionless forms of the models and the data, the model parameters were adjusted to improve their accuracy and identify the dominant forces. At low concentrations: for liquid/solid flow from a bed of solids and gas/solid flow from the bottom of pipelines, the particle weight, and inertial and viscous forces dominate; for gas/solid flow from a bed of solids, the particle weight, and inertial, viscous, and adhesive forces play a role; and gaps exist in the data for large-diameter pipes and high-density gases. © 2013 American Institute of Chemical Engineers *AIChE J*, 60: 76–122, 2014
Keywords: particulate flows, experimental solids transport database, solid transport model evaluation

Introduction

Solids transport models are used to predict the fluid velocity needed to transport solid particles in hydraulic and pneumatic systems. The study of solids transport has found applications in many different fields, including pharmaceutical industries,[1] where dry powder inhalers are used to transport drug particles through a breathing tube; geology,[2] where geologists can study the transport of sediments to deduce the environmental conditions of the past; civil engineering,[3] where the concept of solids transport is applied to the dredging of rivers; sand management,[4] where the goal is to prevent the deposition of sand beds in pipelines; chemical processes,[5] where deposits need to be removed from heat exchangers; and meteorology,[6] where the seasonal patterns of other planets, such as Mars, can be determined based on the transport of dust particles from one part of the planet to another.

In the chemical industry, the transport of solids is applied in different areas, such as the recovery of solids from chemical processes[7] or the cleaning of deposits from the insides of tubes.[5] For instance, in slurry bubble column reactors,[8] thorough mixing of the catalyst powder in the liquid is required, and several flow regimes exist that describe the homogeneity of the mixture.[9] Hence, it is important that the liquid carrying the catalyst powder has the required flow rate to ensure that the solution is well mixed. As another example, in heat exchangers, fouling inside the tubes may occur, in which deposits from the flowing fluid or the corrosion of the tube surface create an accumulation of solid materials in the tube. "Clean-out operations" are needed to remove the accumulated solids, and the fluid used for cleaning needs to have a flow rate such that the solid deposits are swept from inside the tubes.[10]

Mixed-flow dryers are used in the agricultural industry to dry grain, corn, and rice.[11] To ensure uniform drying of the solid particles, there needs to be even grain and air flow distributions, but small changes in grain properties or process conditions can affect the quality of the grain. Therefore, the optimal grain and air flow rates need to be quantified for homogeneity in the drying process, and energy efficiency. In addition, gas-solid transport in risers has found applications in fluidized catalytic cracking in petrochemical industries, coal combustion in utility industries, and pneumatic transport of drug powders in pharmaceutical industries.[12] Along a riser, properties such as the solid holdup and velocity are typically nonuniformly distributed depending on the

Additional Supporting Information may be found in the online version of this article.

Correspondence concerning this article should be addressed to S. Cremaschi at selen-cremaschi@utulsa.edu.

operating condition, including the solid mass flux and the gas velocity. Estimating the values of the solid holdup distribution and velocity is required to determine the optimum design of the riser for an efficient operation.

Natural gas productions require the removal of solids, as the solids can interfere with the treating and dehydration processes.[13] These solids are mostly mill scale and rust from the pipe wall, and iron sulfide, and they can be removed in a scrubber, filter, or filter-coalescer separator. For these solids to reach the separator unit, the flow rate of the natural gas needs to be maintained such that the solids do not accumulate in the pipe. In addition, solid desiccant pellets are used for natural gas dehydration.[13] To ensure that the desiccants are working properly, the flow rate of the natural gas should be sufficient to transport the desiccants throughout the piping system. In the oil field, the presence of solid particles, composed mainly of sand, in the pipeline can be prevented by installing gravel packs or screens as part of the "downhole sand exclusion systems."[14] For many reservoirs, the accumulation of sand particles in the pipe tends to occur at a later stage in the oil production, and for prevention, options include installing a downhole sand exclusion system in the well, or designing a facility to manage the accumulation of the sand particles. The latter option is often preferred due to the risk of loss of production that arise after installing a downhole sand exclusion system.[14] The oil production system needs to be designed and operated such that the fluid velocity is sufficient to prevent the sand particles from settling to the bottom of the pipe.[4]

In the above-mentioned applications, among others, the solid particles are transported by means of a working fluid, where the fluid can be a liquid, a gas, or a mixture. Therefore, it is important that the processes in these applications are designed and operated at a sufficient fluid velocity to ensure particle transport. Solids transport models are used to provide a reasonable estimate for the minimum fluid velocity needed to transport the particles. Due to the wide range of possible operating conditions that exist, and the different possible mechanisms for particle transport, many solids transport models were developed by different authors throughout the years.

The possible mechanisms for the initiation of particle motion include rolling, sliding, and suspension (Figure 1a).[6] The conditions to which the particles are exposed determine the mechanisms responsible for starting the motion of the particle. For instance, based on the results of laboratory experiments, Ramadan et al.[15] observed that in inclined channels, the particles that form a bed at the bottom of the conduit begin their movement by rolling. Stevenson et al.[5] added that the shape of the particle affects the mechanisms for particle transport. They concluded that for non-spherical particles initially at rest at the bottom of a conduit, dragging, rather than rolling, will occur. Cabrejos[16] observed that solid particles start their motion by sliding or rolling before being lifted by the carrier fluid, and Hayden et al.[1] considered particle pick-up to take place when the particles are entrained in the carrier fluid, where vertical motion, or lifting, takes place.

The size of the particle also affects the mechanisms for particle transport due to the presence of the boundary layer near the surface at which the particles are lying.[16] Figure 1b illustrates the effects of the particle size on the velocity profile to which the particle is exposed. Smaller particles may lie within the viscous sublayer, where the velocity profile of the carrier fluid is linear, whereas larger particles are generally exposed to the main turbulent stream, where the velocity profile of the carrier fluid is nearly flat.[16] For cases where the turbulence of the carrier fluid plays a role, effects of the turbulent eddies on particle transport need to be considered.[17,18]

Different definitions for the solids transport velocity are also encountered in the literature due to the different mechanisms that exist for solids transport. Furthermore, for some instances, different velocity names were used to refer to the same solids transport mechanism by different authors. This article adopts the critical velocity definition of Oroskar and Turian,[17] the pick-up velocity definition of Hayden et al.,[1] the incipient motion velocity definition of Rabinovich and Kalman,[19] the saltation velocity definition of Zenz,[20] and the equilibrium velocity definition of Gruesbeck et al.[21] These velocity definitions are depicted in Figure 2, and used consistently to classify the experimental data, models, and findings throughout the article. Oroskar and Turian[17] describe the critical velocity as the velocity that marks the transition from the settling of solid particles at the bottom of the pipe to the full suspension of the particles. This definition of critical velocity is illustrated in Figure 2. Initially, the solid particles are resting at the bottom of the pipe (marked "Initial State" in Figure 2). When the fluid's velocity reaches the critical velocity, all the particles are lifted and transported within the fluid (marked "Final State" in Figure 2). A similar approach is used to illustrate the pick-up and incipient motion velocity definitions in Figure 2, where the left sketches show the initial positions of the particles in the carrier fluid, and the right sketches represent the final position and distribution of the particles within the carrier fluid at the transition velocity indicated on the right. The pick-up velocity defines the fluid velocity where particles initially at rest begin their motion with the fluid,[1] while the incipient motion velocity represents the fluid velocity required to initiate the movement of a single particle initially at rest at the bottom of a conduit.[19] As can be seen in Figure 2, the difference between the pick-up velocity and the incipient motion

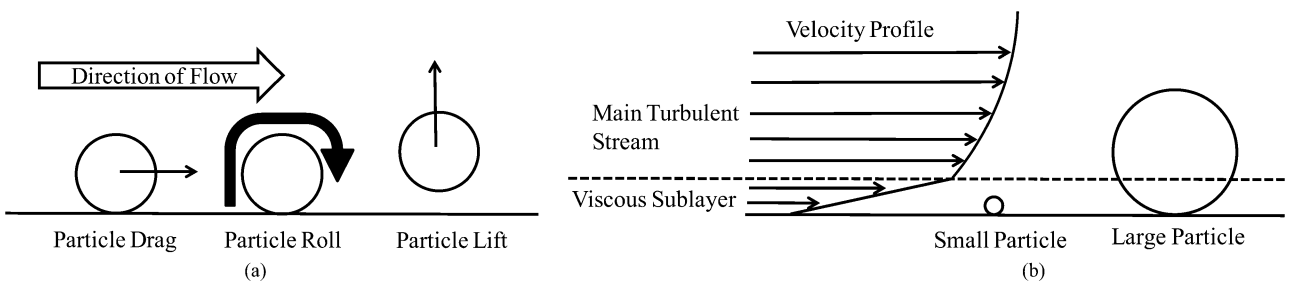

Figure 1. (a) Different solids transport mechanisms, and (b) effect of particle size on the velocity profile to which the particle is exposed.

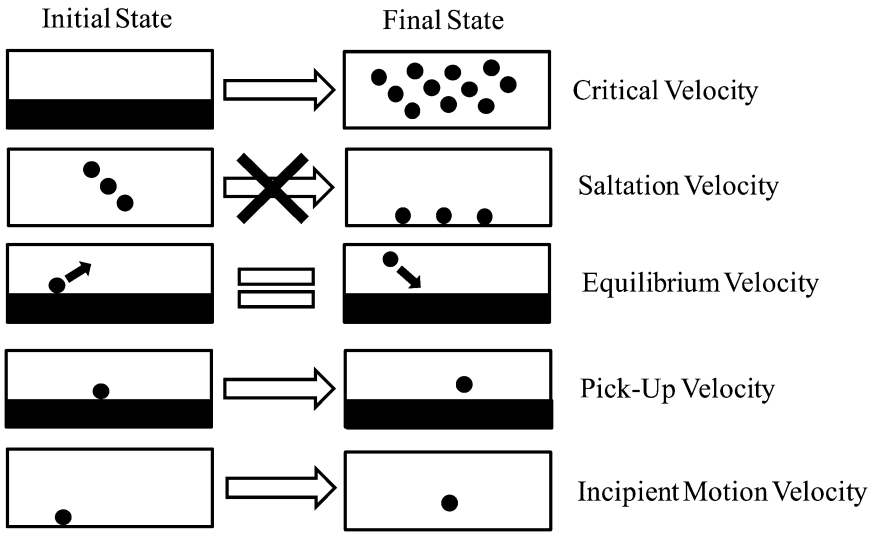

Figure 2. Graphical representations of the solids transport velocity definitions used in this study.

velocity is the initial location of the particle in the pipe. For the case of the incipient motion velocity, the pipe initially contains a single particle resting at the bottom, whereas for the case of the pick-up velocity, the particle is initially at rest on a bed of solid particles. When solid particles are suspended, the saltation velocity can be used to describe the minimum fluid velocity for which the particles do not settle to the bottom of the pipe.[20] As depicted in Figure 2, the particles that are initially moving with the fluid will start to settle to the bottom of the pipe when the fluid velocity falls below the saltation velocity. The equilibrium velocity is defined as the fluid velocity where the rate at which the particles are picked up by the fluid equals the rate at which the particles settle to the bottom of the pipe.[21] As shown in Figure 2, at the equilibrium velocity, while a particle is being lifted by the fluid, another particle settles. Operating at or below the saltation velocity will cause a bed of solids to form at the bottom of the pipe that initially has no bed of solids; whereas operating at the equilibrium velocity will cause the pipe to have a bed of solids for which the height is steady.

Given the different mechanisms the solids transport models consider, and the number of available models, it was observed that for the same operating condition (i.e., inputs), the velocity predictions generated by the models can differ by several orders of magnitude. Therefore, it is important that a practicing engineer is able to determine which models provide accurate velocity predictions at a specific transport mechanism for a given operating condition to design and operate the relevant processes, such as the transport of sand in oil and gas pipelines,[22] the pneumatic transport of dry and free-flowing powders,[16] and the transport of mining products.[3]

The objective of this article is to analyze the applicability of the 44 different models for predicting the pick-up (liquid/solid and gas/solid flow systems) and the incipient motion (gas/solid flow system) velocities for horizontal flow with single-phase carrier fluid at low particle concentrations of less than 100 ppm. Compared to larger particle concentrations, at concentrations below 100 ppm, one can study the conditions for initiating the motion of a single particle more easily.[23] The following section provides a critical review of these 44 solids transport models[1,2,4,5,9,15–19,21,22,24–51,154] by comparing their development methods, the ranges of the experimental data used to develop or validate them, and the forces used to develop them (where applicable). To test the performance of these models, a database that consists of experimental data for solids transport at low particle concentrations was compiled,[5,6,15,16,19,27,30,33,52–58] and the overview of this database is provided in the "Experimental Database" section. The statistics and methods used to compare the performance of the models for the database is summarized in the "Methodology Used to Evaluate the Performance of the Models" section. To identify the proper model forms and the dominant forces for each velocity type for horizontal, single-phase fluid flow at low particle concentrations, the parameters, or constants, of the dimensionless forms of the solids transport models are fine-tuned, or adjusted, using the appropriate data from the compiled database. The methodology and the formulation used for fine-tuning are provided in the "Fine-Tuning Process" section. The "Results and Discussions" section discusses the performances of the models for the experimental database, and the values of the statistics for the original models and the fine-tuned model-forms. This section also provides an analysis of the forces, mechanisms, and dimensionless groups that were most commonly encountered in the better-performing models for the hydraulic conveying (at the pick-up velocity) and pneumatic conveying (at the pick-up and incipient motion velocities) of particles. Lastly, the manuscript provides the conclusions regarding the dominant forces and mechanisms for initiating the motion of particles in conduits for horizontal, single-phase fluid flow at low particle concentrations, and the solids transport models and experimental database.

Review of the Solids Transport Models

The solids transport models can be classified to three categories based on the approach used to develop them: empirical, mechanistic, and semi-mechanistic. Empirical models are developed using experimental data of specific ranges,[15,19] whereas mechanistic models are developed using force balances, where assumptions are made regarding the dominant forces.[15] Semi-mechanistic models are developed with a

combination of force balances and model parameter fine-tuning using experimental data.[59] Mechanistic and semi-mechanistic models can be organized based on the assumptions used to develop these models (e.g., turbulent flow, particle motion by lift, drag, or roll), and empirical models can be grouped based on the approach used to develop the models (e.g., the use of dimensional analysis). Table 1 provides an overview of the 44 models studied in this article. Table 1 groups the solids transport models based on the type of velocity predicted by the models (incipient motion velocity, pick-up velocity, equilibrium velocity, saltation velocity, and critical velocity), the concentration dependence of the models, and the carrier phase used for the development of the models (liquid, gas, liquid or gas). Those models that have "liquid or gas" listed as the carrier phase were developed for solid/liquid and solid/gas flows. Table 1 also provides information regarding the technique used to derive the models (empirical, mechanistic, and semi-mechanistic). The equations for the models in both dimensional and dimensionless forms are given in Appendix Table A1.

The input variables for most of these 44 solids transport models include the fluid properties (density and viscosity), the particle properties (density and diameter), the particle concentration (for concentration-dependent models), and the hydraulic diameter of the conduit. There are a limited number of models that consider the effect of pipe inclination. Table 2 presents the sources of the experimental data that were used to develop the empirical and semi-mechanistic models, and validate the mechanistic models. The ranges of these experimental data are shown in Supporting Information Figure S1.

Upon studying the ranges of the experimental data used to develop or validate the models, for hydraulic conveying of particles, the Kalman et al.,[30] Mantz,[33] Miller et al.,[2] Rabinovich and Kalman,[19,35,36] Ramadan et al.,[15] Rampall and Leighton,[37] Han and Hunt,[47] Ling,[51] Dey,[49] Wu and Chou,[48] Stevenson and Thorpe,[41] and Stevenson et al.[5,42,43] models were developed for low particle concentrations; the widest particle concentration ranges were used by Babcock,[25] Oroskar and Turian,[17] Turian et al.,[45] and Zandi and Govatos,[46] whereas the smallest ranges were used by Doron et al.,[28] and Thomas.[44,154] All the models, except the Almutahar,[22] Bain and Bonnington,[26] Doron et al.,[28] Gruesbeck et al.,[21] Ponagandla,[34] and Rose and Duckworth[38] models, were developed only for horizontal flow. All the models were developed or validated using at least water, with Gruesbeck et al.,[21] Oroskar and Turian,[17] Rabinovich and Kalman,[35] Rampall and Leighton,[37] and Turian et al.[45] using the widest ranges of fluid densities and viscosities. The Thomas[44] model has the largest upper bound for the particle density; the Shook,[39] Thomas,[154] and Turian et al.[45] models have the widest particle density ranges; and Almutahar,[22] Danielson,[4] Davies,[18] Kalman et al.,[30] Ponagandla,[34] Rabinovich and Kalman,[36] Ramadan et al.,[15] Spells,[40] and Stevenson et al.[42] used only a few particle densities to develop or validate their models. For the particle diameter, the widest range was used by Bain and Bonnington,[26] and Shook;[39] the smallest range was used by Almutahar,[22] Davies,[18] Gruesbeck et al.,[21] Oroskar and Turian,[17] Ponagandla,[34] Spells,[40] Stevenson and Thorpe,[41] and Stevenson et al.;[42,43] and Danielson,[4] and Rabinovich and Kalman[36] used one or two discrete values. For the pipe diameter, Bain and Bonnington,[26] Davies,[18] Shook,[39] Thomas,[154] and Turian et al.[45] used the widest range, whereas Danielson,[4] Kalman et al.,[30] Rabinovich and Kalman,[19] and Ramadan et al.[15] utilized the smallest range.

Table 1. An Overview of the Solids Transport Models Used in this Study

Concentration-Dependent	Liquid	–	–	*Gruesbeck et al.*[21]	*Spells*,[40] Almutahar,[22a] Davies,[18] Ponagandla,[34] *Turian et al.*[45]	*Zandi and Govatos*,[46] *Babcock*,[25] *Shook*,[39] *Bain and Bonnington*,[26] Oroskar and Turian,[17] *Kökpınar and Gögüş*[31]	
Concentration-Independent	Liquid or Gas	–	–	–	*Rose and Duckworth*,[38] Thomas[154]	–	
	Liquid	Han And Hunt[47]	*Mantz*,[33] Doron et al.,[28] Rampall and Leighton,[37] *Stevenson et al.*,[42,43] Ramadan et al.,[15] *Stevenson and Thorpe*,[41] Ling,[51] Dey,[49] Wu and Chou[48]	–	Danielson[4]	*Newitt et al.*[9a]	–
	Gas	Cabrejos[16] (single particle), Ibrahim et al.[50]	Hayden et al.,[1] Cabrejos[16] (multiple particle), *Cabrejos and Klinzing*,[27] *Fletcher*[29]	–	–	*Adánez et al.*,[24] *Lee and Kim*[32]	
	Liquid or Gas	Stevenson et al.;[5] *Rabinovich and Kalman*,[19] Rabinovich and Kalman[36]	*Miller et al.*,[2] *Kalman et al.*;[30] *Rabinovich and Kalman*[35]	–	Thomas[44]	–	
Legend: Mechanistic, *Empirical*, Semi-Mechanistic		Incipient Motion Velocity	Pick-Up Velocity	Equilibrium Velocity	Saltation Velocity	Critical Velocity	

[a]Multiple models were obtained from the same source.
The dashes signify that there are no models in the subset. For example, in our model database, there is no concentration-independent model that was developed to predict the equilibrium velocity.

Table 2. Sources of the Experimental Data Used to Develop and/or to Validate the Solids Transport Models

Model	References for the Sources of the Experimental Data
Thomas[44]	44, 61–63
Adánez et al.[24]	24, 32, 64–72
Lee and Kim[32]	32, 65–67, 69–74
Newitt et al.[9] (heterogeneous flow)	9
Miller et al.[2]	53, 57, 75–88
Mantz[33]	33, 53, 57, 75, 79, 80, 89–94
Danielson[4]	95
Stevenson et al.[43]	42, 43, 96
Stevenson and Thorpe[41]	41
Newitt et al.[9] (homogeneous flow)	9
Stevenson et al.[42]	42
Cabrejos and Klinzing[27]	27, 97
Rampall and Leighton[37]	98–102
Stevenson et al.[5]	5, 6, 20, 97, 103
Doron et al.[28]	28, 104–107
Rabinovich and Kalman[35]	15, 33, 49, 53, 57, 58, 75, 78–82, 108–111
Rabinovich and Kalman[19]	5, 6, 19, 47, 54, 97
Kalman et al.[30]	1, 15, 27, 30, 97, 112
Hayden et al.[1]	1, 16
Cabrejos[16] (single particle)	16
Rabinovich and Kalman[36]	6, 19
Ramadan et al.[15]	15
Cabrejos[16] (multiple particle)	16
Fletcher[29]	29, 113–115
Turian et al.[45]	40, 45, 116–141
Almutahar[22] (new approach)	31, 106, 107, 117, 118, 120, 127, 134, 137, 142–144
Davies[18]	127, 130
Spells[40]	Settle JJ, Parkins R (Private Communication), Williams JC (Private Communication), Smith RA, Carruthers GA (Private Communication), 145–147
Rose and Duckworth[38]	38, 148–151
Gruesbeck et al.[21]	21
Thomas[154]	3, 9, 44, 61, 134, 145–148, 152–156
Zandi and Govatos[46]	9, 147, 157–164
Babcock[25]	25, 46, 147
Shook[39]	9, 40, 134, 165–168
Bain and Bonnington[26]	116, 169–172
Kökpınar and Göğüş[31]	31, 120, 142–144, 173, 174
Ponagandla[34]	31, 106, 107, 117, 118, 120, 127, 134, 137, 142–144
Oroskar and Turian[17]	40, 129, 175–178
Almutahar[22] (initial approach)	31, 106, 107, 117, 118, 120, 127, 134, 137, 142–144
Han and Hunt[47]	47
Wu and Chou[48]	179–183
Dey[49]	33, 53, 57, 58, 75, 78–82, 90, 92, 108, 109, 184
Ibrahim et al.[50]	50
Ling[51]	77, 81, 90

For the pneumatic conveying of particles, the following qualitative observations can be made regarding the models. The Cabrejos,[16] Cabrejos and Klinzing,[27] Fletcher,[29] Hayden et al.,[1] Kalman et al.,[30] Miller et al.,[2] Rabinovich and Kalman,[19,35,36] Ibrahim et al.,[50] and Stevenson et al.[5] models were developed for low particle concentration ranges, and the Thomas[154] model used the widest range of particle diameters to develop the model. All the models were developed for horizontal flow, except for the Adánez et al.,[24] and Lee and Kim[32] models; and the Rose and Duckworth[38] model were developed for inclined flow in addition to horizontal and vertical flows. All the models were developed or validated using experimental data with air at room temperature and atmospheric pressure as the carrying phase, with the Thomas[154] model using the widest ranges of fluid density and viscosity. The Miller et al.,[2] and Rabinovich and Kalman[19,36] models used the widest particle density ranges, whereas the Thomas[44] model used only a single particle density value. The models developed by Cabrejos,[16] Kalman et al.,[30] and Rabinovich and Kalman[19] used the widest range of particle diameter, and the Thomas[44] model used a single particle diameter. The widest range of pipe diameter was used by Lee and Kim,[32] and Rose and Duckworth;[38] and a single pipe diameter experimental data were used by Fletcher,[29] and Hayden et al.[1]

Empirical Models

Models developed from dimensional analysis for solids transport in single-phase fluid flow

Models in this category are developed by Gruesbeck et al.,[21] Kökpınar and Göğüş,[31] Spells,[40] Turian et al.,[45] and Zandi and Govatos[46] for hydraulic conveying; Adánez et al.,[24] Cabrejos and Klinzing,[27] Fletcher,[29] and Lee and Kim[32] for pneumatic conveying; and Rose and Duckworth[38] for hydraulic and pneumatic conveying. Table 3 shows that the particle Reynolds number, the Froude number, and the density ratio between the particle and the fluid are the most commonly used dimensionless groups in these models.

The models developed by Spells,[40] Zandi and Govatos,[46] Turian et al.,[45] Kökpınar and Göğüş,[31] Cabrejos and

Table 3. Dimensionless Groups Used in the Development of the Empirical Models

			Dimensionless Groups								
		Model	N_{Re}	$N_{Re,p}$	N_{Ar}	N_{Fr}	C_D	Density Ratio	Diameter Ratio	Conc.	Others
Models Developed from Dimensional Analysis for Single Phase Fluid Flow	Hydraulic Conveying	Gruesbeck et al.[21]	$\frac{Dv_S\rho_f}{\mu}$	$\frac{d_p v_S \rho_f}{\mu}$	–	–	–	$\frac{\rho_S-\rho_f}{\rho_f}$	–	C	–
		Kökpınar and Göğüş[31]	–	$\frac{d_p v_S \rho_f}{\mu}$	–	$\frac{v}{\sqrt{gD}}$	–	$\frac{\rho_S-\rho_f}{\rho_f}$	$\frac{d_p}{D}$	C	–
		Spells[40]	$\frac{Dv\rho_m}{\mu}$	–	–	$\frac{v^2}{gd_p}$	–	$\frac{\rho_f}{\rho_S-\rho_f}$	–	C	–
		Turian et al.[45]	$\frac{D\rho_f\sqrt{gD\left(\frac{\rho_S}{\rho_f}-1\right)}}{\mu}$	–	–	$\frac{v}{\sqrt{gD}}$	–	$\frac{\rho_S-\rho_f}{\rho_f}$	$\frac{d_p}{D}$	C and $(1-C)$	–
		Zandi and Govatos[46]	–	–	–	$\frac{v^2}{gD}$	C_D	$\frac{\rho_f}{\rho_S-\rho_f}$	–	C	–
	Pneumatic Conveying	Adánez et al.[24]	–	$\frac{d_p v \rho_f}{\mu}$	$\frac{gd_p^3\rho_f(\rho_S-\rho_f)}{\mu^2}$	–	–	–	–	–	–
		Cabrejos and Klinzing[27]	–	$\frac{d_p v \rho_f}{\mu}$	–	$\frac{v}{\sqrt{gd_p}}$	–	$\frac{\rho_S}{\rho_f}$	$\frac{D}{d_p}$	–	N_{Shape}
		Fletcher[29]	–	$\frac{d_p v_* \rho_f}{\mu}$	$\frac{gd_p^3\rho_f^2}{\mu^2}$	–	–	$\frac{\rho_S}{\rho_f}$	–	–	$\left(\frac{\gamma}{\rho_f}\right)^{0.5}\frac{d_p\rho_f}{\mu}$

DOI 10.1002/aic Published on behalf of the AIChE January 2014 Vol. 60, No. 1 AIChE Journal

Table 3. *Continued*

			Dimensionless Groups								
		Model	N_{Re}	$N_{Re,p}$	N_{Ar}	N_{Fr}	C_D	Density Ratio	Diameter Ratio	Conc.	Others
		Lee and Kim[32]	–	$\frac{d_p v \rho_f}{\mu}$	$\frac{g d_p^3 \rho_f (\rho_S - \rho_f)}{\mu^2}$	–	–	–	–	–	–
	Hydraulic and Pneumatic Conveying	Rose and Duckworth[38]	–	–	–	$\frac{v^2}{gD}$	–	$\frac{\rho_S}{\rho_f}$	$\frac{d_p}{D}$	C_W	θ
Models Developed Using Hydraulic Gradient		Babcock[25]	–	–	–	$\frac{v^2}{gD}$	C_D	$\frac{\rho_f}{\rho_S - \rho_f}$	–	C	$\frac{P - P_w}{P_w}$
		Bain and Bonnington[26]	–	–	–	$\frac{v^2}{gD}$	C_D	$\frac{\rho_S - \rho_f}{\rho_f}$	–	C	$\frac{P - P_w}{P_w}$
		Newitt et al.[9]	–	–	–	$\frac{v^2}{gD}$	–	$\frac{\rho_f}{\rho_S - \rho_f}$	–	C	$\frac{P - P_w}{P_w}$, v_S/v
		Shook[39]	–	–	–	$\frac{v^2}{gD}$	C_D	$\frac{\rho_S - \rho_f}{\rho_f}$	–	C	$\frac{P - P_w}{P_w}$
Models Developed Using the Shields Parameter		Mantz[33]	$\frac{D v_* \rho_f}{\mu}$	–	–	–	–	–	–	–	$N_{Sh} = \frac{\tau_W}{g d_p (\rho_S - \rho_f)}$
		Miller et al.[2]	$\frac{D v_* \rho_f}{\mu}$	–	–	–	–	–	–	–	N_{Sh}

Table 3. *Continued*

	Model	Dimensionless Groups								
		N_{Re}	$N_{Re,p}$	N_{Ar}	N_{Fr}	C_D	Density Ratio	Diameter Ratio	Conc.	Others
Models with Diameter Corrections	Kalman et al.[30]	$\frac{d_p v \rho_f}{\mu}$	–	$\frac{g d_p^3 \rho_f (\rho_S - \rho_f)}{\mu^2}$	–	–	–	$\frac{D}{D_{50}}$	–	N_{Sph}
	Rabinovich and Kalman[35]	$\frac{d_p v \rho_f}{\mu}$	–	$\frac{g d_p^3 \rho_f (\rho_S - \rho_f)}{\mu^2}$	–	–	–	$\frac{D}{D_{50}}$	–	N_{Sph}
	Rabinovich and Kalman[19]	$\frac{d_p v \rho_f}{\mu}$	–	$\frac{g d_p^3 \rho_f (\rho_S - \rho_f)}{\mu^2}$	–	–	–	$\frac{D}{D_{50}}$	–	f_S
Models Developed for Multiphase Flow	Stevenson et al.[42]	$\frac{D v_{sl} \rho_l}{\mu_l}$	–	–	$\frac{\sqrt{gD}}{v_{sl}}$	–	$\frac{\rho_S}{\rho_l}$	$\frac{d_p}{D}$	–	$\frac{v_p}{v_{sl}}, \frac{v_{sg}}{v_{sl}}$
	Stevenson et al.[43]	$\frac{D v_{sl} \rho_l}{\mu_l}$	–	–	$\frac{\sqrt{gD}}{v_{sl}}$	–	$\frac{\rho_S}{\rho_l}, \frac{\rho_S - \rho_l}{\rho_l}$	$\frac{d_p}{D}$	–	$\frac{v_p}{v_{sl}}, \frac{v_{sg}}{v_{sl}}$
	Stevenson and Thorpe[41]	–	$\frac{d_p v_{sl} \rho_l}{\mu_l}$	–	$\frac{g D_l}{v_{sl}^2}$	–	$\frac{\rho_S - \rho_l}{\rho_l}$	–	–	$\frac{v_p}{v_{sl}}$

Klinzing,[27] and Rose and Duckworth[38] incorporate the Froude number[185,186] $\left(N_{Fr}=\frac{v}{\sqrt{gl_0}}\right)$ with different characteristic lengths, l_0. Some models[31,38,45,46] use the pipe diameter as the characteristic length, whereas the rest[27,40] use the particle diameter. The use of the pipe diameter and the particle diameter as the characteristic length implies that the Froude number represents the ratio of the inertial force to the gravity force[185,186] for the fluid and the particle, respectively. It should be noted that the Froude number that incorporates the hydraulic diameter of the conduit is most commonly used to classify the flow (subcritical, critical, or supercritical) in a free surface or open channel,[185] as it is governed by gravitational forces.

Spells,[40] Kökpınar and Göğüş,[31] Gruesbeck et al.,[21] Lee and Kim,[32] Adánez et al.,[24] Cabrejos and Klinzing,[27] and Fletcher[29] incorporate dimensionless groups with the same form as the Reynolds number[185,186] $\left(N_{\mathrm{Re}}=\frac{l_0 v \rho_f}{\mu}\right)$. Similar to the case of the Froude number, the models use different characteristic lengths, l_0, to calculate the Reynolds number, where some models[21,40] use the pipe diameter, while others[21,24,27,29,31,32] use the particle diameter, yielding the particle Reynolds number. As the Reynolds number represents the ratio between the inertial force and the viscous force, the use of the pipe diameter as the characteristic length implies that the Reynolds number quantifies the ratio of the forces acting on the fluid. The particle Reynolds number quantifies the ratio of the inertial and viscous forces acting on the particle. Although most of the above models estimate the average fluid velocity, the model developed by Fletcher[29] determine the shear velocity; and the models developed by Kökpınar and Göğüş,[31] and Gruesbeck et al.[21] use the settling velocity to quantify the average fluid velocity.

The effect of the apparent weight[187] of the particles is incorporated into most of the models, either through the quantity $\left(\frac{\rho_S}{\rho_f}-1\right)=\left(\frac{\rho_S-\rho_f}{\rho_f}\right)$, or the Archimedes number $\left(N_{Ar}=\frac{g d_p^3 \rho_f\left(\rho_S-\rho_f\right)}{\mu^2}\right)$, which takes into account the inertial, buoyancy, and viscous forces,[30] as the Archimedes number "is related with the Froude number, the Reynolds number, and the ratio of the gravity force to the buoyant force."[16] However, in the models developed by Cabrejos and Klinzing,[27] and Fletcher,[29] the effect of the particle weight is considered using the specific mass of the particle $\left(\frac{\rho_S}{\rho_f}\right)$.[29] The Fletcher[29] model also considers the ratio of the weight of the particle to viscous forces $\left(\frac{g d_p^3 \rho_f^2}{\mu^2}\right)$; and the ratio of the cohesive to viscous forces $\left[\left(\frac{\gamma}{\rho_f}\right)^{0.5}\left(\frac{d_p \rho_f}{\mu}\right)\right]$.

Models developed using hydraulic gradients

The Newitt et al.,[9] Babcock,[25] Bain and Bonnington,[26] and Shook[39] models took into account the effects of pressure losses in the pipes. In general, the authors were interested in correlating the head losses in slurry-transporting pipes, and in the process, models that can be used to predict the solids transport velocity were obtained.

Newitt et al.[9] obtained relations for the transitions from the flow with a sliding bed of particles to the heterogeneous suspension of particles, and from the heterogeneous to the homogeneous flow of suspensions in the pipe. Shook[39] studied the transport of solids in a "short-distance pipeline" designed using only information from the literature, where the "costs do not justify an extensive testing program." Bain and Bonnington[26] differentiated between the possible definitions for the critical velocity. The "critical velocity" was defined as the velocity for which the pressure drop was lowest for a mixture of constant particle concentration, whereas the "critical deposit velocity" was defined as the velocity below which particles began to deposit to the bottom of the pipe.[116] Based on Bain and Bonnington's[26] experimental data (shown in Supporting Information Figure S1), for most cases, the critical velocity exceeded the critical deposit velocity for the same operating condition. Hence, it was advantageous to operate at the critical velocity instead of the critical deposit velocity to minimize the power requirements for the pumps, and to provide a "margin above the critical deposit (velocity) … thereby reducing the likelihood of (particle) deposition."[26] Babcock[25] developed a solids transport model to characterize the transition to the heterogeneous flow of particles in pipes, where the same dimensionless groups used by Zandi and Govatos[46] were incorporated into the model.

The four models in this category were all developed using the Froude number $\left(\frac{v^2}{gD}\right)$, the density ratio, the concentration, and the ratio $\frac{P-P_W}{P_W}$, where P and P_W denote the hydraulic gradients due to particle suspension in the fluid and due to the pure fluid, respectively. The models developed by Bain and Bonnington,[26] and Babcock[25] were derived by determining the fluid velocity that minimized the hydraulic gradient, while the Shook[39] model was developed by determining the maximum concentration for which the solid particles are transported for a given velocity. Despite the different approaches used to derive these three models, when solved for the solids transport velocity, they yield the same form as the Zandi and Govatos[46] model. The Newitt et al.[9] model predicts two different velocities: (1) the fluid velocity where the flow transitions to a heterogeneous flow of solids in the pipe, and (2) the fluid velocity where the flow transitions to a homogeneous flow of solids in the pipe.

Models developed using the Shields parameter

The Shields parameter $\left(N_{Sh}=\frac{\tau_W}{g d_p\left(\rho_S-\rho_f\right)}\right)$, which incorporates the shear stress τ_W due to the fluid flow, is similar to the Froude number as it represents the "relative magnitudes of the inertial and gravitational force on a grain acted upon by fluid flow."[2] The models in this group, that is, the Miller et al.,[2] and the Mantz[33] models, have similar forms due to the use of the same dimensionless groups in their development: N_{Sh}, and the particle Reynolds number calculated using the shear velocity ($N_{Re,p,*}$). The models were obtained by fitting a curve to the experimental data using the above-mentioned dimensionless groups. The two models differ in that the model by Miller et al.[2] was developed using experimental data for the pneumatic conveying of particles, and a broader range of particle densities compared to the Mantz[33] model.

Models with diameter corrections

The Kalman et al.,[30] and the Rabinovich and Kalman[19,35] models were derived for the hydraulic and pneumatic conveying of particles in conduits. They correlate the particle

Reynolds number with the Archimedes number and include corrections to account for the effect of the pipe diameter. The values of the parameters of these three models differ due to the difference in experimental data sets used to estimate them. The Rabinovich and Kalman[19] model was developed to predict the incipient motion velocity of a particle, whereas the remaining two models were developed to predict the pick-up velocity. While the Rabinovich and Kalman[35] model parameters were estimated using experimental data with a broader range of fluid properties (density and viscosity), particle diameter, and pipe diameter compared to the other two models for hydraulic transport of the particles, Kalman et al.[30] used a broad range of fluid properties (density of 1.2–2.0 kg/m^3) for the pneumatic conveying of particles to derive their model. Both Kalman et al.,[30] and Rabinovich and Kalman[19] estimated their model parameters using a broad range of experimental data in terms of particle properties (including particles of diameters up to 5 mm). For the pipe diameter, Rabinovich and Kalman[35] included data that originate from experiments conducted in wind tunnels of heights 1.2 and 2.5 m.

Models developed for solids transport in multiphase fluid flow that can be extended to single-phase carrier liquids

The Stevenson and Thorpe,[41] and Stevenson et al.[42] models were developed for the transport of solids in stratified flow and slug flow, respectively; and Stevenson et al.[43] expanded their previous model to account for the transport of solids in liquid-only flow in addition to slug flow. Similar dimensionless groups incorporating different types of velocities (particle velocity v_p, superficial gas velocity v_{sg}, and superficial liquid velocity v_{sl}) were used to derive all three models. To extend the applications of the models to solids transport in single-phase liquids, the models assume that v_p is equal to zero at the threshold of particle movement, and v_{sg} is set to zero for single-phase flow.

Mechanistic Models

The mechanistic solids transport models include those developed by Davies,[18] Doron et al.,[28] Stevenson et al.,[5] Rampall and Leighton,[37] Hayden et al.,[1] Cabrejos,[16] Rabinovich and Kalman,[36] Wu and Chou,[48] and Ramadan et al.[15] The performances of most of the mechanistic models were tested using data for flow at low particle concentrations in horizontal or near-horizontal conduits. The models for hydraulic and pneumatic conveying of solids were validated using experiments with water and air as the carrying phase, respectively. Broader ranges of particle diameters and densities were used to validate the models developed for pneumatic flow compared to hydraulic flow. Finally, most of the mechanistic models were tested using experimental data for flow in conduits with hydraulic diameters of about 0.1 m or less. The mechanisms and forces assumed to be significant for particle transport are shown in Table 4: F_D (drag force), F_L (lift force), F_F (friction force between the particle and the pipe wall), F_A (adhesive force), F_W (apparent weight of the particle in the fluid), F_P (plastic force), F_T (forces acting on the particle caused by the turbulence of the fluid), F_{sed} (sedimentation force), F_{ef} (eddy fluctuation force), and F_N (normal force exerted by the column of particles lying above the particle of interest).

Model developed for the initiation of particle motion by lift

The Hayden et al.[1] model, which was derived for pneumatic conveying of particles in horizontal conduits, was developed with the assumption that particle pick-up took place when the particle was "entrained in the moving fluid." Hence, the lift force, the apparent weight of the spherical particle in the fluid, and the adhesive force were identified as the dominant forces.

Models developed for horizontal initiation of particle motion

These models, where it was assumed that the particle commences motion by dragging or rolling, were developed by Doron et al.,[28] who studied the roll of spherical particles from a layer of particles, and Stevenson et al.,[5] who focused on the dragging of a hemispherical particle on the conduit wall. Doron et al.[28] assumed that the particle rotates at its point of contact with the adjacent particle, and hence, unlike the Stevenson et al.[5] model, ignored the effects of friction. In terms of the flow regime, Stevenson et al.[5] assumed that the particle is initially lying at the bottom of the conduit within the viscous sublayer, whereas Doron et al.[28] assumed three flow regions (the stationary bed, the moving bed, and the heterogeneous mixture region) in the pipe for the transport of solids from a bed of particles. According to Doron et al.,[28] the bottom layer of the bed (the stationary bed) is not in motion even though the upper layer of the bed (the moving bed) may be in motion, and the particles that are in motion occupy the heterogeneous mixture region. With the incorporation of the normal force F_N, the Doron et al.[28] model can be used to predict the fluid velocity needed to move particles in any location within the layer of particles

Table 4. Mechanisms and Forces Considered in the Development of the Mechanistic Models

	Mechanism			Forces							
Model	Drag	Lift	Roll	F_D	F_L	F_F	F_A	F_W	F_P	F_T	Others
Cabrejos[16] (single particle)	✓	✓	–	✓	✓	✓	✓	✓	–	–	–
Davies[18]	–	✓	–	–	–	–	–	–	–	✓	F_{sed}
Doron et al.[28]	–	–	✓	✓	–	–	–	✓	–	–	F_N
Hayden et al.[1]	–	✓	–	–	✓	–	✓	✓	–	–	–
Rabinovich and Kalman[36]	✓	✓	✓	✓	✓	✓	✓	✓	–	–	–
Ramadan et al.[15]	–	✓	✓	✓	✓	–	–	✓	✓	–	–
Rampall and Leighton[37]	–	✓	–	–	✓	–	–	✓	–	✓	–
Stevenson et al.[5]	✓	–	–	✓	–	✓	–	✓	–	–	–
Wu and Chou[48]	–	✓	✓	✓	✓	–	–	✓	–	–	–

(i.e., the particle of interest does not necessarily have to be the topmost particle in the bed).

Models developed for horizontal and vertical initiation of particle motion

The models developed by Cabrejos,[16] Ramadan et al.,[15] Wu and Chou,[48] and Rabinovich and Kalman[36] considered the possibility of both horizontal and vertical initiation of particle motion. Cabrejos[16] determined that for both particles larger and smaller than the thickness of the viscous sublayer, the particle is transported with the fluid due to dragging. Cabrejos[16] also developed a model to predict the fluid velocity needed to initiate the lift of the solid particles. Ramadan et al.,[15] and Wu and Chou[48] developed their models to predict the fluid velocity needed to initiate the motion of a solid particle from a bed of particles by considering the possibilities of particle lift and roll. Rabinovich and Kalman[36] developed different equations for predicting the solids transport velocity, and the selection of the equation depended on the size of the particle relative to the thickness of the viscous sublayer, and the type of continuous phase (i.e., liquid or gas). It was assumed that non-spherical particles larger than the thickness of the viscous sublayer drag, spherical particles larger than the thickness of the viscous sublayer roll, particles smaller than the thickness of the viscous sublayer flowing in a gaseous-carrying phase roll or bounce (i.e., are lifted), and particles flowing in a liquid-carrying phase drag or roll initially.

The drag force, lift force, and apparent weight of the particle were considered in all these models. Cabrejos,[16] and Rabinovich and Kalman[36] included the adhesive and the friction forces between the particle and the pipe wall because these models were developed for particles initially at rest at the bottom of the pipe. Furthermore, these two models incorporated the effect of particle size relative to the thickness of the viscous sublayer. Ramadan et al.[15] included the plastic force to account for the yield stress of the fluid, if applicable. Cabrejos,[16] Wu and Chou,[48] and Ramadan et al.[15] assumed a spherical shape for the particles, whereas Rabinovich and Kalman[36] took into account the shape of the particle through the force balances for non-spherical and spherical particles.

Models developed using turbulence theory

The models by Davies,[18] and Rampall and Leighton[37] were developed by considering the effect of turbulence on the solids transport mechanism. Davies[18] balanced the sedimentation force F_{sed} with the eddy fluctuation force F_{ef}, and accounted for the presence of multiple particles through concentration. Rampall and Leighton[37] studied the movement of the particle from the viscous sublayer to the turbulent core of the fluid. The Rampall and Leighton[37] model predicts the velocity at the initiation of particle motion, whereas the Davies[18] model predicts the velocity needed to transport the solid particles such that there is no solids deposition and no bed formation.

Semi-mechanistic Models

The semi-mechanistic solids transport models include those developed by Almutahar,[22] Thomas,[44,154] Danielson,[4] Ponagandla,[34] Oroskar and Turian,[17] Ibrahim et al.,[50] Ling,[51] Dey,[49] Han and Hunt,[47] and Cabrejos.[16] The forces and mechanisms considered by the above authors are shown in Table 5. Most semi-mechanistic models were developed for near-horizontal flow, with two of the models developed for an inclination of up to $\sim 30^{\circ}$.[22,34] Unlike mechanistic models, some parameters of the semi-mechanistic models are adjusted using experimental data, and therefore, it is important to know the ranges of data used in their developments. The forces used in the development of the models depended on the mechanisms (drag, lift, or roll) considered in the development of the models.

Models developed using the lift, drag, or roll mechanisms

Thomas[44] developed his solids transport model by taking into account the lift force; Cabrejos[16] developed his model by taking into account both the drag and lift mechanisms; Ling[51] derived equations to predict the fluid velocity needed to lift and roll the solid particle; Ibrahim et al.[50] considered the possibility of particle drag, lift and roll; and Dey,[49] and Han and Hunt[47] studied the requirement for particle motion by rolling. Thomas[44] was interested in quantifying the solids transport velocity needed to prevent the accumulation of a layer of stationary particles at the bottom of a horizontal conduit, and the model was developed by considering the lift due to Bernoulli forces. Cabrejos[16] derived the correlation for a multiple-particle system by incorporating the velocity from the single-particle model[16] (described in the "Models Developed for Horizontal and Vertical Initiation of Particle Motion" subsection). The effects of particle-particle interaction and particle shape were incorporated empirically into

Table 5. Mechanisms and Forces Considered in the Development of the Semi-Mechanistic Models

	Mechanism			Forces							
Model	Drag	Lift	Roll	F_D	F_L	F_F	F_A	F_W	F_P	F_T	Others
Almutahar[22] (initial approach)	–	✓	–	✓	–	–	–	–	–	✓	–
Almutahar[22] (new approach)	–	✓	–	–	–	–	–	–	–	✓	F_{sed}
Cabrejos[16] (multiple particle)	✓	✓	–	✓	✓	✓	✓	✓	–	–	–
Danielson[4]	–	✓	–	✓	–	–	–	–	–	✓	–
Oroskar and Turian[17]	–	✓	–	✓	–	–	–	–	–	✓	–
Ponagandla[34]	✓	✓	–	–	–	–	–	✓	–	✓	–
Thomas[44]	–	✓	–	–	✓	–	–	✓	–	–	–
Thomas[154]	–	✓	–	✓	–	✓	–	✓	–	✓	F_{spin}
Ibrahim et al.[50]	✓	✓	✓	✓	✓	✓	✓	✓	–	–	–
Ling[51]	–	✓	✓	✓	✓	–	–	✓	–	–	–
Dey[49]	–	–	✓	✓	✓	–	–	✓	–	–	–
Han and Hunt[47]	–	–	✓	✓	✓	✓	–	✓	–	–	–

the model. Han and Hunt[47] assumed that the lift force is negligible compared to the apparent weight of the particle, and that the particle is either a "truncated sphere" initially resting on a flat surface, or a sphere initially resting on a "spherical depression of the same radius as the particle." Similar to Han and Hunt,[47] Ibrahim et al.[50] assumed the particle's shape to be that of a "truncated sphere,"[47] and that the particle is initially resting at the bottom of the conduit. Ling[51] developed his model to predict the fluid velocity needed to roll or lift a particle initially at rest on a bed of particles, and expressed the lift force as the sum of the shear lift, the Magnus force or spin lift, and the centrifugal force. Similar to Ling,[51] Dey[49] developed his model for the initiation of the motion of the particle initially at rest on a bed of particles. However, Dey[49] considered the possibility that the particle of interest has a different diameter compared to the rest of the particles comprising the bed.

Thomas[44] designed his model for the prediction of the solids transport velocity at "dilute suspensions" to prevent the deposition of solid particles; Cabrejos,[16] Dey,[49] and Ling[51] were interested in the pick-up of solids from a layer of particles; and Han and Hunt,[47] and Ibrahim et al.[50] were interested in initiating the motion of a single particle. Instead of balancing the lift force with the apparent weight of the particle, Thomas[44] used the ratio of the two forces to quantify the solids transport velocity. Compared to Thomas[44] and Ibrahim et al.,[50] for the pneumatic transport of particles, Cabrejos[16] incorporated experimental data with greater variations in the particle properties (density and diameter), although the largest particle density used by Ibrahim et al.[50] exceeded the values of the particle densities used by Cabrejos.[16] For the hydraulic transport of particles, Thomas[44] was mainly interested in fine particles, where the largest particle diameter used in the experiments was about 66 μm, but there was a variation in the values used for the pipe diameter (the largest value is about 0.3 m) and particle density (which includes values of 6400, 1.0×10^4, and 1.89×10^4 kg/m^3). In their experiments, Han and Hunt[47] used particles with smaller densities compared to those of Thomas,[44] but of larger diameters. Dey[49] developed his model using experimental data with greater variations in the fluid density compared to the Thomas,[44] Han and Hunt,[47] and Ling[51] models.

Models developed using turbulence theory

The models developed by Oroskar and Turian,[17] Almutahar,[22] Danielson,[4] Ponagandla,[34] and Thomas[154] took into account the effects of the turbulence of the fluid on the solids transport mechanism. Oroskar and Turian[17] were interested in predicting the velocity that marked the transition between the formation of a bed of solids at the bottom of the pipe to the full suspension of the particles, where an energy balance that incorporated the drag force and the turbulence of the fluid was used to develop the model. Oroskar and Turian[17] developed their model by balancing the energy required to maintain the particles in suspension with the "total turbulent energy" of the fluid. Building upon the Oroskar and Turian[17] model, Almutahar[22] (initial approach) incorporated additional terms to account for the effects of the particle size and the pipe inclination angle. Danielson[4] also referred to Oroskar and Turian,[17] where the energy required to keep the particles in suspension was balanced with the fraction of the turbulent energy effective in suspending them. Ponagandla[34] assumed that the turbulent velocity fluctuation force needs to overcome the apparent weight of the particle for transport. Four of these models[17,22,34,154] accounted for the effect of particle concentration on the solids transport velocity.

Thomas[154] defined the "minimum transport velocity" as the fluid velocity where "the particles cease to slide along the bottom of the pipe" but are instead transported by bouncing motion. Thomas[154] considered the following forces: the force of the apparent weight of the particle, the Bernoulli forces caused by the mean velocity gradient and instantaneous velocity differences, the forces caused by the spin of the particle giving the Magnus effect, the viscous drag force, and the friction force between the particle and the pipe wall as the particle bounces. It was found that the dominant upward forces were the Bernoulli forces caused by the instantaneous velocity differences following turbulent fluctuation, and it was assumed that the turbulent fluctuations and the friction velocities were proportional.

All models in this category were developed for hydraulic flow except the Thomas[154] model, which was also developed using gas data with a broad range for the fluid density (1.2–2.9 kg/m^3), but small particle densities ($\sim$1000 to $\sim$2500 kg/m^3). For the liquid data, Oroskar and Turian[17] used a broad range for the fluid properties, with densities in the range of 900–1350 kg/m^3, and viscosities in the range of 0.47–38 mPa·s.

Most of the semi-mechanistic models incorporate the drag force and the forces due to turbulence into the force balance. Despite this similarity, the models produce different velocity predictions due to the different methods used to calculate the drag and turbulent forces. For instance, the equation for the turbulent force used by Ponagandla[34] has a similar form to the drag force equations used by other authors,[15,28,36,185,188] with the drag coefficient, C_D, replaced with the drag and lift coefficient, $C_{D,L}$, and the average fluid velocity, v, replaced with the turbulent velocity fluctuation, v'. The models developed by Davies,[18] Almutahar[22] (new approach), and Ponagandla[34] use similar force balances in their derivation, but each relate the turbulent velocity fluctuation to the average fluid velocity differently, resulting in different velocity predictions for the same operating condition.

A more detailed review of 18 of these 44 solid transport models,[1,5,15,19,25,27,30,31,35,36,38,40,46–51] among others, can be found in Rabinovich and Kalman,[60] where the discussion was divided based on the velocity types: incipient motion velocity, pick-up velocity, saltation velocity, and minimum pressure velocity. Rabinovich and Kalman[60] discussed the ranges of the particle diameter and dimensionless groups for which the models are applicable, and classified the models based on their applicability for particles with diameters smaller and larger than the thickness of the viscous sublayer. The origins of the equations that are used to calculate the forces, such as the one developed by Saffman[189] for the lift force, were summarized, and the effect of the location of the particle prior to motion for the cases of particle pick-up from a flat layer of particles was discussed. Finally, an empirical model was suggested to predict the above-mentioned velocity types. However, a thorough assessment of the performances of these models using comparison of their predictions against experimental data was not performed.

Experimental Database

To test the performances of the models, we have compiled a database for the hydraulic and pneumatic conveying of

Table 6. Data Ranges of the Low Concentration Database

Variable	Liquid Data	Gas Data	
Velocity type	Pick-up	Pick-up	Incipient motion
Particle concentration (ppm)	1 (i.e., ~0)	1 (i.e., ~0)	1 (i.e., ~0)
Pipe inclination angle (degree)	0–3.21	0	0–40
Fluid density (kg/m^3)	820–1500	1.18–1.80	1.18–3.13
Fluid viscosity (mPa·s)	0.85–447.66	0.015–0.020	0.015–0.020
Particle density (kg/m^3)	1053–3100	930–8785	180–11640
Particle diameter (μm)	15–5000	4.65–5400	2.65–5930
Pipe diameter (m)	0.02–0.44	0.02–0.10	0.04–0.10
Total number of data points	151	284	167

particles at low particle concentrations from open literature.[5,6,15,16,19,27,30,33,52–58] (Please see Supporting Information Tables S1–S3 for the complete database.) The focus of this article is the transport of solids initially at rest. Thus, the database only includes experiments where the pick-up and the incipient motion velocities were measured. For experiments where only a single particle is placed in the conduit, the incipient motion velocity is quantified, and in those experiments where a flat bed of particles is used, the pick-up velocity is quantified. Table 6 summarizes the range of the experimental data in our database based on the type of the carrying phase. For the transport of particles in a liquid-carrying phase at low particle concentrations, the database contains 151 experimental data points for which the pick-up velocity was quantified, 117 of which are for horizontal flow. We were able to locate only three experimental data points for the incipient motion of particles in a liquid-carrying phase. Thus, the analysis is not performed for incipient motion velocity for liquid/solid flows. For the transport of particles in a gaseous-carrying phase at low particle concentrations, the experimental database consists of 284 experimental data points where the pick-up velocity was measured; and 167 experimental data points, 137 of which are for horizontal flow, where the incipient motion velocity was measured. For the liquid/solid flow experimental data, there are 34 experimental data points where the pipe inclination angles range from 0 to 5 degrees; and for the gas/solid flow experimental data at the incipient motion velocity, there are 30 experimental data points where the pipe inclination angles range from 0 to 40 degrees.

The shear velocity, which is the reported velocity in some experimental work,[33,53,55,57] is converted to the average fluid velocity via Eq. 1 for noncircular duct flow[35] and Eq. 2 for pipe flow:[186]

$$v = \frac{v_*}{k_V}\left[\frac{z_0}{h} + \ln\left(\frac{h}{z_0}\right) - 1\right] \tag{1}$$

and

$$\frac{v}{v_*} = 2.5 \times \ln\left(0.5\frac{Dv_*\rho_f}{\mu}\right) + 1.75 \tag{2}$$

In the above equations, v and v_* denote the average fluid velocity and the shear velocity, respectively. k_V represents the von Karman constant (the value of 0.4 was used), h the flow depth, z_0 the zero velocity level ($z_0 = 0.033\ k_S$), and k_S the equivalent roughness height ($k_S = 2d_p$).

Because our study focuses on the horizontal transport of solid particles, only the experimental data for horizontal flow were used to assess the performances of the models. Figure 3 provides the plots of the particle Reynolds number versus the Archimedes number for the experimental data subsets (i.e., particle transport in liquid at pick-up velocity, in gas at pick-up velocity and at incipient motion velocity) for horizontal flow. The particle Reynolds number and Archimedes numbers were chosen because they incorporate some of the most significant forces for particle transport. These plots suggest a power-law relationship between the particle Reynolds number and the Archimedes number for each of the subsets. However, because these plots were developed using the log-log scale, fitting a power-law function may generate large percent errors for the prediction of the particle Reynolds number at the lower ranges of the Archimedes numbers and large absolute errors for the predictions at the higher ranges. Table 7 shows the type of velocity measured in the experiments (based on the velocity definitions given in Figure 2) for horizontal flow, and the mechanisms observed by the authors for these experiments.

Different authors made different observations regarding the initiation of the solid particles' motion. In the experiments conducted for liquid/solid flow, for the pick-up velocity experiments: Bohling[52] interpreted the solids transport velocity as the fluid velocity where there is "constant transport on the entire sediment's surface"; Mantz[33] observed particle motion in ripples; White[57] interpreted the solids transport velocity as the fluid velocity where there is movement of a few particles; Grass[53] observed the particles "on the bed surface (fluctuating) between general motion and complete stability"; and Ramadan et al.[15] observed that particles initially lying on a bed of solids initiate their motion by rolling, and that at higher pipe inclinations, the particles move by rolling and bouncing (i.e., by lifting).

In the experiments conducted for gas/solid flow, for the pick-up velocity experiments: Cabrejos and Klinzing[27] observed the particle eroding from a layer of particles; Hubert and Kalman,[54] and Kalman et al.[30] observed three stages of particle transport: (1) the particles start to roll along the layer of particles, (2) the particles bounce (i.e., are lifted) after colliding with other particles in the bed of solids, and (3) the particles collide with the particles that are carried by the moving fluid; and Cabrejos[16] observed particle pick-up. For the incipient motion velocity experiments: Cabrejos,[16] and Villareal and Klinzing[56] observed particle pick-up; Halow[6] observed that spherical particles initiate their motion by rolling, whereas non-spherical particles initiate their motion by dragging; for particles initially at rest at the bottom of the conduit, Hubert and Kalman[54] considered the solids transport velocity to be the fluid velocity for which the particles start rolling; Rabinovich and Kalman[19] noted that "the motion (of the particles) can start by rolling, sliding, or blowing away" (i.e., by rolling, dragging, or lifting); and Stevenson et al.[5] used one of the criteria for particle motion described by Zenz,[20] namely, the initiation of motion by rolling or bouncing (i.e., lifting) along the bottom of the pipe.

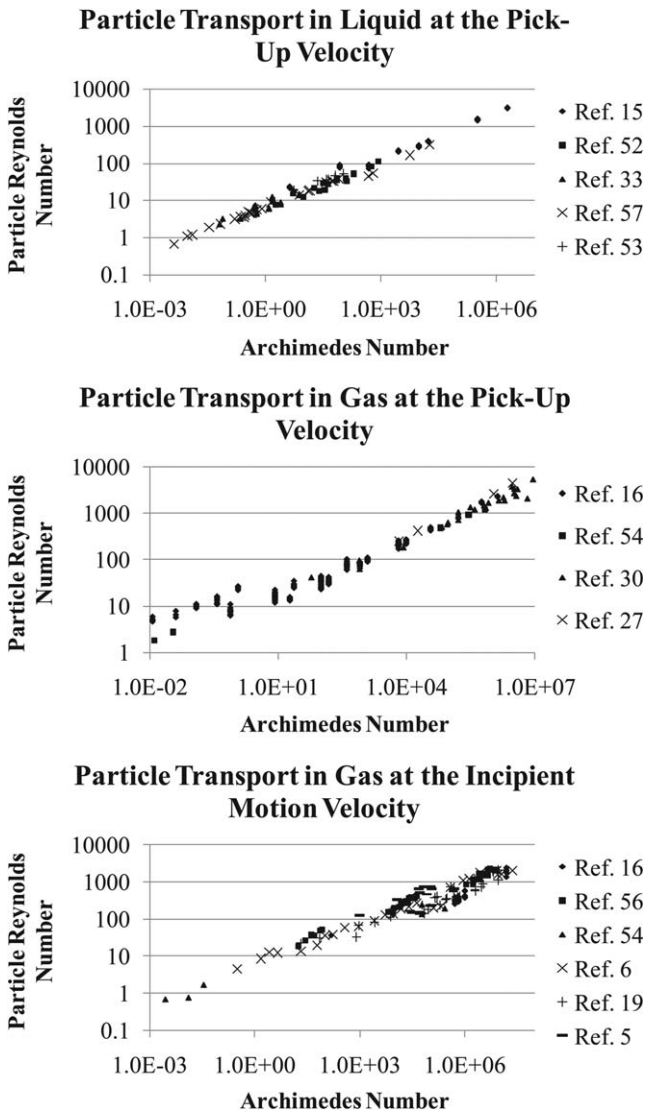

Figure 3. The graphs of $N_{Re,p}$ versus N_{Ar} for the experimental data subsets for horizontal flow

As mentioned above, for some of the experimental data, only general descriptions were given regarding the motion of the solid particles. For the experimental data from Mantz,[33] we interpreted the motion of the particles as rolling; for the experimental data from Cabrejos,[16] and Villareal and Klinzing,[56] we interpreted the motion of the particles as lifting; and for the rest of the sources for which the authors did not define a specific solids transport mechanism,[27,52,53,57] we assumed the possibility of the particle moving by dragging, lifting, or rolling.

Table 7 provides information regarding the accuracy of the measuring instruments used by the experimenters for measuring the fluid velocity, or the volumetric flow rate of the fluid. All instruments (shown in Table 7) have similar accuracies that fall to within $\pm 10\%$. The uncertainties in the fluid velocity and volumetric flow rate are larger compared to the uncertainties in the other independent variables (the fluid density and viscosity, the particle density and diameter, and the pipe diameter). This discrepancy may be attributed to the velocity and flow rate measurements being recorded based on the experimenter's observation of the movement of the particle, and inability to measure the velocity or the flow rate accurately with existing instruments. Thus, the uncertainty in the measurements of the fluid velocity or volumetric flow rate is the main source of uncertainty in the experimental data.

The Methodology Used to Evaluate the Performance of the Models: Model Screening and Ranking

To evaluate the performances of the solids transport models against the experimental data, a method that consists of two parts is used: a model screening protocol and a model ranking protocol. The purpose of the model screening protocol is to use statistical analysis to discard the models that grossly under or overestimate the solids transport velocities from further consideration, and hence to reduce the computational burden. The model ranking protocol ranks the remaining models based on the accuracy of the velocity predictions using a procedure that combines different statistical quantities. Although the scope of the current study involves flow in horizontal conduits at low particle concentrations, models that were developed for vertical flow or for high particle concentrations were included in the analysis to evaluate the

Table 7. Velocity Measured and Mechanisms Observed in the Experimental Data for Horizontal Flow

	Source	Velocity Measured	Number of Data Points	Observed Mechanism	Measuring Instrument for the Fluid Velocity or Flow Rate	Instrument Accuracy
Hydraulic Conveying	Ramadan et al.[15]	Pick-up	43	Lift, roll	Magnetic flowmeter	±3%[190]
	Bohling[52]	Pick-up	13	Drag, lift, roll	Acoustic Doppler-Velocimeter	±0.5%[191]
	Mantz[33]	Pick-up	28	Roll	Not specified	N/A
	White[57]	Pick-up	26	Drag, lift, roll	Orifice plate flow gauge	±3%[30]
	Grass[53]	Pick-up	7	Drag, lift, roll	Hydrogen Bubble Method of Velocity Measurement	±0.5%[191,192]
Pneumatic Conveying	Cabrejos[16]	Incipient motion	31	Lift	Two rotameters in parallel	±10%[193,194]
		Pick-up	247	Lift		
	Kalman et al.[30]	Pick-up	27	Lift, roll	Mass flow meters (for flow rates below 2500 L/min)	±0.1%[30]
					Thin-plate orifice (for higher flow rates)	±3%[30]
	Halow[6]	Incipient motion	26	Drag, roll	Rotameters manufactured by Fischer Porter	±10%[195]
	Rabinovich and Kalman[19]	Incipient motion	29	Drag, lift, roll	Mass flow meters (for flow rates below 2500 L/min)	±0.1%[30]
					Thin-plate orifice (for higher flow rates)	±3%[30]
	Stevenson et al.[5]	Incipient motion	14	Lift, roll	Two rotameters in parallel	±10%[193,194]
	Hubert and Kalman[54]	Incipient motion	7	Roll	Mass flow meters (for flow rates below 2500 L/min)	±0.1%[54]
					Thin-plate orifice (for higher flow rates)	±3%[54]
		Pick-up	6	Roll, lift	Mass flow meters (for flow rates below 2500 L/min)	±0.1%[54]
					Thin-plate orifice (for higher flow rates)	±3%[54]
	Cabrejos and Klinzing[27]	Pick-up	4	Drag, lift, roll	Pressure transducer	±1%[196]
	Villareal and Klinzing[56]	Incipient motion	30	Lift	Pressure transducer	±7% (this value represents the reproducibility of the experimental results)[56]

performances of the model screening and ranking procedures. Because our experimental database contains data for horizontal flow at low particle concentrations, models developed for these conditions should have higher rankings compared to the rest of the models.

The model screening analysis uses the following statistics: the modified adjusted-R^2 ($R^2_{\text{mod,adj},j}$) of each model j, and the slope m_j of the best-fitting line between the predicted versus experimental velocity with the intercept of the line set as the origin for each model j. The modified adjusted-R^2 is calculated as

$$R^2_{\text{mod, adj},j} = 1 - \left(\frac{E_{SS,j}}{T_{SS,\text{mod}}}\right)\left(\frac{N_{\text{data}} - 1}{N_{\text{data}} - n_{\text{indep},j} - 1}\right) \tag{3}$$

where $E_{SS,j}$ denotes the error sum of squares[197] of model j, N_{data} the total number of liquid or gas data in the database, $n_{\text{indep},j}$ the number of independent variables in model j, and $T_{SS,\text{mod}}$ the modified total sum of squares of the experimental velocity in the liquid or gas database. The modified total sum of squares quantifies the square of the overall variation in the experimental velocity.[197,198] Hence, the modified adjusted-R^2 provides information regarding the ratio of the variation of the velocity prediction error and the overall variation in the experimental velocity. This information can be used to assess the accuracy of a model's velocity prediction, where a negative value of the modified adjusted-R^2 implies that the variation between the experimental and the predicted velocities are greater than the variation within the experimental velocities.

The conditions that were used to discard the models are specified in Eqs. 4–6

$$R^2_{\text{mod,adj},j} < 0 \tag{4}$$

$$m_j < 0.5 \tag{5}$$

or

$$m_j > 1.5 \tag{6}$$

The models were discarded if at least one of the above conditions was satisfied. Here, the values of 0.5 and 1.5 were selected as the lower and upper limits, respectively, for the slope to keep the velocity predictions of the models within ±50% of the experimental velocities. Ideally, the slope of this line is expected to be close to unity (i.e., the values of the predicted velocity are almost equal to the values of the experimental velocity). Therefore, having the

slope falling between 0.5 and 1.5 implies that most of the predicted versus experimental velocity pairings considered for analysis fall within the ±50% lines.

For the model ranking, because different statistics provide different information regarding the accuracy of the models, the following statistical quantities are used

$$E_{MS,j}=\frac{E_{SS,j}}{N_{\text{data}}} \tag{7}$$

$$E_{MAP,j}=\frac{100}{N_{\text{data}}}\sum_{i=1}^{N_{\text{data}}}\frac{|v_{calc,i,j}-v_{\text{exp},i}|}{v_{\text{exp},i}} \tag{8}$$

$$E_{MA,j}=\frac{1}{N_{\text{data}}}\sum_{i=1}^{N_{\text{data}}}|v_{calc,i,j}-v_{\text{exp},i}| \tag{9}$$

and

$$R^2_{\text{mod,adj,dev},j}=1-R^2_{\text{mod,adj},j} \tag{10}$$

The statistics shown in Eqs. 7–10 include: $E_{MS,j}$ (the mean squared error of model j), $E_{MAP,j}$ (the mean absolute percent error of model j), $E_{MA,j}$ (the mean absolute error of model j), and $R^2_{\text{mod,adj,dev},j}$ (the deviation of the adjusted-R^2 statistic of model j from one). In addition to the above statistics, the following information are used to rank the models: $P_{50\%,j}$ (the percent of velocity predictions that lie outside the ±50% lines in the graph of predicted versus experimental velocity for model j), $\max_{\%,j}$ ($\max_{\%,j}=\max\left[over_{\%,j}, under_{\%,j}\right]$, with $\text{over}_{\%,j}$ and $\text{under}_{\%,j}$ denoting the percent of experimental velocity overestimated by model j and the percent of experimental velocity underestimated by model j, respectively), and k_j (the number of parameters in model j, used if the model parameters are fine-tuned—discussed in the "Fine-Tuning Process" section).

The values of the seven statistics were normalized using

$$\overline{y_j}=\frac{|y_j|-\min\left(|y_1|,\ldots,|y_J|\right)}{\max\left(|y_1|,\ldots,|y_J|\right)-\min\left(|y_1|,\ldots,|y_J|\right)},\quad j=1,\ldots,J \tag{11}$$

In the preceding equation, J corresponds to the total number of models that were ranked, and y_j denotes the statistics of model j ($E_{MS,j}$, $E_{MAP,j}$, $E_{MA,j}$, $R^2_{\text{mod,adj,dev},j}$, $P_{50\%,j}$, $\max_{\%,j}$, and k_j), with $\overline{y_j}$ representing the normalized value of y_j $\left(\overline{E_{MS,j}}, \overline{E_{MA,j}}, \overline{E_{MAP,j}}, \overline{R^2_{\text{mod},adj,dev,j}}, \overline{P_{50\%,j}}, \overline{\max_{\%,j}}, \text{and } \overline{k_j}\right)$. For each model j, the normalized values of the six (or seven) statistics were summed to obtain the total score S_j of the model

$$S_j=w_1\overline{E_{MS,j}}+w_2\overline{E_{MA,j}}+w_3\overline{E_{MAP,j}}+w_4\overline{P_{50\%,j}}+w_5\overline{\max_{\%,j}}+w_6\overline{R^2_{\text{mod},adj,dev,j}}+\left(w_7\overline{k_j}\right) \tag{12}$$

where w_1 to w_7 represent the weight of each statistic. $\overline{k_j}$ is only used in the model ranking for the cases where the model parameters are fine-tuned prior to ranking, and thus, the term $w_7\overline{k_j}$ is enclosed in parentheses in Eq. 12. For this study, all weights are equal to one. Those models with scores closest to zero are the ones that are ranked higher. These seven statistics are used to rank the models because the strength of each statistic offset the limitations of the others, as will be discussed below. Equal weights ensure that the strength(s) or limitation(s) of any statistic is not amplified. However, the analysis can be repeated with different weights if the characteristic(s) quantified by a subset of the statistics were more significant to the user compared to the rest.

The mean squared error represents the sum of the variance of the model's prediction and the bias of the model's prediction.[197] Thus, the mean squared error quantifies the "spread" of the error. However, the value of the squared error may become very small for small velocity predictions, and may become very large for large velocity predictions.[197] To overcome this shortcoming, absolute errors are used. However, using the mean absolute percent error can pose a problem if the value of the observation is equal to zero (which means that $E_{MAP,j}$ cannot be calculated), or if the value of the observation is nearly equal to zero (which means that the value of $E_{MAP,j}$ will become very large). The statistic $E_{MA,j}$ can be used to overcome the weaknesses of $E_{MS,j}$ and $E_{MAP,j}$, as the calculations of $E_{MA,j}$ does not involve squaring the errors, or dividing by the experimental velocity. The values of $E_{MA,j}$ need to be compared against the values of the experimental velocity to assess the accuracy of the model. For instance, an absolute error of 0.1 m/s for the model may be acceptable if the value of the experimental velocity is 10 m/s. However, if the value of the experimental velocity is 0.15 m/s, such absolute error implies that the model is inadequate. Thus, $E_{MAP,j}$ can overcome the shortcoming of $E_{MA,j}$, as $E_{MAP,j}$ provides information on the accuracy of the model relative to the value of the experimental velocities.

The modified adjusted-R^2 statistic quantifies the model's accuracy by comparing the errors produced by the model against the overall variation in the experimental velocity. The modified adjusted-R^2 statistic would have a value of one for a model that does not produce any error, and zero for models which produce errors that are equal to the overall variation in the experimental velocity. Therefore, the model will have a lower ranking as the value of its modified adjusted-R^2 statistic deviates farther from one.

Ideally, a model should neither underestimate nor overestimate the experimental velocity. In reality, this is not the case. Therefore, one would prefer unbiased models, where the amounts of underestimates and overestimates produced by the model are approximately equal. The model is unbiased if its value $\max_{\%,j}$ is approximately equal to 50%. If the model generates more overestimates than underestimates, or vice versa, its value of $\max_{\%,j}$ will exceed 50%. By including $\max_{\%,j}$ as a statistic for the model ranking, one can ensure that the greater the bias of the model (i.e., the closer the value of $\max_{\%,j}$ is to 100%), the lower the ranking of the model. And to ensure that most, if not all, the estimates of the models fall to within ±50% of the experimental velocity, $P_{50\%,j}$ is used as a statistic for the model ranking. With this inclusion, models that produce estimates that exceed +50% or fall below −50% of the experimental velocity are ranked lower compared to those whose estimates fall to within ±50% of the experimental velocity. The values of ±50% is used to stay consistent with the criteria used in the model screening (shown in Eqs. 5 and 6). k_j is used as a statistic for the model ranking if the model parameters are fine-tuned prior to ranking, because we would like to prevent the model from overfitting the experimental data. Thus, if two models have very similar values of all the statistics except for k_j, the model with the larger value of k_j will have a lower ranking.

Fine-Tuning Process

The goal of the fine-tuning process is to identify the proper model forms and dominant forces for the experimental database for the hydraulic conveying of particles at the pick-up velocity, and the pneumatic conveying of particles at the pick-up and incipient motion velocities. Hence, the analysis outlined in this section is performed separately for each of the above three experimental data sets.

To generate a model-form list, we converted all available solid transport models into dimensionless forms. This is done by multiplying both sides of the velocity equations of the models by $\left(\frac{d_p \rho_f}{\mu}\right)$, which yields the particle Reynolds number on the left-hand side of the equation. Upon performing this procedure, for many of the model forms, the independent variables on the right-hand side of the equations can be rearranged to form the Archimedes number. The particle Reynolds number was selected as the dimensionless group that contains the solids transport velocity (the dependent variable) because this dimensionless group represents the ratio between the inertial force and the viscous force acting on the particle. Thus, the particle Reynolds number represents the relative magnitude of the force that causes particle motion, as the inertial force is "proportional to the fluid density and the square of the fluid velocity," while the viscous force is the force that prevents "the random and rapid fluctuations of the fluid."[185] For some of the models, the conversion into dimensionless form revealed the existing small dimensional inconsistencies in the original models, and these models are summarized in Supporting Information Table S4. Then, the numerical constants in the dimensionless models, that is, the coefficients and the powers, are replaced with k-constants. At the end of this step, the models with the same forms are grouped together, yielding a model-form list.

The dimensionless forms of the models with their original constants (second column), and with the k-constants (third column) are given in Appendix Table A1. Here, $N_{Re,p,\text{lift}}$, $N_{Re,p,\text{drag}}$, and $N_{Re,p,\text{roll}}$ denote the particle Reynolds number required for particle lift, drag, and roll, respectively, and $N_{Re,p,0}$ denotes the particle Reynolds number required to initiate the motion of a single particle in the absence of additional particles. For the multiple-particle model developed by Cabrejos,[16] the values of v_0 and $N_{Re,p,0}$ are obtained from the single-particle model developed by Cabrejos.[16]

The parameters of the model forms are adjusted by minimizing the error sum of squares ($E_{SS,j}$) of the velocity predictions made by each model form j for the database. The method of minimizing $E_{SS,j}$ is chosen for the fine-tuning process because this method proves to be more robust compared to using $E_{MAP,j}$ or $E_{MA,j}$, as absolute values are used in the calculations of $E_{MAP,j}$ and $E_{MA,j}$.[198] The optimization formulation is

$$\text{MIN} : E_{SS,j} = \sum_{i=1}^{N_{data}} \left(v_{calc,i,j} - v_{\text{exp},i}\right)^2 \tag{13}$$

subject to

$$k_{l,j} \geq 0 \tag{14}$$

where $k_{l,j}$ represents the lth parameter of model form j, N_{data} the number of data points in the data set, $v_{\text{calc},i,j}$ the velocity prediction of model form j for datum point i, and $v_{\text{exp},i}$ the experimental velocity for datum point i. The nonnegativity constraint shown in Eq. 14 ensures that the forms of the models are unchanged by preventing the inversions of the dimensionless groups. The values of the parameters of the solids transport model forms after they are fine-tuned using the horizontal liquid-carrying phase at the pick-up velocity, and gas-carrying phase experimental data at the pick-up and incipient motion velocities are shown in the second, third, and fourth columns of Appendix Table A2, respectively.

Results and Discussion

The model ranking is performed for the original models and different model forms after fine-tuning to compare the performances of both sets separately for the experimental data for liquid/solid flow at the pick-up velocity, gas/solid flow at the pick-up velocity, and gas/solid flow at the incipient motion velocity. The experimental database was divided into these three subsets to study the differences between the solids transport mechanisms for the hydraulic and pneumatic conveying of particles, and between the initiation of the motion of the solid particles from a bed of particles and the bottom of the conduit. The following subsections discuss the results of the model ranking for the three experimental data subsets, and the implications of the model ranking results.

Hydraulic conveying of particles at the pick-up velocity

The statistics of the ranked original models, without the parameter fine-tuning, for the horizontal, hydraulic conveying of solid particles at the pick-up velocity are shown in Table 8, and the graphs of the predicted versus experimental velocities for the models are given in Supporting Information Figure S2. The same information is provided for the model forms after the parameter fine-tuning in Table 9 and Supporting Information Figure S3. An initial glance at the rankings and the graphs of the predicted versus experimental velocity reveals that the rankings are consistent with these graphs, that is, similar results for the model ranking would have been yielded had the model ranking been performed using only the graphs.

The normalized values of the statistics (obtained using Eq. 11 by normalizing the first six statistics shown in Table 8 and the first seven statistics shown in Table 9) are given in Supporting Information Tables S5 and S6. The score S_j of each model is obtained as the summation of the normalized values (given in Supporting Information Tables S5 and S6) using Eq. 12, and are given in the rightmost columns of Supporting Information Tables S5 and S6. It should be noted here that because the scores of the models (S_j) are obtained through the normalizations of the statistics, these scores can only be used to compare the performances of the models in the same set against each other (e.g., the ranked original models for hydraulic flow). For example, from the values shown in Table 8, the minimum and maximum values of $E_{MS,j}$ for the ranked models, without the parameter fine-tuning, are 0.0128 and 0.0813 m^2/s^2, respectively. And from the values shown in Table 9, the minimum and maximum values of $E_{MS,j}$ for the fine-tuned ranked model forms are 0.0067 and 0.0533 m^2/s^2, respectively. As shown in Eq. 11, the calculations of the normalized statistics depend on the minimum and maximum values of the statistic. Because the minimum and maximum values of $E_{MS,j}$ differ for the models with and without the parameter fine-tuning, the values of

Table 8. Statistics of the Ranked Original Models for the Liquid Data for the Pick-Up Velocity

Model	Rank	$E_{MS,j}$ (m^2/s^2)	$E_{MA,j}$ (m/s)	$E_{MAP,j}$ (%)	$P_{50\%,j}$ (%)	$\max_{\%,j}$ (%)	$R^2_{\text{mod,adj},j}$	$P_{+50\%,j}$ (%)	$P_{-50\%,j}$ (%)	$\text{over}_{\%,j}$ (%)	$\text{under}_{\%,j}$ (%)
Mantz[33]	1	0.0157	0.0865	26.32	13.68	50.43	0.8719	7.69	5.98	49.57	50.43
Rabinovich and Kalman[35]	2	0.0128	0.0731	21.79	10.26	69.23	0.8954	4.27	5.98	30.77	69.23
Dey[49]	3	0.0187	0.0960	30.14	17.09	71.79	0.8479	0.00	17.09	28.21	71.79
Miller et al.[2]	4	0.0223	0.1027	27.58	7.69	84.62	0.8179	1.71	5.98	15.38	84.62
Fletcher[29]	5	0.0280	0.1092	29.82	15.38	88.03	0.7719	0.00	15.38	11.97	88.03
Rabinovich and Kalman[19]	6	0.0364	0.1455	43.49	44.44	56.41	0.7035	21.37	23.08	43.59	56.41
Oroskar and Turian[17]	7	0.0453	0.1522	50.24	35.90	53.85	0.6274	22.22	13.68	46.15	53.85
Ramadan et al.[15]	8	0.0535	0.1819	62.49	70.09	94.87	0.5602	0.00	70.09	5.13	94.87
Rampall and Leighton[37]	9	0.0809	0.2455	92.27	68.38	62.39	0.3404	49.57	18.80	62.39	37.61
Cabrejos[16] (single particle)	10	0.0813	0.2552	102.75	71.79	76.07	0.3373	58.12	13.68	76.07	23.93

the normalized statistics and the scores for the different sets of models cannot be compared against each other.

For the original models, Table 8 shows that as the ranking of the model decreases, the value of the modified adjusted-R^2 statistic decreases, while the values of $E_{MS,j}$, $E_{MA,j}$, and $E_{MAP,j}$ increase (starting with the third-ranked model). When the values of these statistics are fairly close to each other, as is the case with the Mantz,[33] and Rabinovich and Kalman[35] models, the value of $\max_{\%,j}$ determines the ranking. The value of $\max_{\%,j}$ for the Rabinovich and Kalman[35] model is significantly larger than for the Mantz[33] model. Based on the values of $\max_{\%,j}$ and $\text{under}_{\%,j}$, and the graphs in Supporting Information Figure S2, the Rabinovich and Kalman[35] model more frequently underestimates the experimental velocity compared to the Mantz[33] model. Hence, the Rabinovich and Kalman[35] model is ranked lower than the Mantz[33] model.

For the original models with the highest rankings for the hydraulic conveying of solids at the pick-up velocity, the two highest-ranked models[33,35] were developed empirically using experimental data with liquid/solid flow. These models have the highest modified adjusted-R^2 statistic, and the lowest $E_{MS,j}$, $E_{MA,j}$, and $E_{MAP,j}$ compared to the remaining ranked models (shown in Table 8). The data ranges used to develop these models[33,35] were similar to the ranges of the liquid data in our database, and thus, it should be expected that these models provide the most accurate velocity predictions among the available models. Although the Rabinovich and Kalman[19] model (the sixth-ranked model) was developed using experimental data for both gas/solid and liquid/solid

Table 9. Statistics of the Ranked Model Forms for the Liquid Data for the Pick-Up Velocity (After Fine-Tuning Process)

Model Form No.	Rank	$E_{MS,j}$ (m^2/s^2)	$E_{MA,j}$ (m/s)	$E_{MAP,j}$ (%)	$P_{50\%,j}$ (%)	$\max_{\%,j}$ (%)	$R^2_{\text{mod,adj},j}$	k_j	$P_{+50\%,j}$ (%)	$P_{-50\%,j}$ (%)	$\text{over}_{\%,j}$ (%)	$\text{under}_{\%,j}$ (%)
2	1	0.0072	0.0569	20.04	5.98	59.83	0.9416	2	5.98	0.00	59.83	40.17
3	2	0.0072	0.0569	20.04	5.98	59.83	0.9411	3	5.98	0.00	59.83	40.17
9	3	0.0072	0.0569	20.04	5.98	59.83	0.9411	4	5.98	0.00	59.83	40.17
22	4	0.0072	0.0569	20.04	5.98	59.83	0.9405	4	5.98	0.00	59.83	40.17
4	5	0.0069	0.0567	20.39	6.84	59.83	0.9439	4	6.84	0.00	59.83	40.17
32	6	0.0070	0.0584	20.80	5.98	57.26	0.9428	6	5.98	0.00	57.26	42.74
5	7	0.0098	0.0633	23.63	5.13	52.14	0.9207	3	5.13	0.00	52.14	47.86
30	8	0.0067	0.0560	19.06	5.13	59.83	0.9440	7	5.13	0.00	59.83	40.17
10	9	0.0072	0.0569	20.04	5.98	59.83	0.9411	5	5.98	0.00	59.83	40.17
19	10	0.0072	0.0569	20.04	5.98	59.83	0.9405	5	5.98	0.00	59.83	40.17
24	11	0.0072	0.0569	20.04	5.98	59.83	0.9405	5	5.98	0.00	59.83	40.17
20	12	0.0072	0.0569	20.04	5.98	59.83	0.9405	5	5.98	0.00	59.83	40.17
26	13	0.0072	0.0570	20.09	5.98	59.83	0.9405	5	5.98	0.00	59.83	40.17
27	14	0.0069	0.0567	20.39	6.84	59.83	0.9434	6	6.84	0.00	59.83	40.17
6	15	0.0076	0.0587	21.93	6.84	59.83	0.9380	4	6.84	0.00	59.83	40.17
21	16	0.0072	0.0569	20.04	5.98	59.83	0.9405	7	5.98	0.00	59.83	40.17
11	17	0.0069	0.0540	19.66	5.98	59.83	0.9436	9	5.98	0.00	59.83	40.17
28	18	0.0072	0.0569	20.04	5.98	59.83	0.9405	8	5.98	0.00	59.83	40.17
17	19	0.0071	0.0543	19.58	5.13	60.68	0.9423	11	5.13	0.00	60.68	39.32
8	20	0.0071	0.0584	20.73	6.84	60.68	0.9424	9	6.84	0.00	60.68	39.32
29	21	0.0116	0.0644	20.47	11.97	51.28	0.9048	11	5.98	5.98	51.28	48.72
25	22	0.0110	0.0693	26.95	13.68	52.99	0.9093	9	12.82	0.85	52.99	47.01
12	23	0.0107	0.0704	25.22	14.53	52.14	0.9126	11	11.11	3.42	52.14	47.86
1	24	0.0132	0.0750	25.93	19.66	59.83	0.8923	2	13.68	5.98	59.83	40.17
13	25	0.0148	0.0784	24.91	15.38	56.41	0.8790	6	9.40	5.98	56.41	43.59
18	26	0.0132	0.0750	25.93	19.66	59.83	0.8923	4	13.68	5.98	59.83	40.17
33	27	0.0156	0.0899	27.94	15.38	50.43	0.8731	5	9.40	5.98	50.43	49.57
7	28	0.0131	0.0749	25.87	18.80	61.54	0.8930	4	12.82	5.98	61.54	38.46
35	29	0.0132	0.0749	25.95	19.66	59.83	0.8925	16	13.68	5.98	59.83	40.17
14	30	0.0141	0.0899	29.99	14.53	60.68	0.8855	12	11.97	2.56	60.68	39.32
31	31	0.0275	0.1120	35.42	29.91	62.39	0.7777	3	16.24	13.68	62.39	37.61
16	32	0.0533	0.1811	62.28	70.09	93.16	0.5616	11	0.00	70.09	6.84	93.16
15	33	0.0485	0.1801	61.21	61.54	88.89	0.6049	36	0.85	60.68	11.11	88.89

flow, the liquid used in the experiments was water, which is consistent with the experimental data in our database, as most of the liquid data in our database consists of experimental data for solids transport in water. The selection of the Fletcher[29] and Dey[49] models among the highest-ranked models suggest that the weight and specific mass of the particle, viscous forces, and drag and lift forces play a role in the hydraulic conveying of solids. However, the cohesion between the particles become significant only in the cases of fine particles.[29] It is also worth noting that the five highest-ranked models were developed to predict the pick-up velocity, which is the velocity quantified in the experimental database subset currently discussed. This observation validates the model ranking method, in which the method is capable of identifying the models that were developed for the same type of velocity as those quantified in the experimental data. Three of the five highest-ranked models[2,33,35] also have similar forms, where the particle Reynolds number is a function of the Archimedes number. However, the incorporation of the hydraulic diameter of the conduit differs, where D is incorporated via the quantity $\left(\frac{D}{d_p}\right)$ in the Miller et al.[2] and Mantz[33] models, via the exponential function in the Rabinovich and Kalman[19,35] models, and through the conversion from the shear velocity to the solids transport velocity in the Fletcher[29] and Dey[49] models.

The inclusion of the Oroskar and Turian,[17] Rampall and Leighton,[37] and Cabrejos[16] models among the ranked models suggests that the turbulence of the fluid affects the motion of the particle, and the solids transport mechanisms differ for particles larger and smaller than the viscous sublayer thickness. However, these three models fall among the lowest four ranked models, and hence, the rankings suggest that the effects of the turbulence of the fluid and the viscous sublayer are not as significant compared to the forces suggested by the Fletcher[29] and Dey[49] models for low concentration flow at the pick-up velocity with liquid as the carrier phase.

As a further validation, we compared the mechanisms that were used to develop the higher-ranked mechanistic or semi-mechanistic models[15–17,37,49] against the mechanisms observed by the experimenters (shown in Table 7). It was seen that the mechanisms assumed to be dominant by the authors who developed the above-mentioned models are consistent with the mechanisms observed by the experimenters. For instance, most of the authors who conducted the experiments for solids transport in liquid-continuous phase observed particle motion by rolling,[15,33,53,54,58] which is consistent with the dominant mechanisms assumed by Dey[49] and Ramadan et al.[15] Many observations were made for the initiation of the particle's motion by lift,[15,52,53,57] which is consistent with the mechanisms assumed to be dominant by four of the mechanistic or semi-mechanistic models[15–17,37] included among the ranked models. Thus, the model ranking method is capable of identifying the models that predict the appropriate solids transport mechanisms for an experimental database.

To identify the appropriate model forms and dominant forces for the hydraulic conveying of solids at the pick-up velocity, the parameters of the model forms were fine-tuned using the experimental data. For the 20 highest-ranked model forms, the values of all the statistics, except for the number of adjusted parameters, are nearly equal to each other (Table 9). The effect of incorporating the number of adjusted parameters (i.e., constants) into the model ranking can be seen here, where the model forms with more parameters are ranked lower compared to those with less parameters.

The values of the parameters of the fine-tuned model forms in Appendix Table A2 suggest that for flow in the liquid-continuous phase at low particle concentrations at the pick-up velocity, many of the models reduce to the same form, resulting in similar values of the statistics (shown in Table 9). For instance, eight of the model forms reduce to the form where the particle Reynolds number is a function of the Archimedes number only, three of the model forms reduce to the form where the particle Reynolds number based on the shear velocity is a function of the Archimedes number only, and two of the model forms reduce to the form where the particle Reynolds number is a function of the Archimedes number and the ratio $\left(\frac{\rho_f}{\rho_S-\rho_f}\right)$. Hence, although 35 different model forms were identified initially, the fine-tuning process using the liquid experimental data quantifying the pick-up velocity reduces the number of model forms to 25 different forms. The results of the fine-tuning process imply that for the hydraulic conveying of solids at low concentrations, the inertial force, viscous force, and apparent weight of the particle dominate, as the Reynolds number represents the ratio of the inertial force to the viscous force, and the Archimedes number quantifies the ratio $\frac{F_I F_W}{F_V^2}$,[30,185,186] where F_I and F_V represent the inertial and viscous forces, respectively.

The results of the fine-tuning process suggest that the effects of the ratio of the fluid and particle density should be considered. However, most of the original models do not take into account the density ratio, with the exception of the Fletcher[29] and Dey[49] models. Among the five highest-ranked fine-tuned model forms, differences can be seen regarding the incorporation of the density ratio in some of the models. For instance, Model Forms 4 and 22 incorporate the density ratio through $\left(\frac{\rho_f}{\rho_S-\rho_f}\right)$ and $\left[1+C\left(\frac{\rho_S-\rho_f}{\rho_f}\right)\right]$, respectively. Thus, the density ratio can be incorporated into the models in more than one way.

At first glance, it seems that for the liquid data for the pick-up velocity in our database, the hydraulic diameter does not affect the solids transport velocity, as the exponent for the ratio $\frac{D}{d_p}$ become zero after the fine-tuning process for 13 of the model forms where $N_{Re,p}$ is a function of $\frac{D}{d_p}$. However, it was found that the correlation between v and $\frac{D}{d_p}$ is about -0.58 for the liquid/solid flow data. (The ratio $\frac{D}{d_p}$ is where D appears most often in the dimensionless model forms.) The negative value of the correlation implies that as the value of $\frac{D}{d_p}$ increases, the value of v decreases in our experimental data set for hydraulic conveying. This observation suggests that the behaviors of the models can be further investigated if the nonnegativity constraint shown in Eq. 14 is removed during fine-tuning. In fact, when the nonnegativity constraint is removed, the results of the fine-tuned parameters for the above model forms suggest nonzero, negative parameters (between -0.012 and -0.31) for the exponent of $\frac{D}{d_p}$. Thus, in developing models for liquid/solid pick-up velocity predictions, the fine-tuning results suggest that it may be more appropriate to incorporate the effects of the hydraulic diameter of the conduit through the ratio $\frac{d_p}{D}$ instead of $\frac{D}{d_p}$ for low solids concentrations. Because the scope of the fine-tuning

analysis in this article was defined to identify the best parameter values for the identified model forms, the complete analysis of these results is left as a future study.

Pneumatic conveying of particles at the pick-up velocity

Tables 10 and 11 (and Supporting Information Tables S7 and S8), and Supporting Information Figures S4 and S5 summarize the results for the horizontal, pneumatic conveying of solid particles at the pick-up velocity. The information in these tables and figures are organized in the same way as the liquid/solid case, and the model ranking for the gas/solid case was obtained using the same method as that for the liquid/solid case. The results of the model ranking for the gas data are consistent with the graphs of the predicted versus experimental velocity (Supporting Information Figures S4 and S5).

For the original models, the highest-ranked model[30] has the largest value of the modified adjusted-R^2 statistic, and the smallest values of $E_{MS,j}$, $E_{MA,j}$, $E_{MAP,j}$, and $P_{50\%,j}$ compared to the remaining ranked models (shown in Table 10). After the sixth-ranked model, the values of the statistics differ significantly, where the seventh to the last-ranked models[5,15,16,27,33,34,37,45,49] have larger values of $E_{MS,j}$, $E_{MA,j}$, $E_{MAP,j}$, $P_{50\%,j}$, and smaller values of the modified adjusted-R^2 statistic compared to the six highest-ranked models.[2,17,19,30,35,36]

Five of the six highest-ranked original models[2,19,30,35,36] (shown in Table 10) were developed or validated using experimental data for gas/solid flow (Supporting Information Figure S1). For three of the six highest-ranked models,[19,35,36] the ranges of the experimental data used to develop the models are similar to the ranges of the gas data for pick-up velocity in our database. In addition, three of the four highest-ranked models[2,30,35] were developed to predict the pick-up velocity for pneumatic conveying, which is the velocity quantified in the current experimental data subset being discussed. The selection of mechanistic and semi-mechanistic models[5,15–17,34,36,37,49] among the ranked original models may suggest the possible mechanisms for the pneumatic transport of solids at low particle concentrations. The selection of the models developed by Rabinovich and Kalman,[36] Cabrejos,[16] and Stevenson et al.[5] suggests that for at least some experimental data points, the particle motion was initiated by dragging. In addition, Rabinovich and Kalman,[36] and Stevenson et al.[5] developed their models assuming non-spherical particle shapes, and most of the pneumatic conveying experimental data for the pick-up velocity in our database are for non-spherical particles. The selection of the Rampall and Leighton,[37] Ponagandla,[34] Oroskar and Turian,[17] and Ramadan et al.[15] models implies that for some of the experimental data points, the particle transport takes place due to the lift mechanism; and the selection of the Dey,[49] Ramadan et al.,[15] and Rabinovich and Kalman[36] models suggests the possibility of the initiation of the particle's motion by rolling. The selection of the models developed by Rabinovich and Kalman,[36] Cabrejos,[16] and Rampall and Leighton[37] suggest that for the pneumatic conveying of particles from a bed of solids, the solids transport mechanisms for particles smaller and larger than the thickness of the viscous sublayer differ. Here, the viscous sublayer thickness is measured relative to the topmost particles that remain at rest. Finally, the inclusion of the Oroskar and Turian,[17] and Ponagandla[34] model among the ranked models suggests that the turbulence of the fluid contributes to the motion of particle. Most of the ranked original models incorporate the Archimedes number, and the Cabrejos,[16] and Rabinovich and Kalman[36] models also incorporate the adhesive force term. Similar to the five highest-ranked original models for liquid flow at the pick-up velocity, the five highest-ranked original models for gas flow at the pick-up velocity incorporate the hydraulic diameter through $\left(\frac{D}{d_p}\right)$,[2,17] or the exponential function.[19,30,35]

It can be seen from Table 11 that for the nine highest-ranked fine-tuned model forms, the values of $E_{MS,j}$, $E_{MA,j}$, $E_{MAP,j}$, $\max_{\%,j}$, and $P_{50\%,j}$ are smaller, and the values of the adjusted-R^2 statistics are larger, when compared to the remaining models. The values of all the statistics, except for the number of parameters, of the nine highest-ranked fine-tuned model forms are nearly equal to each other. The inclusion of model forms with larger number of parameters among the nine highest-ranked suggests that for the gas data for flow at the pick-up velocity, the number of parameters in the model have limited impact on the model ranking compared to the remaining statistics. The effects of the number of model parameters are different for the pick-up velocity experiments in liquid/solid and gas/solid flows due to the greater number of experimental data points in the database

Table 10. Statistics of the Ranked Original Models for the Gas Data for the Pick-Up Velocity

Model	Rank	$E_{MS,j}$ (m^2/s^2)	$E_{MA,j}$ (m/s)	$E_{MAP,j}$ (%)	$P_{50\%,j}$ (%)	$\max_{\%,j}$ (%)	$R^2_{\mathrm{mod,adj},j}$	$P_{+50\%,j}$ (%)	$P_{-50\%,j}$ (%)	$\mathrm{over}_{\%,j}$ (%)	$\mathrm{under}_{\%,j}$ (%)
Kalman et al.[30]	1	7.18	1.73	23.51	8.80	53.87	0.9031	8.80	0.00	46.13	53.87
Miller et al.[2]	2	14.29	2.25	25.57	13.73	60.56	0.8072	2.46	11.27	39.44	60.56
Oroskar and Turian[17]	3	14.81	2.47	29.34	22.89	50.70	0.7994	11.62	11.27	50.70	49.30
Rabinovich and Kalman[35]	4	15.51	2.36	26.45	14.79	67.25	0.7907	2.11	12.68	32.75	67.25
Rabinovich and Kalman[19]	5	16.64	3.11	33.82	21.48	81.34	0.7755	0.70	20.77	18.66	81.34
Rabinovich and Kalman[36]	6	19.46	2.99	32.53	19.01	83.10	0.7375	0.70	18.31	16.90	83.10
Rampall and Leighton[37]	7	24.47	4.03	55.18	46.48	51.76	0.6699	29.93	16.55	48.24	51.76
Stevenson et al.[5]	8	24.03	3.37	37.07	29.23	83.10	0.6758	2.11	27.11	16.90	83.10
Dey[49]	9	30.23	3.59	40.36	28.17	65.14	0.5922	13.38	14.79	65.14	34.86
Mantz[33]	10	25.32	3.79	44.82	34.15	70.07	0.6584	22.89	11.27	70.07	29.93
Ponagandla[34]	11	26.83	4.04	48.05	51.41	65.49	0.6367	16.90	34.51	34.51	65.49
Cabrejos and Klinzing[27]	12	33.99	3.74	41.92	40.14	83.80	0.5414	5.63	34.51	16.20	83.80
Ramadan et al.[15]	13	32.03	4.17	51.25	51.41	83.10	0.5664	4.93	46.48	16.90	83.10
Cabrejos[16] (single particle)	14	29.11	4.90	74.70	64.79	76.41	0.6072	50.00	14.79	76.41	23.59
Turian et al.[45]	15	34.80	5.31	79.50	66.20	83.80	0.5288	64.08	2.11	83.80	16.20

Table 11. Statistics of the Ranked Model Forms for the Gas Data for the Pick-Up Velocity (After Fine-Tuning Process)

Model Form No.	Rank	$E_{MS,j}$ (m^2/s^2)	$E_{MA,j}$ (m/s)	$E_{MAP,j}$ (%)	$P_{50\%,j}$ (%)	$\max_{\%,j}$ (%)	$R^2_{\mathrm{mod,adj},j}$	k_j	$P_{+50\%,j}$ (%)	$P_{-50\%,j}$ (%)	$\mathrm{over}_{\%,j}$ (%)	$\mathrm{under}_{\%,j}$ (%)
8	1	4.46	1.39	18.64	5.99	50.35	0.9398	9	5.28	0.70	49.65	50.35
13	2	4.61	1.36	18.64	8.10	52.46	0.9378	6	6.69	1.41	52.46	47.54
12	3	4.63	1.46	19.59	8.10	51.41	0.9375	11	7.39	0.70	51.41	48.59
18	4	6.32	1.63	21.95	10.92	50.70	0.9147	4	8.10	2.82	50.70	49.30
7	5	6.70	1.65	21.84	9.86	51.06	0.9096	4	8.10	1.76	51.06	48.94
25	6	5.63	1.56	21.49	10.56	52.46	0.9238	9	8.80	1.76	47.54	52.46
17	7	5.12	1.50	20.99	10.92	52.46	0.9309	11	9.51	1.41	52.46	47.54
11	8	6.51	1.99	28.59	14.79	51.06	0.9122	9	14.44	0.35	51.06	48.94
15	9	7.08	1.79	22.12	5.63	51.41	0.9044	36	3.52	2.11	48.59	51.41
5	10	10.66	2.23	30.49	19.72	61.62	0.8567	3	15.14	4.58	61.62	38.38
6	11	10.50	2.22	30.21	21.48	63.73	0.8584	4	14.79	6.69	63.73	36.27
4	12	10.50	2.22	30.21	21.48	63.73	0.8584	4	14.79	6.69	63.73	36.27
27	13	10.53	2.22	30.15	21.13	64.08	0.8574	6	14.44	6.69	64.08	35.92
2	14	11.01	2.32	30.88	23.94	65.49	0.8520	2	14.79	9.15	65.49	34.51
1	15	11.30	2.37	31.35	22.89	65.14	0.8475	2	14.44	8.45	65.14	34.86
23	16	11.58	2.34	30.63	22.54	60.21	0.8432	7	14.08	8.45	60.21	39.79
3	17	11.01	2.32	30.88	23.94	65.49	0.8515	3	14.79	9.15	65.49	34.51
26	18	11.02	2.31	30.73	23.94	64.08	0.8508	5	14.79	9.15	64.08	35.92
9	19	11.01	2.32	30.88	23.94	65.49	0.8515	4	14.79	9.15	65.49	34.51
22	20	11.01	2.32	30.88	23.94	65.49	0.8509	4	14.79	9.15	65.49	34.51
20	21	11.01	2.32	30.88	23.94	65.49	0.8509	5	14.79	9.15	65.49	34.51
19	22	11.01	2.32	30.88	23.94	65.49	0.8509	5	14.79	9.15	65.49	34.51
24	23	11.01	2.32	30.88	23.94	65.49	0.8509	5	14.79	9.15	65.49	34.51
31	24	11.83	2.50	32.75	23.59	61.97	0.8409	3	14.44	9.15	61.97	38.03
32	25	11.01	2.32	30.88	23.94	65.49	0.8515	6	14.79	9.15	65.49	34.51
30	26	11.01	2.31	30.76	23.94	64.79	0.8504	7	14.79	9.15	64.79	35.21
21	27	11.01	2.32	30.88	23.94	65.49	0.8509	7	14.79	9.15	65.49	34.51
28	28	11.01	2.32	30.88	23.94	65.49	0.8509	8	14.79	9.15	65.49	34.51
29	29	11.01	2.32	30.88	23.94	65.49	0.8509	11	14.79	9.15	65.49	34.51
35	30	11.30	2.37	31.35	22.89	65.14	0.8475	16	14.44	8.45	65.14	34.86
14	31	11.99	2.74	34.38	23.24	61.27	0.8382	12	11.97	11.27	38.73	61.27
33	32	37.75	3.39	35.48	26.06	57.04	0.4907	5	6.69	19.37	42.96	57.04
16	33	28.85	3.97	49.72	47.89	88.03	0.6094	11	2.46	45.42	11.97	88.03
10	34	29.67	4.35	55.65	52.46	91.55	0.5997	5	1.06	51.41	8.45	91.55

for gas/solid flow compared to liquid/solid flow. Thus, for the gas/solid case, the model forms with large numbers of parameters do not run the risk of overfitting the experimental data.

The results of the parameter fine-tuning for the pneumatic conveying of solid particles at the pick-up velocity show that 10 of the model forms reduce to the form where the particle Reynolds number is a function of the Archimedes number only, and two of the model forms reduce to the form where the particle Reynolds number based on the shear velocity is a function of the Archimedes number only (shown in Appendix Tables A1 and A2). Here, the number of model forms reduces from 35 to 25 different forms. For the model forms that consider the adhesive force between the particle and the pipe wall, and the cohesive force between the particles, the coefficients for the adhesive and cohesive forces are nonzero after the parameters are fine-tuned. This implies that in addition to the apparent weight of the particle, and the inertial and viscous forces, the adhesive and cohesive forces play a role in the solids transport mechanism in pneumatic flow from a bed of solids.

Similar to the results for the ranking of the original models, the results of the fine-tuning process suggest that for the pneumatic conveying of solids from a bed, different equations should be used based on the ranges of a dimensionless group, such as the Archimedes number. Similar to the experimental data for liquid/solid flow, the mechanisms assumed to be dominant by the ranked mechanistic or semi-mechanistic models[5,15–17,34,36,37,49] are compared against the mechanisms observed by the experimenters. For the gas case, most of the experimental data for the pick-up of solids from a bed include lift as a solids transport mechanism,[16,27,30,54] which is consistent with the mechanisms assumed by Cabrejos,[16] Rabinovich and Kalman,[36] Rampall and Leighton,[37] Oroskar and Turian,[17] Ramadan et al.,[15] and Ponagandla[34] in developing their models. Thus, for both the experimental data for liquid/solid flow and gas/solid flow at the pick-up velocity, the mechanisms assumed to be dominant in the development of the higher-ranked mechanistic and semi-mechanistic models are consistent with those observed by the experimenters.

Similar to the liquid/solid case, the parameters of some of the fine-tuned model forms suggest that for the gas/solid case, the hydraulic diameter has little effect on the solids transport velocity. It was found that the correlation between v and $\frac{D}{d_p}$ is about 0.05 for the gas/solid flow data at the pick-up velocity. This observation implies the possibility of a limited number of experimental data with a wide range of diameter values in the literature for gas/solid flow from a bed of solids. As shown in Table 6, for the gas/solid flow data in our experimental database for which the pick-up velocity was measured, the pipe diameters range from 0.02 to 0.10 m. Hence, to accurately quantify the impact of the hydraulic diameter on the velocity for pneumatic conveying of solid particles from a bed, experiments comparing a range of pipe diameters are necessary.

Pneumatic conveying of particles at the incipient motion velocity

Tables 12 and 13 (and Supporting Information Tables S9 and S10), and Supporting Information Figures S6 and S7

Table 12. Statistics of the Ranked Original Models for the Gas Data for the Incipient Motion Velocity

Model	Rank	$E_{MS,j}$ (m^2/s^2)	$E_{MA,j}$ (m/s)	$E_{MAP,j}$ (%)	$P_{50\%,j}$ (%)	$\max_{\%,j}$ (%)	$R^2_{\text{mod,adj},j}$	$P_{+50\%,j}$ (%)	$P_{-50\%,j}$ (%)	$\text{over}_{\%,j}$ (%)	$\text{under}_{\%,j}$ (%)
Hayden et al.[1]	1	4.73	1.62	38.48	25.55	62.04	0.8030	19.71	5.84	37.96	62.04
Ling[51]	2	5.18	1.73	36.39	30.66	62.04	0.7841	5.11	25.55	37.96	62.04
Rampall and Leighton[37]	3	7.38	2.13	49.68	40.88	52.55	0.6924	24.82	16.06	52.55	47.45
Ponagandla[34]	4	10.90	2.42	51.57	40.15	62.77	0.5423	18.98	21.17	37.23	62.77
Stevenson et al.[5]	5	8.47	2.32	66.18	41.61	68.61	0.6471	37.23	4.38	68.61	31.39
Rabinovich and Kalman[19]	6	9.21	2.40	63.31	40.88	69.34	0.6159	37.96	2.92	69.34	30.66
Ibrahim et al.[50]	7	9.75	2.28	46.93	35.77	81.75	0.5966	8.03	27.74	18.25	81.75
Adánez et al.[24]	8	16.53	3.29	84.33	57.66	62.04	0.3159	43.80	13.87	62.04	37.96
Rabinovich and Kalman[36]	9	15.78	3.18	84.24	50.36	80.29	0.3421	49.64	0.73	80.29	19.71
Almutahar[22] (initial approach)	10	23.50	3.94	91.83	71.53	54.01	0.0050	45.99	25.55	54.01	45.99

summarize the results for the horizontal, pneumatic conveying of solid particles at the incipient motion velocity. The information in these tables and figures are organized in the same way as the previous two cases. The model ranking was obtained using the same method as the previous two cases, and the results of the model ranking are consistent with the graphs of the predicted versus experimental velocity (Supporting Information Figures S6 and S7).

For the original models, the highest-ranked model[1] has the largest value of the modified adjusted-R^2 statistic, and the smallest values of $E_{MS,j}$, $E_{MA,j}$, and $P_{50\%,j}$ compared to the remaining ranked models (shown in Table 12). After the third-ranked model, the values of the statistics differ significantly, where the remaining ranked models have larger values of $E_{MS,j}$ and $E_{MA,j}$, and smaller values of the modified adjusted-R^2 statistic compared to the three highest-ranked models.[1,37,51]

Two of the five highest-ranked models[1,5] (shown in Table 12) were developed or validated using experimental data for gas/solid flow. In addition, the Hayden et al.[1] model was developed with the assumption that the particle's motion is initiated by lift, which is consistent with the experimenters' observations for most of the data points for the pneumatic conveying of particles at the incipient motion velocity. In observing the remaining ranked mechanistic or semi-mechanistic models, the inclusion of the Stevenson et al.,[5] Ibrahim et al.,[50] and Rabinovich and Kalman[36] models suggest that similar to the pneumatic conveying of particles from a bed

Table 13. Statistics of the Ranked Model Forms for the Gas Data for the Incipient Motion Velocity (After Fine-Tuning Process)

Model Form No.	Rank	$E_{MS,j}$ (m^2/s^2)	$E_{MA,j}$ (m/s)	$E_{MAP,j}$ (%)	$P_{50\%,j}$ (%)	$\max_{\%,j}$ (%)	$R^2_{\text{mod,adj},j}$	k_j	$P_{+50\%,j}$ (%)	$P_{-50\%,j}$ (%)	$\text{over}_{\%,j}$ (%)	$\text{under}_{\%,j}$ (%)
8	1	2.98	1.36	33.31	18.98	51.09	0.8758	9	16.06	2.92	51.09	48.91
25	2	3.29	1.35	34.27	23.36	50.36	0.8619	9	18.98	4.38	50.36	49.64
7	3	3.50	1.45	35.65	25.55	52.55	0.8539	4	21.17	4.38	47.45	52.55
6	4	3.35	1.43	37.45	24.82	51.82	0.8604	4	21.90	2.92	48.18	51.82
4	5	3.35	1.43	37.45	24.82	51.82	0.8604	4	21.90	2.92	48.18	51.82
31	6	3.53	1.46	35.17	25.55	55.47	0.8540	3	20.44	5.11	44.53	55.47
27	7	3.31	1.43	37.36	23.36	53.28	0.8609	6	21.17	2.19	46.72	53.28
5	8	3.68	1.43	37.83	25.55	50.36	0.8476	3	21.90	3.65	50.36	49.64
28	9	3.33	1.40	35.78	27.01	52.55	0.8601	8	22.63	4.38	47.45	52.55
26	10	3.38	1.49	38.17	23.36	53.28	0.8580	5	21.17	2.19	46.72	53.28
2	11	3.46	1.50	38.22	24.09	54.74	0.8567	2	21.17	2.92	45.26	54.74
32	12	3.35	1.49	38.33	24.09	52.55	0.8603	6	21.90	2.19	47.45	52.55
1	13	3.66	1.49	36.74	26.28	54.74	0.8476	2	21.90	4.38	45.26	54.74
3	14	3.46	1.50	38.22	24.09	54.74	0.8556	3	21.17	2.92	45.26	54.74
22	15	3.47	1.49	38.12	24.09	54.74	0.8544	4	21.17	2.92	45.26	54.74
9	16	3.46	1.50	38.48	24.09	54.74	0.8558	4	21.17	2.92	45.26	54.74
23	17	3.53	1.47	37.79	25.55	52.55	0.8517	7	21.90	3.65	47.45	52.55
29	18	3.55	1.45	35.46	25.55	54.01	0.8509	11	21.17	4.38	45.99	54.01
19	19	3.46	1.50	38.22	24.09	54.74	0.8545	5	21.17	2.92	45.26	54.74
20	20	3.46	1.50	38.22	24.09	54.74	0.8545	5	21.17	2.92	45.26	54.74
24	21	3.46	1.50	38.22	24.09	54.74	0.8545	5	21.17	2.92	45.26	54.74
18	22	3.66	1.49	36.73	26.28	55.47	0.8476	4	21.90	4.38	44.53	55.47
11	23	3.40	1.51	38.55	23.36	52.55	0.8583	9	21.17	2.19	47.45	52.55
21	24	3.46	1.50	38.22	24.09	54.74	0.8545	7	21.17	2.92	45.26	54.74
30	25	3.46	1.50	38.22	24.09	54.74	0.8533	7	21.17	2.92	45.26	54.74
13	26	3.48	1.50	38.35	24.82	54.74	0.8548	6	21.90	2.92	45.26	54.74
12	27	3.36	1.48	37.77	24.82	55.47	0.8598	11	21.90	2.92	44.53	55.47
35	28	3.52	1.46	36.04	26.28	53.28	0.8533	16	21.90	4.38	46.72	53.28
17	29	3.48	1.50	38.27	24.82	54.74	0.8550	11	21.90	2.92	45.26	54.74
14	30	3.48	1.50	38.38	25.55	54.74	0.8549	12	22.63	2.92	45.26	54.74
15	31	3.48	1.50	38.24	24.09	55.47	0.8550	36	21.17	2.92	44.53	55.47
16	32	5.15	1.85	42.15	40.15	66.42	0.7835	11	18.25	21.90	33.58	66.42
10	33	7.05	2.21	48.99	49.64	67.15	0.7060	5	13.87	35.77	32.85	67.15
34	34	9.75	2.28	46.93	35.77	81.75	0.5966	33	8.03	27.74	18.25	81.75

of solids, the effects of the particle's shape need to be taken into account for the transport of a particle from the bottom of the conduit. This observation is consistent with the experimental data, where nearly 50% of the experimental data for the incipient motion of solids in gases involve non-spherical particles. With the Hayden et al.,[1] Ibrahim et al.,[50] and Rabinovich and Kalman[36] models included among the ranked models, the adhesion between the particle and the conduit wall may play a role in the incipient motion of a particle in addition to the drag force, the lift force, and the apparent weight of the particle. Similar to the five highest-ranked original models for the previous two cases, the five highest-ranked original models for gas flow at the incipient motion velocity incorporate the hydraulic diameter through $\left(\frac{D}{d_p}\right)$,[1,5,34] or the conversion from the shear velocity to the average fluid velocity.[37,51]

Based on the information in Table 13, among the ranked fine-tuned model forms, the two highest-ranked model forms have the smallest values of $E_{MS,j}$, $E_{MA,j}$, $E_{MAP,j}$, $P_{50\%,j}$, and $\max_{\%,j}$, and the largest values of the adjusted-R^2 statistic. The values of the above statistics for the third ranked to the 31st-ranked model forms are very similar to each other. This observation suggests that after the parameters are fine-tuned, the model forms produce to very similar estimations. Because the values of the six statistics are very similar for the model forms ranked third to 31st, those model forms with greater number of parameters have lower rankings compared to those with fewer number of parameters.

The results of the parameter fine-tuning for the pneumatic conveying of solid particles at the incipient motion velocity show that six of the model forms reduce to the form where the particle Reynolds number is a function of the Archimedes number only, and two of the model forms reduce to the form where the particle Reynolds number based on the shear velocity is a function of the Archimedes number only (shown in Appendix Tables A1 and A2). Here, the number of models is reduced from 35 to 29 different forms. After the parameters of Model Form 18 is fine-tuned, the coefficient for the cohesive force term becomes zero, which is consistent with the definition of the incipient motion velocity. However, the coefficients for the adhesive force term becomes zero after the model parameters are fine-tuned for three of the model forms that incorporate this term (Model Forms 13, 14, and 15). This observation implies that although the adhesive force plays a role in the solids transport mechanism at the incipient motion, as suggested by the ranking for the original models, the magnitude of the adhesive force is not as large as those of the remaining forces. These forces include the inertial and viscous forces, and the apparent weight of the particle.

For the incipient motion of particles in gaseous flow, the higher-ranked original models and fine-tuned model forms have forms similar to the models developed by Rampall and Leighton,[37] and Stevenson et al.[5] Similar to the results for the ranking of the original models, the results of the fine-tuning process suggest that for the pneumatic conveying of solids from the bottom of conduits, the solids transport mechanisms differ for particles smaller and larger than the viscous sublayer thickness, and are dependent on the shape of the particle. For the ranked original models, all the models are mechanistic or semi-mechanistic, with the exception of the Rabinovich and Kalman,[19] and the Adánez et al.[24] models. Most of the experimental data for single particle motion in pneumatic conveying include lift as a solids transport mechanism,[5,16,19,56] which is consistent with the assumed dominant mechanism in the Hayden et al.,[1] Ling,[51] Rampall and Leighton,[37] Ponagandla,[34] Ibrahim et al.,[50] Rabinovich and Kalman,[36] and Almutahar[22] (initial approach) models. One can also observe that there are experimental data for which the particle's motion is initiated by dragging or rolling.[5,6,19,54] The models that assume the above mechanisms to be dominant are included among the ranked models.[5,34,36,50,51] Thus, the model ranking methodology is capable of selecting the models that make the proper assumption regarding the dominant solids transport mechanism given the experimental data.

Similar to the gas/solid case at the pick-up velocity, the parameters of some of the fine-tuned model forms suggest that the hydraulic diameter has little effect on the solids transport velocity. This inconsistency is explained with the value of -0.10 for the correlation between v and $\frac{D}{d_p}$ for the gas/solid flow data at the incipient motion velocity. Table 6 shows that the range of the pipe diameter for the gas/solid flow data at the incipient motion is narrower compared to the other two experimental data subsets. Thus, the impact of the hydraulic diameter on the incipient motion velocity can be better understood if data from experiments comparing a range of pipe diameters are available.

Conclusions and Future Directions

Forty four different solids transport models are reviewed to determine the methods used to develop the models and the experimental data used in their development or validation. An extensive database that consists of experimental data at low particle concentrations is compiled. The accuracy of the models for this database is tested using statistical analysis. To determine the dominant forces for the low particle concentration case, the parameters of the 35 identified model forms were fine-tuned using the compiled database. The same statistical analysis is applied to compare the performances of the fine-tuned model forms.

For the original models, the selection of the five highest-ranked models suggest that the inertial and viscous forces, the drag and lift forces, and the apparent weight of the particle affect the motion of the particle in the conduit for the hydraulic conveying of solids from a bed of particles. For the pneumatic conveying of particles from a bed of solids, the results suggest that lift is the dominant solids transport mechanism, and that models that use different equations based on the ranges of a dimensionless group (e.g., the Archimedes number) can better explain the solids transport phenomena compared to models that use single equations. Finally, for the pneumatic conveying of a single particle from the bottom of conduits, the initiation of motion by lifting has been observed in many experimental data points, while the initiation of motion by dragging or rolling depends on the particle's shape. It was also found that the solids transport mechanisms differ depending on the particle size relative to the thickness of the viscous sublayer for this case.

The fine-tuning process using the experimental data for low particle concentrations shows that although there are 35 solids transport model forms in our model database, this number reduces to 25–29 different forms for the three above-mentioned cases. Based on the results of the fine-tuning process, for liquid-mediated transport of particles from a bed of solids, and gas-mediated transport of particles

from the bottom of conduits, the inertial and viscous forces, and apparent weight of the particle are dominant. For gas-mediated transport of particles from a bed of solids, the apparent weight of the particle, and the inertial, viscous, cohesive, and adhesive forces play a role in the solids transport mechanism.

The values of the parameters of the model forms upon fine-tuning using the experimental data suggest that several key gaps in the solid transport database exist, particularly for applications in the petroleum industry. Most notable are the lack of experimental data in large pipe diameters and high-density (or high pressure) gases, and the narrow range of viscosities. In addition, there is a lack of experimental data for the initiation of the motion of solids from the bottom of conduits for liquid/solid flow.

In observing the parity plots of the solids transport models (Supporting Information Figures S2–S7), it can be seen that there are numerous experimental data where the same solids transport velocity is predicted when the experimental data are widely spread. This observation could be due to an incomplete model. When such experimental data are checked, one can find spreads in the experimental data for the same conditions, even if the experiments were ran by the same experimenter. Therefore, one can suggest that the experimental uncertainty due to measurement error and/or definition of solids transport velocity is large, or something may be missed in the characterization of the experiment. This uncertainty limits our confidence in the ranking and selection of the models and, ultimately, in the prediction of the solids transport velocity, and a better understanding of the experimental uncertainty is recommended for improving the state-of-the-art in solids transport analysis.

Based on the scores S_j of each model, shown in Supporting Information Tables S6, S8, and S10, it is concluded that after the fine-tuning process, the scores of the model forms can be nearly equal to each other for a subset of the ranked model forms. For instance, from Supporting Information Table S6, the 10th to the 12th-ranked model forms have scores that are nearly equal to each other; from Supporting Information Table S8, the 11th and 12th-ranked model forms have scores of nearly equal values; and from Supporting Information Table S10, the 19th to the 21st-ranked model forms have scores of nearly equal values. This suggests that instead of using a serial ranking, the model ranking can be performed using a cluster analysis, where models with similar scores are given the same ranking. In addition, methods for fine-tuning the parameters that use a combination of the different statistics will be investigated. The uncertainties in the experimental data and the model predictions will also be estimated to determine the confidence of the model velocity predictions, and in the model ranking results. These tasks are left as a future study.

Notation

A_H = Hamaker constant
B = coefficient used in the Ling[51] model
C = particle volumetric concentration
C_D = drag coefficient
$C_{D,L}$ = drag and lift coefficient
$C_{D,\text{mult}}$ = ratio of the drag coefficient at the corresponding range of $N_{Re,h}$ to the drag coefficient at $N_{Re,h} \leq 0.5$
C_f = wall friction coefficient
C_l = term that accounts for the effects of the particle-wall interaction and particle diameter
C_L = lift coefficient
C_{mb} = moving bed concentration
C_W = solids mass fraction
C_1 = constant term used in the Ponagandla[34] model
d_p = particle diameter
D = pipe diameter
D_l = hydraulic diameter of the liquid stratum for a gas/liquid stratified flow in a pipe
D_R = ratio of the drag forces with the presence of other particles to those without
D_{50} = hydraulic diameter of a 50-mm conduit
E_D = total energy per unit length of pipe needed to maintain all of the particles in suspension
$E_{MA,j}$ = mean absolute error of model j
$\overline{E_{MA,j}}$ = normalized $E_{MA,j}$
$E_{MAP,j}$ = mean absolute percent error of model j
$\overline{E_{MAP,j}}$ = normalized $E_{MAP,j}$
$E_{MS,j}$ = mean squared error of model j
$\overline{E_{MS,j}}$ = normalized $E_{MS,j}$
$E_{SS,j}$ = error sum of squares of the velocity predictions made by model j
E_T = turbulent energy per unit length of pipe used in maintaining the particles in suspension
f_C = variable that takes into account particle concentration effects
f_F = Fanning friction factor
f_S = static friction coefficient
f_1 = non-dimensional function that incorporates the effect of particle-particle interaction
f_2 = non-dimensional function that incorporates the effect of particle shape
$f(C, d_p)$ = function used to account for the effect of the particle concentration, the particle-wall interaction, and the particle diameter
F_1 = coefficient used in the Ling[51] model
F_2 = coefficient used in the Ling[51] model
F_3 = coefficient used in the Ling[51] model
F_A = adhesive force
F_D = drag force
F_{ef} = eddy fluctuation force
F_F = frictional force
F_I = inertial force
F_L = lift force
F_N = normal force exerted by a column of particles lying above the particle of interest
F_P = plastic force
F_{sed} = sedimentation force
F_{turb} = turbulent velocity fluctuation force
F_V = viscous force
F_W = apparent weight of the particle in the fluid
g = gravitational acceleration
h = flow depth
H_1 = coefficient used in the Ling[51] model
H_2 = coefficient used in the Ling[51] model
i = index used for the data points
j = index used for the solids transport models
k_j = number of parameters in model j
$\overline{k_j}$ = normalized k_j
$k_{l,j}$ = lth parameter of model j
k_S = equivalent roughness height
k_V = von Karman constant
k_{1-36} = parameter, or constant, in the equation of the solids transport model
l = index used for the parameters in a model
l_e = mean eddy length
l_t = turbulent length scale
l_0 = length scale used in the Reynolds number and the Froude number
L_D = perpendicular distance from the line of action of the drag force to the particle's center of rotation
L_L = perpendicular distance from the line of action of the lift force to the particle's center of rotation
L_W = perpendicular distance from the line of action of the apparent weight to the particle's center of rotation
L_1 = perpendicular distance from the line of action of the apparent weight of the particle to the particle's center of rotation
L_2 = perpendicular distance from the line of action of the normal force to the particle's center of rotation

$max_{\%,j}$ = maximum value of the percent of experimental velocity overestimated or underestimated by model j

$\overline{max_{\%,j}}$ = normalized $max_{\%,j}$

m_j = the slope between the predicted and the experimental velocity for model j

n_C = exponent value that accounts for the effect of the presence of additional particles

n_D = coefficient of wall effect on the drag force

$n_{\text{indep},j}$ = number of independent variables incorporated in model j

N_{Ar} = Archimedes number $\left(N_{Ar}=\frac{gd_p^3\rho_f\left(\rho_S-\rho_f\right)}{\mu^2}\right)$

$N_{Ar,m}$ = modified Archimedes number that takes into account the shape of the particle or the friction between the particle and the pipe wall

N_{data} = the number of liquid or gaseous data points in the database

N_{Fr} = Froude number $\left(N_{Fr}=\frac{v}{\sqrt{gl_0}}\right)$

N_l = dimensionless group used to quantify the lower limit below which the settling of solid particles to the bottom of the pipe will occur

N_{part} = average number of particles lying in a column above the particle of interest

N_{Re} = pipe Reynolds number $\left(N_{\text{Re}}=\frac{Dv\rho_f}{\mu}\right)$

$N_{Re,h}$ = hemispherical Reynolds number $\left(N_{\text{Re,h}}=\frac{\rho_f Q\left(\frac{d_p}{2}\right)^2}{\mu}\right)$

$N_{Re,l}$ = Reynolds number based on the liquid properties $\left(N_{\text{Re},l}=\frac{Dv_{sl}\rho_l}{\mu_l}\right)$

$N_{Re,OT}$ = modified particle Reynolds number used by Oroskar and Turian[17] $\left(N_{\text{Re},OT}=\frac{D\rho_f\left[gd_p\left(\frac{\rho_S}{\rho_f}-1\right)\right]^{0.5}}{\mu}\right)$

$N_{Re,p}$ = particle Reynolds number $\left(N_{\text{Re},p}=\frac{d_p v\rho_f}{\mu}\right)$

$N_{Re,p,\text{lift}}$ = particle Reynolds number required for particle lift

$N_{Re,p,m}$ = modified particle Reynolds number that takes into account the effects of the hydraulic diameter of the conduit

$N_{Re,p,\text{roll}}$ = particle Reynolds number required for particle roll

$N_{Re,p,S}$ = particle Reynolds number based on the settling velocity of the particle $\left(N_{\text{Re},p,S}=\frac{d_p v_S\rho_f}{\mu}\right)$

$N_{Re,p,0}$ = particle Reynolds number required to initiate the motion of a single particle in the absence of additional particles

$N_{Re,p,*}$ = particle Reynolds number based on the shear velocity $\left(N_{\text{Re},p,*}=\frac{d_p v_*\rho_f}{\mu}\right)$

$N_{Re,S}$ = Reynolds number based on the settling velocity of the particle $\left(N_{\text{Re},S}=\frac{Dv_S\rho_f}{\mu}\right)$

$N_{Re,*}$ = Reynolds number based on the shear velocity $\left(N_{\text{Re},*}=\frac{Dv_*\rho_f}{\mu}\right)$

N_{Sh} = dimensionless Shields parameter $\left(N_{Sh}=\frac{\tau_W}{\left(\rho_S-\rho_f\right)gD}\right)$

N_{Shape} = dimensionless group that takes into account the effect of the shape of the particle

N_{Sph} = sphericity of the particle

N_{St} = Stokes number $\left(N_{St}=\frac{\rho_S d_p^2}{18\mu\left(\frac{l_f}{v'}\right)}\right)$

$\text{over}_{\%,j}$ = percent of experimental velocity overestimated by model j

p = constant coefficient for the lift force expression

P = hydraulic gradients due to the particle suspension in the fluid

P_w = hydraulic gradients due to the pure fluid

$P_{50\%,j}$ = percent of velocity predictions that lie outside the $\pm 50\%$ lines in the graph of predicted versus experimental velocity for model j

$\overline{P_{50\%,j}}$ = normalized $P_{50\%,j}$

$P_{+50\%,j}$ = percent of velocity predictions of model j with values greater than $1.5v_{\text{exp},i}$, for $i = 1, 2, \ldots, N_{\text{data}}$

$P_{-50\%,j}$ = percent of velocity predictions of model j with values less than $0.5v_{\text{exp},i}$, for $i = 1, 2, \ldots, N_{\text{data}}$

q = constant coefficient for the lift force expression

Q = shear rate within the viscous sublayer

$R^2_{\text{mod,adj,dev},j}$ = deviation of the modified adjusted-R^2 statistic of model j from unity

$\overline{R^2_{\text{mod,adj,dev},j}}$ = normalized $R^2_{\text{mod,adj,dev},j}$

$R^2_{\text{mod,adj},j}$ = modified adjusted-R^2 statistic of model j

s = separation distance between the particle and the pipe wall

S_j = score of model j that is used to rank model j based on the accuracy of its velocity predictions

T_{SS} = total sum of squares of the experimental velocity in the database

$\text{under}_{\%,j}$ = percent of experimental velocity underestimated by model j

v = solids transport velocity

$v_{\text{calc},i,j}$ = velocity prediction of model j for datum point i

v_{drag} = fluid velocity required for particle drag

$v_{\text{exp},i}$ = experimental velocity for datum point i

v_{lift} = fluid velocity required for particle lift

v_p = particle velocity

v_{roll} = fluid velocity required for particle roll

v_S = settling velocity of a particle at its terminal velocity in an unbounded fluid

v_{sg} = superficial gas velocity

v_{sl} = superficial liquid velocity

v_0 = single-particle transport velocity

$v_{0,*}$ = friction velocity for the limiting case of infinite dilution

v_{50} = solids transport velocity sufficient to transport particles in a 50-mm conduit

v_* = shear, or friction, velocity

v' = turbulent fluctuation velocity

v'_x = turbulent velocity fluctuation component in the direction perpendicular to v'_z and v'_y

v'_y = turbulent velocity fluctuation component in the vertical direction

v'_z = turbulent velocity fluctuation component in the direction of the flow

w_1 = weight placed in $\overline{E_{MS,j}}$ to obtain the score of a model

w_2 = weight placed in $\overline{E_{MA,j}}$ to obtain the score of a model

w_3 = weight placed in $\overline{E_{MAP,j}}$ to obtain the score of a model

w_4 = weight placed in $\overline{P_{50\%,j}}$ to obtain the score of a model

w_5 = weight placed in $\overline{max_{\%,j}}$ to obtain the score of a model

w_6 = weight placed in $\overline{R^2_{\text{mod,adj,dev},j}}$ to obtain the score of a model

w_7 = weight placed in $\overline{k_j}$ to obtain the score of a model

x = fraction of eddies with velocities exceeding $v_S\,(1-C)^2$

y = vertical distance from the bed level

y_b = height from the bed level where the area-averaged mean fluid velocity is equal to the temporal mean velocity at height y

y_{mb} = height of the moving bed layer

z_0 = zero velocity level

α = surface tilting angle

α_D = constant term used in the Davies[18] model

γ = particle cohesion

δ = thickness of the laminar sublayer

θ = pipe inclination angle from the horizontal

θ_V = pipe inclination angle from the vertical

κ = magnitude of the velocity gradient

λ = ratio of $v_S\,(1-C)^2$ to v

μ = fluid viscosity

μ_l = liquid viscosity

ρ_f = fluid density

ρ_l = liquid density

ρ_m = slurry density

ρ_S = particle density

τ_W = shear stress of the fluid flow

τ_y = yield stress for Bingham plastics

φ = angle of repose

Ω = turbulent dissipation term

Subscripts

calc = calculated

exp = experimental

Acknowledgments

The authors would like to thank Dr. Jose Gamboa of the McDougall School of Petroleum Engineering at The

University of Tulsa (TU) for his work on compiling the initial list of the solids transport models, and for providing them with the references for the models when needed; Dr. Peyton Cook of the Department of Mathematics at TU for assisting them with the statistical analysis; and Dr. Brenton McLaury of the Department of Mechanical Engineering at TU for helping them better understand the calculations for one of the solids transport model. The authors would also like to thank Dr. Alexander Zazovsky of Chevron Energy Technology Company (Chevron ETC) for his constructive questions and comments regarding some of the solids transport models to ensure that the correct equations were reported for the models; David Lee of TU for his preliminary work on reviewing the solids transport models; and Spencer Copeland of TU for compiling the initial list of the development ranges of the solids transport models. Finally, the authors would like to acknowledge the Tulsa University Center of Research Excellence (TUCoRE) program, a partnership between Chevron ETC and TU to conduct oil and gas industrial research, for providing the financial support for their research.

Literature Cited

1. Hayden KS, Park K, Curtis JS. Effect of particle characteristics on particle pickup velocity. *Powder Technol*. 2003;131:7–14.
2. Miller MC, McCave IN, Komar PD. Threshold of sediment motion under unidirectional currents. *Sedimentology*. 1977;24:507–527.
3. Durand R. Basic relationships of the transportation of solids in pipes—experimental research. *Proceedings of Minnesota International Hydraulics Convention. Minneapolis*, MN: University of Minnesota, September 1–4, 1953:89–103.
4. Danielson TJ. Sand transport modeling in multiphase pipelines. *2007 Offshore Technology Conference*. Houston, TX: Offshore Technology Conference, 2007:1–11.
5. Stevenson P, Thorpe RB, Davidson JF. Incipient motion of a small particle in the viscous boundary layer at a pipe wall. *Chem Eng Sci*. 2002;57:4505–4520.
6. Halow JS. Incipient rolling, sliding and suspension of particles in horizontal and inclined turbulent flow. *Chem Eng Sci*. 1973;28: 1–12.
7. Kramp M, Thon A, Hartge E-U, Heinrich S, Werther J. The role of attrition and solids recovery in a chemical looping combustion process. *Oil Gas Sci Technol Rev IFP Energies Nouvelles*. 2011;66(2): 277–290.
8. Roberts GW. *Chemical Reactions and Chemical Reactors*. Hoboken: Wiley, 2009.
9. Newitt DM, Richardson JF, Abbott M, Turtle RB. Hydraulic conveying of solids in horizontal pipes. *Trans Inst Chem Eng*. 1955; 33:93–110.
10. Buthod P, Thompson RE, Wilson AJ. *Process Component Design*. Tulsa: The University of Tulsa, 1993.
11. Mellmann J, Teodorov T. Solids transport in mixed-flow dryers. *Powder Technol*. 2011;205:117–125.
12. Zhu C, You J. An energy-based model of gas-solid transport in a riser. *Powder Technol*. 2007;175:33–42.
13. Manning FS, Thompson RE. *Oilfield Processing of Petroleum*, Vol. 1. Tulsa: PennWell Corporation, 1991.
14. Salama MM. Sand production management. *J Energy Resour Technol*. 2000;122:29–33.
15. Ramadan A, Skalle P, Johansen ST. A mechanistic model to determine the critical flow velocity required to initiate the movement of spherical bed particles in inclined channels. *Chem Eng Sci*. 2003; 58:2153–2163.
16. Cabrejos FJ. *Incipient Motion of Solid Particles in Pneumatic Conveying*, MS Thesis. Pittsburgh, PA: University of Pittsburgh, 1991.
17. Oroskar AR, Turian RM. The critical velocity in pipeline flow of slurries. *AIChE J*. 1980;26(4):550–558.
18. Davies JT. Calculation of critical velocities to maintain solids in suspension in horizontal pipes. *Chem Eng Sci*. 1987;42(7):1667–1670.
19. Rabinovich E, Kalman H. Incipient motion of individual particles in horizontal particle-fluid systems: A. Experimental analysis. *Powder Technol*. 2009;192:318–325.
20. Zenz FA. Conveyability of materials of mixed particle size. *Ind Eng Chem Fundam*. 1964;3(1):65–75.
21. Gruesbeck C, Salathiel WM, Echols EE. Design of gravel packs in deviated wellbores. *J Pet Technol*. 1979;31:109–115.
22. Almutahar FM. *Modeling of Critical Deposition Velocities of Sand in Horizontal and Inclined Pipes*, MS Thesis. Tulsa, OK: The University of Tulsa, 2006.
23. Yang CT. Noncohesive sediment transport. *Erosion and Sedimentation Manual*. In: Reclamation Bo, editor. Denver, CO: Sedimentation and River Hydraulics Group, 2006:1–111.
24. Adánez J, de Diego LF, Gayán P. Transport velocities of coal and sand particles. *Powder Technol*. 1993;77:61–68.
25. Babcock HA. Heterogeneous flow of heterogeneous solids. In: Zandi I, editor. *Advances in Solid-Liquid Flow in Pipes and its Application*. Oxford: Pergamon Press Inc., 1971:125–148.
26. Bain AG, Bonnington ST. *The Hydraulic Transport of Solids by Pipeline*. Oxford: Pergamon Press Ltd., 1970.
27. Cabrejos FJ, Klinzing GE. Pickup and saltation mechanisms of solid particles in horizontal pneumatic transport. *Powder Technol*. 1994;79:173–186.
28. Doron P, Simkhis M, Barnea D. Flow of solid-liquid mixtures in inclined pipes. *Int J Multiphase Flow*. 1997;23(2):313–323.
29. Fletcher B. The incipient motion of granular materials. *J Phys D Appl Phys*. 1976;9:2471–2478.
30. Kalman H, Satran A, Meir D, Rabinovich E. Pickup (critical) velocity of particles. *Powder Technol*. 2005;160:103–113.
31. Kökpınar MA, Göğüş M. Critical flow velocity in slurry transporting horizontal pipelines. *J Hydraul Eng*. 2001;127(9):763–771.
32. Lee GS, Kim SD. Bed expansion characteristics and transition velocity in turbulent fluidized beds. *Powder Technol*. 1990;62:207–215.
33. Mantz PA. Incipient transport of fine grains and flakes by fluids—extended Shields diagram. *J Hydraul Div*. 1977;103(HY6):601–615.
34. Ponagandla V. *Critical Deposition Velocity Method for Dispersed Sand Transport in Horizontal Flow*, MS Thesis. Tulsa, OK: The University of Tulsa, 2008.
35. Rabinovich E, Kalman H. Pickup, critical and wind threshold velocities of particles. *Powder Technol*. 2007;176:9–17.
36. Rabinovich E, Kalman H. Incipient motion of individual particles in horizontal particle-fluid systems: B. *Theoretical analysis*. *Powder Technol*. 2009;192:326–338.
37. Rampall I, Leighton DT Jr. Influence of shear-induced migration on turbulent resuspension. *Int J Multiphase Flow*. 1994;20(3): 631–650.
38. Rose HE, Duckworth RA. Transport of solid particles in liquids and gases. *The Engineer*. 1969;227:478–483.
39. Shook CA. Pipelining solids: the design of short-distance pipelines. *The Symposium on Pipeline Transport of Solids*. Toronto, Canada, 1969.
40. Spells KE. Correlations for use in transport of aqueous suspensions of fine solids through pipes. *Trans Inst Chem Eng*. 1955;33:79–84.
41. Stevenson P, Thorpe RB. Velocity of isolated particles along a pipe in stratified gas-liquid flow. *AIChE J*. 2002;48(5):963–969.
42. Stevenson P, Thorpe RB, Kennedy JE, McDermott C. The transport of particles at low loading in near-horizontal pipes by intermittent flow. *Chem Eng Sci*. 2001;56:2149–2159.
43. Stevenson P, Thorpe RB, Kennedy JE, McDermott C. *The similarity of sand transport by slug flow and hydraulic conveying*. 10th International Conference, Multiphase '01. Cannes, France, June 13–15, 2001.
44. Thomas DG. Transport characteristics of suspensions: II. Minimum transport velocity for flocculated suspensions in horizontal pipes. *AIChE J*. 1961;7(3):423–430.
45. Turian RM, Hsu F-L, Ma T-W. Estimation of the critical velocity in pipeline flow of slurries. *Powder Technol*. 1987;51:35–47.
46. Zandi I, Govatos G. Heterogeneous flow of solids in pipelines. *J Hydraul Div*. 1967;93(HY3):145–159.
47. Han Q, Hunt JD. Particle pushing: critical flow rate required to put particles into motion. *J Cryst Growth*. 1995;152(3):221–227.
48. Wu F-C, Chou Y-J. Rolling and lifting probabilities for sediment entrainment. *J Hydraul Eng*. 2003;129(2):110–119.
49. Dey S. Sediment threshold. *Appl Math Modell*. 1999;23(5):399–417.
50. Ibrahim AH, Dunn PF, Brach RM. Microparticle detachment from surfaces exposed to turbulent air flow: controlled experiments and modeling. *J Aerosol Sci*. 2003;34:765–782.
51. Ling C-H. Criteria for incipient motion of spherical sediment particles. *J Hydraul Eng*. 1995;121(6):472–478.
52. Bohling B. Measurements of threshold values for incipient motion of sediment particles with two different erosion devices. *J Mar Syst*. 2009;75:330–335.

53. Grass AJ. Initial instability of fine bed sand. *J Hydraul Div*. 1970; 96(HY3):619–632.
54. Hubert M, Kalman H. Measurements and comparison of saltation and pickup velocities in wind tunnel. *Granul Matter*. 2004;6:159–165.
55. Lee H-Y, Hsu I-S. Investigation of saltating particle motions. *J Hydraul Eng*. 1994;120(7):831–845.
56. Villareal JA, Klinzing GE. Pickup velocities under higher pressure conditions. *Powder Technol*. 1994;80:179–182.
57. White SJ. Plane bed thresholds of fine grained sediments. *Nature*. 1970;228:152–153.
58. Yalin MS, Karahan E. Inception of sediment transport. *J Hydraul Div*. 1979;105(HY11):1433–1443.
59. te Braake HAB, van Can HJL, Verbruggen HB. Semi-mechanistic modeling of chemical processes with neural networks. *Eng Appl Artif Intell*. 1998;11(4):507–515.
60. Rabinovich E, Kalman H. Threshold velocities of particle-fluid flows in horizontal pipes and ducts: literature review. *Rev Chem Eng*. 2011;27:215–239.
61. Murphy G, Young DF, Burian RJ. *Progress Report on Friction Loss of Slurries in Straight Tubes*, Ames, IA: Ames Laboratory, 1954.
62. Cairns RC. Fluid flow studies of simulated suspensions for a liquid metal fuel suspension reactor. *The Second United Nations International Conference on the Peaceful Uses of Atomic Energy*. Geneva, Switzerland, September 1–13, 1958.
63. Patterson RC. Pulverized-coal transport through pipes. *Am Soc Mech Eng Trans J Eng Power*. 1959;81(1):43–52.
64. Perales JF, Coll T, Llop MF, Puigjaner L, Arnaldos J, Casal J. On the transition from bubbling to fast fluidization regimes. In: Basu P, Horio M, Hasatami M, editors. *Circulating Fluidized Bed Technology III*. Oxford: Pergamon Press Inc., 1991:73–78.
65. Han GY, Lee GS, Kim SD. Hydrodynamic characteristics of a circulating fluidized bed. *Korean J Chem Eng*. 1985;2(2):141–147.
66. Shin BC, Koh YB, Kim SD. Hydrodynamics and coal combustion characteristics of circulating fluidized beds. *Hwahak Konghak*. 1984;22:253–258.
67. Le Palud T, Zenz FA. Supercritical phase behavior of fluid particle systems. In: Grace JR, Shemilt LW, Bergougnou MA, editors. *Fluidization VI*. New York: Engineering Foundation, 1989:121.
68. Horio M, Ishii H, Nishimuro M. On the nature of turbulent and fast fluidized beds. *Powder Technol*. 1992;70(3):229–236.
69. Li J, Tung Y, Kwauk M. Energy transport and regime transition in particle-fluid two-phase flow. In: Basu P, Large JF, editors. *Circulating Fluidized Bed Technology II*. Oxford: Pergamon Press Inc., 1988:75.
70. Li Y, Kwauk M. The dynamics of fast fluidization. In: Grace JR, Matsen JM, editors. *Fluidization*. New York: Springer US, 1980:537–544.
71. Avidan AA, Yerushalmi J. Bed expansion in high velocity fluidization. *Powder Technol*. 1982;32(2):223–232.
72. Kwauk M, Ningde W, Youchu L, Bingyu C, Zhiyuan S. Fast fluidization at ICM. In: Basu P, editor. *Circulating Fluidized Bed Technology*. Toronto, Canada: Pergamon Press Inc., 1986:33–62.
73. Lee JS, Kim SD. The Vertical Pneumatic Transport of Cement Raw Meal, *Hwahak Konghak*. 1982;20:207.
74. Horio M, Nishimura M, Ishii H. On the nature of turbulent and fast fluidized beds. *Society of Chemical Engineers of Japan Symposium*. Tokyo, Japan, 1989.
75. Casey HJ. *Über die geschiebebewegung*, PhD Thesis. Berlin, Germany: Teknikal Hochschule-Scharlottenburg, 1935.
76. Tison LJ. Studies of the critical shear stress for the entrainment of bed materials. *Joint Meeting of International Association for Hydraulic Research and Hydraulics Division*. Minneapolis, MN, 1953.
77. Shields A. Application of Similarity Principles and Turbulence Research to Bed-Load Movement. Pasadena, CA : California Institute of Technology, 1936:167.
78. Kramer H. Sand mixtures and sand movement in fluvial levels. *Trans Am Soc Civil Eng*. 1935;100:798–838.
79. USWES. Flume Tests Made to Develop a Synthetic Sand Which Will Not Form Ripples When Used in Movable Bed Models. Vicksburg, MS: United States Waterways Experiment Station, 1936.
80. Gilbert GK. *Transportation of Debris by Running Water*. Washington, DC: United States Geological Survey, 1914.
81. Vanoni VA. *Measurements of Critical Shear Stress for Entraining Fine Sediments in a Boundary Layer*. Pasadena, CA: California Institute of Technology, 1964.
82. Neill CR. Mean velocity criterion for scour of course uniform bed material. *The 12th Congress of the International Association for Hydraulic Research*. Fort Collins, CO, 1967.
83. Everts CH. Particle overpassing on flat granular boundaries. *Am Soc Civil Eng J Waterways Harb Coast Eng Div*. 1973;99(WW4):425–438.
84. Paintal AS. A stochastic model for bed load transport. *J Hydraul Res*. 1971;9:527–553.
85. Greeley R, Iversen JD, Pollack JB, Udovich N, White B. Wind tunnel studies of Martian aeolian processes. *Philos Trans R Soc A*. 1974;341:331–360.
86. Chepil WS. Equilibrium of soil grains at the threshold of movement by wind. *Soil Sci Soc Am Proc*. 1959;23(6):422–428.
87. Zingg AW. Wind tunnel studies of the movement of sedimentary material. *The Fifth Hydraulics Conference*. Iowa City, IA, 1952.
88. Lyles L, Woodruff NP. Chapter 2: Boundary-layer flow structure: effects on detachment of non-cohesive particles. In: Shen HW, editor. *Sedimentation*. Fort Collins, CO: H.W. Shen, 1972, 1–16.
89. Vanoni VA. Transport of suspended sediment by water. *Trans Am Soc Civil Eng*. 1946;111:67–102.
90. White CM. The equilibrium of grains on the bed of a stream. *The Royal Society*. London, Great Britain, 1940.
91. Nagy I, Karadi G, Kalmar G. A study into the incipient stage of bed-load movement. *Convegno di Idraulica i Construzioni Idrauliche*. Padova, Italy, 1959.
92. Shields A. Application of similarity principles and turbulence research to bed-load movement. *Mitteilunger der Preussischen Versuchanstalt für Wasserbau und Schiffbau*. 1936;26:5–24.
93. Schoklitsch A. *Uber Schleppkraft und Geschiebebewegung*. Leipzig, Germany: Engelmann, 1914.
94. Ho P-Y. Abhangigkeit der geschiebebewegung von der kornform und der temperatur, *Mitteilungen der Preussischen Versuchsanstalt fur Wasserbau, Erdbau und Schiffbau*, Vol. 37, p. 43, Berlin, Germany, 1939.
95. Dahl AM, Ladam Y, Unander TE, Onsrud G. *SINTEF-IFE Sand Transport 2001–2003: SINTEF Internal Report*, Trondheim, Norway: SINTEF, 2003.
96. Stevenson P. *The Transport of Particles in Horizontal Multiphase Flows*, PhD Thesis. Cambridge, Great Britain: University of Cambridge, 2001.
97. Cabrejos FJ, Klinzing GE. Incipient motion of solid particles in horizontal pneumatic conveying. *Powder Technol*. 1992;72:51–61.
98. Gadala-Maria FA. *The Rheology of Concentrated Suspensions*, PhD Thesis. Stanford, CA: Stanford University, 1979.
99. Leighton D, Acrivos A. Viscous resuspension. *Chem Eng Sci*. 1986;41(6):1377–1384.
100. Leighton DT, Acrivos A. Shear-induced migration of particles in concentrated suspensions. *J Fluid Mech*. 1987;181:415–439.
101. Leighton D, Acrivos A. The lift on a small sphere touching a plane in the presence of a simple shear flow. *J Appl Math Phys (ZAMP)*. 1985;36:174–178.
102. Chapman BK, Leighton DT. Dynamic viscous resuspension. *Int J Multiphase Flow*. 1991;17:469–483.
103. Kennedy JE, McDermott C. *Solids Transport in Subsea Flowlines*. Cambridge, Great Britain: Department of Chemical Engineering, University of Cambridge, 2000.
104. Kao DTY, Hwang LY. Critical slope for slurry pipeline transporting coal and other solid particles. *6th International Conference on the Hydraulic Transport of Solids in Pipes*. Canterbury, Great Britain, 1979.
105. Wilson KC, Tse JKP. Deposition limit for coarse particle transport in inclined pipes. *9th International Conference on the Hydraulic Transport of Solids in Pipes*. Rome, Italy, 1984.
106. Roco MC. Experimental investigation of critical velocity in pipelines for hydrotransport. *J Rom Acad*. 1977;36:111–112.
107. Shook CA, Roco MC. *Slurry Flow: Principles and Practice*. Stoneham, MA: Butterworth-Heinemann, 1991.
108. Meyer-Peter E, Müller R. Formulas for bed-load transport. *The 2nd Congress of the International Association for Hydraulic Research*. Stockholm, Sweden, 1948.
109. Iwagaki Y. Fundamental study on critical tractive force. *Trans Jpn Soc Civil Eng*. 1956;41:1–21.
110. Dong Z, Liu X, Wang H, Wang X. Aeolian sand transport: a wind tunnel model. *Sediment Geol*. 2003;161:71–83.
111. Cornelis WM, Gabriels D. The effect of surface moisture on the entrainment of dune sand by wind: an evaluation of selected models. *Sedimentology*. 2003;50:771–790.
112. Cabrejos FJ, Klinzing GE. Minimum conveying velocity in horizontal pneumatic transport and the pickup and saltation mechanisms of solid particles. *Bulk Solids Handling*. 1994;14(3):541–550.
113. Fletcher B. The erosion of dust by an airflow. *J Phys D Appl Phys*. 1976;9:913–924.
114. Chepil WS. Properties of soil which influence wind erosion: IV. State of dry aggregate structure. *Soil Sci*. 1951;72(5):387–401.

115. Chepil WS. Dynamics of wind erosion: I. Nature of movement of soil by wind. *Soil Sci.* 1945;60(4):397–411.
116. Durand R, Condolios E. Communication de R. Durand, E. Condolios. *Deuxièmes Journées de L'Hydraulique*. Grenoble, France, June 25–29, 1952.
117. Silin NA, Kobernik SG. *Operational Mechanics of Large Dredgers and Pipelines*. Kiev, Ukraine: Ukrainian Academy of Sciences, 1962.
118. Silin NA, Karasik VM, Kondakov VN. The influence of clay fraction on the basic parameters of the hydro-transport of fine free-flowing materials. *Fluid Mech Sov Res.* 1973;2(6):1–5.
119. Silin NA, Vitoshkin YK, Karasik VM, Otcheretko VF. *Hydrotransport*. Kiev, Ukraine: Naukova Dumka, 1971.
120. Sinclair CG. The limit deposit-velocity of heterogeneous suspensions. *Symposium on the Interaction between Fluids and Particles, Third Congress of the European Federation of Chemical Engineers*. London, Great Britain, June 1962.
121. Schriek W, Smith LG, Haas DB, Husband WHW. *Experimental Studies on the Transport of Two Different Sands in Water in 2-, 4-, 6-, 8-, 10- and 12-inch Pipelines*. Saskatoon, Canada: Saskatchewan Research Council, July 1973.
122. Schriek W, Smith LG, Haas DB, Husband WHW. *Experimental Studies on the Hydraulic Transport of Limestone*. Saskatoon, Canada: Saskatchewan Research Council, August 1973.
123. Schriek W, Smith LG, Haas D, Husband WHW. *Experimental Studies on the Hydraulic Transport of Iron Ore*. Saskatoon, Canada: Saskatchewan Research Council, July 1973.
124. Schriek W, Smith LG, Haas DB, Husband WHW. *Experimental Studies on the Hydraulic Transport of Coal*. Saskatoon, Canada: Saskatchewan Research Council, October 1973.
125. Goedde E. To the critical velocity of heterogeneous hydraulic transport. *Fifth International Conference on the Hydraulic Transport of Solids in Pipes*. Hannover, Federal Republic of Germany, May 8–11, 1978.
126. Vodolazski VI, Gruchko VP, Telechkin ED. *An Investigation of the Critical Velocity for Hydraulic Transport of Suspensions from Gas-Scrubbing of Blast Furnace Plants in Metallurgical Factories*. Kiev, Ukraine: Vodosnabchenie Kanalizatsia, Gidrotechnicheskie Sooruzenia, 1971.
127. Parzonka W, Kenchington JM, Charles ME. Hydrotransport of solids in horizontal pipes: effects of solids concentration and particle size on the deposit velocity. *Can J Chem Eng.* 1981;59(3):291–296.
128. Wasp EJ, Kenny JP, Gandhi RL. *Solid-Liquid Flow: Slurry Pipeline Transportation*. Trans Tech Publications, Rockport, MA, 1977.
129. Wasp EJ, Aude TC, Kenny JP, Seiter RH, Jacques RB. Deposition velocities, transition velocities, and spatial distribution of solids in slurry pipelines. *First International Conference on the Hydraulic Transport of Solids in Pipes*. Coventry, UK: The University of Warwick, September 1–4, 1970.
130. Thomas AD. Predicting the deposit velocity for horizontal turbulent pipe flow of slurries. *Int J Multiphase Flow.* 1979;5:113–129.
131. Smith LG, Haas DB, Schriek W, Husband WHW. *Experimental Studies on the Hydraulic Transport of Potash*. Saskatoon, Canada: Saskatchewan Research Council, October 1973.
132. Shook CA, Schriek W, Smith LG, Haas DB, Husband WHW. *Experimental Studies of the Transport of Sands in Liquids of Varying Properties in 2- and 4-inch Pipelines*. Saskatoon, Canada: Saskatchewan Research Council, November 1973.
133. Craven JP. *A Study of the Transportation of Sand in Pipes*, PhD Thesis. Iowa City, IA: State University of Iowa, 1951.
134. Smith RA. Experiments on the flow of sand-water slurries in horizontal pipes. *Trans Inst Chem Eng.* 1955;33:85–92.
135. Yotsukura N. Measurement of sediment-laden flow by means of circular orifice. *US Geol Surv.* 1963:172–173.
136. Bielova NT. *Movement of Uniform and Non-Uniform Fluids*. Moscow, Russia: Moskovski Inzhynierno-Stroitelnyi Institut im Kuybycheva, 1968.
137. Hayden JW, Stelson TE. Hydraulic conveyance of solids in pipes. In: Zandi I, editor. *Advances in Solid-Liquid Flow in Pipes and Its Application*. Oxford: Pergamon Press Inc., 1971:149–163.
138. Wicks M. Transport of solids at low concentration in horizontal pipes. In: Zandi I, editor. *Advances in Solid-Liquid Flow in Pipes and its Application*. Oxford: Pergamon Press Inc., 1971:101–124.
139. Stevens GS, Charles ME. The pipeline flow of slurries: transition velocities. *The Second International Conference on the Hydraulic Transport of Solids in Pipes*. Coventry, UK: The University of Warwick, September 20–22, 1972.
140. Pokrovskaya VN. *Ways of Improving the Efficiency of Hydrotransport*. Moscow, Russia: Nedra, 1972.
141. Wilson KC, Watt WE. Influence of particle diameter on the turbulent support of solids in pipeline flow. *Third International Conference on the Hydraulic Transport of Solids in Pipes*. Golden, CO, May 15–17, 1974.
142. Graf WH, Robinson MP, Yucel O. *Critical velocity for solid-liquid mixtures; the Lehigh experiments*. Bethlehem, PA: Lehigh University, July 1970.
143. Yotsukura N. *Some Effects of Bentonite Suspensions on Sand Transport in a Smooth Four-Inch Pipe*, PhD Thesis. Fort Collins, CO: Colorado State University, 1961.
144. Durand R. The hydraulic transportation of coal and other materials in pipes. College of National Coal Board. London, Great Britain: Laboratoire dauphinois d'hydraulique, Neyrpic, November 1952.
145. Howard GW. Transportation of sand and gravel in four-inch pipe. *Proc Am Soc Civil Eng.* 1938;64(7):1377–1391.
146. Yufin AP. The motion of nonhomogeneous fluids through horizontal partly filled steel tubes, *Proc USSR Acad Sci Fluid Mech (Izvestiya Akademii Nauk SSSR, Mekhanika Zhidkosti i Gaza)*. 1949;8:1146.
147. Blatch NS. Discussion of works for the purification of the water supply of Washington, D.C. *Trans Am Soc Civil Eng.* 1906;57:400–409.
148. Worster RC, Denny DF. Hydraulic transport of solid material in pipes. *Proc Inst Mech Eng.* 1955;169(32):563–573.
149. Durand R, Condolios E. Study of the transport of solids in pipes. *Colloquium on Hydraulic Transport*. National Coal Board, London, Great Britain, November 1952:75.
150. Hitchcock JA, Jones C. The Pneumatic Conveying of Spheres Through Straight Pipes, Mining Research Establishment, Isleworth, Great Britain, Report 2053, December 1956.
151. Segler G. *Pneumatic Grain Conveying: With Special Reference to Agricultural Application*. Great Britain: National Institute of Agricultural Engineering, 1951.
152. Rose HE, Barnacle HE. Flow of suspensions of non-cohesive spherical particles in pipes. *Engineer*. 1957;203(5290):898–901, 939–941.
153. Zenz FA. Two-phase fluid-solid flow. *Ind Eng Chem.* 1949;41(12):2801–2806.
154. Thomas DG. Transport characteristics of suspensions: Part VI. Minimum transport velocity for large particle size suspensions in round horizontal pipes. *AIChE J*. 1962;8(3):373–378.
155. Clark RH, Charles DE, Richardson JF, Newitt D. Pneumatic conveying. Part 1. The pressure drop during horizontal conveyance. *Trans Inst Chem Eng.* 1952;30:209–224.
156. Mehta NC, Smith JM, Comings EW. Pressure drop in air-solid flow systems. *Ind Eng Chem.* 1957;49(6):986–992.
157. Wasp EJ, Regan TJ, Withers J, Cook DAC, Clancey JT. Cross-country coal pipeline hydraulics. *Pipe Line News.* 1963;35(7):20–28.
158. Shih CCS. Hydraulic transport of solids in a sloped pipe. *ASCE J Pipeline Div*. 1964;90(PL2):1–14.
159. Wayment WR, Wilhelm GL, Bardill JP. *Factors Influencing the Design of Hydraulic Backfill Systems, Part I*. Washington, DC: US Bureau of Mines, 1962, pp. 20–28.
160. Bardill JD, Corson DR, Wayment WR. *Factors Influencing the Design of Hydraulic Backfill Systems, Part II*. Washington, DC: US Bureau of Mines, 1962.
161. Bonnington ST. *Estimation of Pipe Friction Involved in Pumping Solid Material*. London, Great Britain: British Hydromechanics Research Association, December 1961.
162. Homayounfar F. *Flow of Multicomponent Slurries*, MS Thesis. Newark, DE: University of Delaware, 1965.
163. Durand R, Condolios E. The hydraulic transport of coal and solid materials in pipes. *International Association for Hydro-Environment Engineering and Research*. Minneapolis, MN, 1953.
164. Abbott M. *The Hydraulics Conveying of Solids in Pipelines*, PhD Thesis. London, Great Britain: University of London, 1955.
165. The Colorado School of Mines Research Foundation, Inc. The Transportation of Solids in Steel Pipelines. Golden, CO: Colorado School of Mines Research Foundation Inc., 1963.
166. Ellis HS, Round GF. Laboratory Studies on the Flow of Nickel-Water Suspensions, *Annual General Meeting, Canadian Institute of Mining and Metallurgy*, 1963.
167. Sinclair CG. The pipe flow properties of suspensions of high density solids, PhD Thesis. Sydney University, Sydney, Australia, 1959.
168. Shook CA, Daniel SM, Fertuck LJ. Transportation of potash by pipeline. *First Annual Meeting Canadian Transportation Research*

Forum. Transportation Research Forum, Quebec City, Canada, September 9–10, 1965:459.
169. Condolios E, Chapus EE. Solids pipelines: transporting solid materials in pipelines. *Chem Eng.* 1963;70(13):93–98.
170. Condolios E, Chapus EE. Operating solids pipelines. *Chem Eng.* 1963;70(15):145–150.
171. Condolios E, Chapus EE. Designing solids-handling pipelines. *Chem Eng.* 1963;70(14):131–138.
172. Schmidt JJ, Limebeer GJN. Preliminary experiences in operating 120-ton-per-hour hydraulic coal transport system. *S Afr Mech Eng.* 1965;14(7):135–152.
173. Avci I. *Experimentally Determination of Critical Flow Velocity in Sediment Carrying Pipeline Systems*. Istanbul, Turkey: Istanbul Technical University, 1981.
174. Wicks M. Transportation of solids at low concentrations in horizontal pipes. *ASCE International Symposium on Solid-Liquid Flow in Pipes.* New York, NY 1968.
175. Turian RM, Yuan T-F. Flow of slurries in pipelines. *AIChE J.* 1977;23(3):232–243.
176. Smith LG, Schriek W, Husband WHW, Shook CA. Pilot-plant facilities for hydraulic transport of solids. *Can Min Metall Bull.* 1973;66:1–3.
177. Schriek W, Smith LG, Haas DB, Husband WHW. The potential of helically ribbed pipes for solids transport. *Can Min Metall Bull.* 1974;67:1–8.
178. Husband WHW, Smith LG, Haas DB, Schriek W, Shook CA. Experimental study of iron ore concentrate slurries in pipelines. *Can Inst Min Metall Pet Bull.* 1976;69:106–108.
179. Guy HP, Simons DB, Richardson EV. *Summary of Alluvial Channel Data from Flume Experiments, 1956-61*. Washington, DC: US Department of the Interior, 1966:I1–I96.
180. Luque RF. *Erosion and Transport of Bed Load Sediment*, PhD Thesis. Delft, The Netherlands: Delft University of Technology, 1974.
181. Jain SC. Note on lag in bedload discharge. *J Hydraul Eng.* 1992; 118(6):904–917.
182. Papanicolaou AN. Discussion of "pickup probability for sediment entrainment." *J Hydraul Eng.* 1999;125(7):788–789.
183. Drake TG, Shreve RL, Dietrich WE, Whiting PJ. Bedload transport of fine gravel observed by motion-picture photography. *J Fluid Mech.* 1988;192:193–217.
184. Karahan E. *Initiation of Motion for Uniform and Nonuniform Materials*, PhD. Thesis. Istanbul, Turkey: Istanbul Technical University, 1975.
185. Cimbala JM, Çengel YA. *Essentials of Fluid Mechanics: Fundamentals and Applications.* New York: The McGraw-Hill Companies Inc., 2008.
186. Bird RB, Stewart WE, Lightfoot EN. *Transport Phenomena*, 2nd ed. New York: Wiley, 2007.
187. Halliday D, Resnick R, Walker J. *Fundamentals of Physics*, 7th ed. Hoboken: Wiley, 2005.
188. Shoham O. *Mechanistic Modeling of Gas-Liquid Two-Phase Flow in Pipes*. Richardson: Society of Petroleum Engineers, 2006.
189. Saffman PG. The lift on a small sphere in a slow shear flow. *J Fluid Mech.* 1965;22(2):385–400.
190. Total Temperature Instrumentation, Inc. Seametrics WMP Series Plastic-Bodied Magmeter. South Burlington, VT, 2013. Available at http://www.instrumart.com/products/36674/seametrics-wmp-series-plastic-bodied-magmeter. Accessed on January 28, 2013.
191. Nortek AS. Vector 3D Acoustic Velocimeter. Rud, Norway: Nortek AS, 2010, 1–4.
192. Meile T, De Cesare G, Blanckaert K, Schleiss AJ. Improvement of acoustic doppler velocimetry in steady and unsteady turbulent open-channel flows by means of seeding with hydrogen bubbles. *Flow Meas Instrum.* 2008;19:215–221.
193. Brooks Instrument. Low-Flow, Glass Variable Area Meters. Hatfield, PA, 2013. Available at http://www.brooksinstrument.com/flowmeter-flowcontroller-products/variable-area-flow-meters/low-flow-glass-tube-flow-meters.html. Accessed on January 28, 2013.
194. Brooks Instrument. High-Flow, Glass Tube Variable Area Meter. Hatfield, PA, 2013. Available at http://www.brooksinstrument.com/flowmeter-flowcontroller-products/variable-area-flow-meters/high-flow-glass-tube-flow-meters.html. Accessed on 28 January, 2013.
195. BSI Controls (Buck Sales, Inc.). Fischer & Porter ABB Series 10A2235A RATOSIGHT™ Rotameter. Succasunna, NJ, 2013. Available at http://www.bucksales.com/abb/abb_rotameters/ratosight.htm. Accessed on 28 January, 2013.
196. Viatran. *Pressure Transmitter Models 245/345 DIGICOMP*. Wheatfield, NY: Viatran, 2012:1–3.
197. Devore JL, Berk KN. *Modern Mathematical Statistics with Applications*. Belmont: Brooks/Cole, Cengage Learning, 2007.
198. Ragsdale CT. *Spreadsheet Modeling and Decision Analysis*, 6th ed. Mason, South-Western: Cengage Learning, 2011.

APPENDIX

Table A1. Dimensional and Dimensionless Forms of the Solids Transport Models (the Equation Presented in the Literatures are Highlighted in Grey)

Model No.	Model	Dimensional Equation	Dimensionless Equation	Dimensionless Form	Model Form No.
1	Thomas[44]	$\frac{v_S}{v_*}=0.0083\left(\frac{d_p v_* \rho_f}{\mu}\right)^{2.61}$	$N_{Re,p,*}=\left(\frac{1}{0.1494}\right)^{1/3.61} N_{Ar}^{1/3.61}$	$N_{Re,p,*}=k_1 N_{Ar}^{k_2}$	1
2	Adánez et al.[24]	N/A	$N_{Re,p}=2.078 N_{Ar}^{0.463}$	$N_{Re,p}=k_1 N_{Ar}^{k_2}$	2
3	Lee and Kim[32]	N/A	$N_{Re,p}=2.916 N_{Ar}^{0.354}$		
4	Newitt et al.[9] (heterogeneous flow)	$v=17 v_S$	$N_{Re,p}=\frac{17}{18} N_{Ar}^{1}$		
5	Miller et al.[2]	$v=1.78\left[g\left(\frac{\rho_S}{\rho_f}-1\right)\right]^{0.469}\times\left(\frac{\mu}{\rho_f}\right)^{0.063} D^{0.141} d_p^{0.263}$ Note: The above equation was obtained by fitting a curve to the Shields threshold curve presented in Miller et al.[2]	$N_{Re,p}=1.78\left(\frac{D}{d_p}\right)^{0.141} N_{Ar}^{0.469}$	$N_{Re,p}=k_1\left(\frac{D}{d_p}\right)^{k_2} N_{Ar}^{k_3}$	3
6	Mantz[33]	$v=2\left[g\left(\frac{\rho_S}{\rho_f}-1\right)\right]^{0.495}\times\left(\frac{\mu}{\rho_f}\right)^{0.006} D^{0.141} d_p^{0.347}$ Note: The above equation was obtained by fitting a curve to the Shields threshold curve presented in Mantz.[33]	$N_{Re,p}=2\left(\frac{D}{d_p}\right)^{0.141} N_{Ar}^{0.495}$		
7	Danielson[4]	$v=0.23\left[gD\left(\frac{\rho_S}{\rho_f}-1\right)\right]^{5/9}\times\left(\frac{\mu}{\rho_f}\right)^{-1/9} d_p^{1/9}$	$N_{Re,p}=0.23\left(\frac{D}{d_p}\right)^{5/9} N_{Ar}^{5/9}$		
8	Stevenson et al.[43]	$v=0.76 g^{0.41}\left(\frac{\rho_S}{\rho_f}-1\right)^{0.41}\times D^{0.5} d_p^{-0.27}\mu_l^{0.18}\rho_l^{-0.18}$	$N_{Re,p}=0.76\left(\frac{D}{d_p}\right)^{0.5} N_{Ar}^{0.41}$		
9	Stevenson and Thorpe[41]	$v=v_{sl}=3.43 d_p^{-0.34}\left(\frac{\mu_l}{\rho_l}\right)^{0.34}\times\left[gD_l\times\left(\frac{\rho_S}{\rho_l}-1\right)\right]^{0.33}$	$N_{Re,p}=3.43\left(\frac{D}{d_p}\right)^{0.33} N_{Ar}^{0.33}$		
10	Newitt et al.[9] (homogeneous flow)	$v=(1800 g D v_S)^{1/3}$	$N_{Re,p}=100^{1/3}\left(\frac{\rho_f}{\rho_S-\rho_f}\right)^{1/3}\left(\frac{D}{d_p}\right)^{1/3}\times N_{Ar}^{2/3}$	$N_{Re,p}=k_1\left(\frac{\rho_f}{\rho_S-\rho_f}\right)^{k_2}\left(\frac{D}{d_p}\right)^{k_3}\times N_{Ar}^{k_4}$	4
11	Stevenson et al.[42]	$v=0.924 g^{0.41}\mu_l^{0.181} d_p^{-0.272} D^{0.5}\rho_l^{-0.181}$	$N_{Re,p}=0.924\left(\frac{D}{d_p}\right)^{0.5}\left(\frac{g d_p^3\rho_f^2}{\mu^2}\right)^{0.41}$	$N_{Re,p}=k_1\left(\frac{D}{d_p}\right)^{k_2}\left(\frac{g d_p^3\rho_f^2}{\mu^2}\right)^{k_3}$	5

DOI 10.1002/aic Published on behalf of the AIChE January 2014 Vol. 60, No. 1 AIChE Journal

Table A1. *Continued*

Model No.	Model	Dimensional Equation	Dimensionless Equation	Dimensionless Form	Model Form No.
12	Cabrejos and Klinzing[27]	$\frac{v}{\sqrt{gd_p}}=0.0428N_{Re,p}^{0.175}\times\left(\frac{\rho_S}{\rho_f}\right)^{0.75}\left(\frac{D}{d_p}\right)^{0.25}$	$N_{Re,p}=(0.0428)^{1/0.825}\times\left(\frac{\rho_S}{\rho_f}\right)^{0.75/0.825}\times\left(\frac{D}{d_p}\right)^{0.25/0.825}\times\left(\frac{gd_p^3\rho_f^2}{\mu^2}\right)^{0.5/0.825}$	$N_{Re,p}=k_1\left(\frac{\rho_S}{\rho_f}\right)^{k_2}\times\left(\frac{D}{d_p}\right)^{k_3}\times\left(\frac{gd_p^3\rho_f^2}{\mu^2}\right)^{k_4}$	6
13	Rampall and Leighton[37]	$N_{Ar}<0.728$: $\frac{v_S}{v_*}=0.05\left(\frac{d_pv_*\rho_f}{\mu}\right)^{4/3}$ $N_{Ar}\geq0.728$: $\frac{v_S}{v_*}=0.061\left(\frac{d_pv_*\rho_f}{\mu}\right)^{3}$	$N_{Ar}<0.728$: $N_{Re,p,*}=\left(\frac{1}{0.9}\right)^{3/7}N_{Ar}^{3/7}$ $N_{Ar}\geq0.728$: $N_{Re,p,*}=\left(\frac{1}{1.098}\right)^{1/4}N_{Ar}^{1/4}$	$N_{Ar}<0.728$: $N_{Re,p,*}=k_1N_{Ar}^{k_2}$ $N_{Ar}\geq0.728$: $N_{Re,p,*}=k_3N_{Ar}^{k_4}$	7
14	Stevenson et al.[5]	$N_{Re,h}\leq0.5$: $v=2.19\left[f_Sg\left(\frac{d_p}{2}\right)\left(\frac{\rho_s}{\rho_f}-1\right)\right]^{0.57}\times D^{0.14}\left(\frac{\mu}{\rho_f}\right)^{-0.14}$ $0.5<N_{Re,h}<500$: $v=3.29\left[f_Sg\left(\frac{\rho_s}{\rho_f}-1\right)\right]^{0.41}\times\left(\frac{d_p}{2}\right)^{0.08}D^{0.14}\left(\frac{\mu}{\rho_f}\right)^{0.18}$ $N_{Re,h}\geq500$: $v=11.67\left[f_Sg\left(\frac{\rho_s}{\rho_f}-1\right)\right]^{0.29}\times\left(\frac{d_p}{2}\right)^{-0.29}D^{0.14}\left(\frac{\mu}{\rho_f}\right)^{0.43}$	$N_{Re,h}\leq0.5$: $N_{Re,p}=\left[2.19\left(\frac{0.55}{2}\right)^{0.57}\right]\times\left(\frac{D}{d_p}\right)^{0.14}N_{Ar}^{0.57}$ $0.5<N_{Re,h}<500$: $N_{Re,p}=\left[3.29\left(\frac{1}{2}\right)^{0.08}0.55^{0.41}\right]\times\left(\frac{D}{d_p}\right)^{0.14}N_{Ar}^{0.41}$ $N_{Re,h}\geq500$: $N_{Re,p}=\left[11.67(2\times0.55)^{0.29}\right]\times\left(\frac{D}{d_p}\right)^{0.14}N_{Ar}^{0.29}$	$N_{Re,h}\leq0.5$: $N_{Re,p}=k_1\left(\frac{D}{d_p}\right)^{k_2}N_{Ar}^{k_3}$ $0.5<N_{Re,h}<500$: $N_{Re,p}=k_4\left(\frac{D}{d_p}\right)^{k_5}N_{Ar}^{k_6}$ $N_{Re,h}\geq500$: $N_{Re,p}=k_7\left(\frac{D}{d_p}\right)^{k_8}N_{Ar}^{k_9}$	8

Table A1. *Continued*

Model No.	Model	Dimensional Equation	Dimensionless Equation	Dimensionless Form	Model Form No.
15	Doron et al.[28]	$v=\left\{1.559 g d_p(\rho_S-\rho_f) \times \frac{\left[\sin\left(\frac{\pi}{6}+\theta\right)+\frac{\cos\theta}{2}C_{mb}\left(\frac{y_{mb}}{d_p}-1\right)\right]}{\rho_f C_D}\right\}^{0.5}$	$N_{Re,p}=\frac{1.559^{0.5}}{C_D^{0.5}}\left[\sin\left(\frac{\pi}{6}+\theta\right)+\frac{\cos\theta}{2}C_{mb} \times\left(\frac{y_{mb}}{d_p}-1\right)\right]^{0.5}N_{Ar}^{0.5}$	$N_{Re,p}=\frac{k_1}{C_D^{k_2}}\left[\sin\left(\frac{\pi}{6}+\theta\right)+\frac{\cos\theta}{2}C_{mb} \times\left(\frac{y_{mb}}{d_p}-1\right)\right]^{k_3}N_{Ar}^{k_4}$	9
16	Rabinovich and Kalman[35]	N/A	$N_{Re,p,m}=5N_{Ar,m}^{3/7}$ $N_{Re,p}=\left[1.4-0.8\times\exp\left(-\frac{D}{1.5\times0.05\,\mathrm{m}}\right)\right]N_{Re,p,m}$ $N_{Ar}=N_{Ar,m}$ $N_{Re,p}=\left[7\left(0.03^{3/7}\right)\exp(1.5)-4\left(0.03^{3/7}\right)\exp(1.5) \times\exp\left(-\frac{D}{1.5\times0.05\,\mathrm{m}}\right)\right]^1 N_{Ar}^{3/7}$	$N_{Re,p}=\left[k_1-k_2\exp\left(-\frac{D}{k_3\,\mathrm{m}}\right)\right]^{k_4}N_{Ar}^{k_5}$	10
17	Rabinovich and Kalman[19]	N/A	$f(D)=1.25-0.5\exp\left(-\frac{D}{1.5\times0.05\,\mathrm{m}}\right)$ $N_{Re,p}=[f(D)]\times N_{Re,p,m}$ $N_{Ar}=N_{Ar,m}$ $N_{Ar}>8000$: $N_{Re,p,m}=2.7N_{Ar,m}^{3/7}$ $N_{Re,p}=2.7[f(D)]^1 N_{Ar}^{3/7}$ $N_{Ar}\le 8000$: $N_{Re,p,m}=8.57N_{Ar,m}^{0.3}$ $N_{Re,p}=8.57[f(D)]^1 N_{Ar}^{0.3}$	$f(D)=k_1-k_2\exp\left(-\frac{D}{k_3\,\mathrm{m}}\right)$ $N_{Ar}>8000$: $N_{Re,p}=k_4[f(D)]^{k_5}N_{Ar}^{k_6}$ $N_{Ar}\le 8000$: $N_{Re,p}=k_7[f(D)]^{k_8}N_{Ar}^{k_9}$	11

DOI 10.1002/aic Published on behalf of the AIChE January 2014 Vol. 60, No. 1 AIChE Journal

Table A1. *Continued*

Model No.	Model	Dimensional Equation	Dimensionless Equation	Dimensionless Form	Model Form No.
18	Kalman et al.[30]	N/A	$f(D)=1.4-0.8\exp\left(-\frac{D}{1.5\times0.05\,\mathrm{m}}\right)$ $N_{Re,p}=[f(D)]\times N_{Re,p,m}$ $N_{Ar}>16.5$: $N_{Re,p,m}=5N_{Ar}^{3/7}$ $N_{Re,p}=5[f(D)]^1N_{Ar}^{3/7}$ $0.45\le N_{Ar}\le 16.5$: $N_{Re,p,m}=16.7$ $N_{Re,p}=16.7[f(D)]^1$ $N_{Ar}<0.45$: $N_{Re,p,m}=21.8N_{Ar}^{1/3}$ $N_{Re,p}=21.8[f(D)]^1N_{Ar}^{1/3}$	$f(D)=k_1-k_2\exp\left(-\frac{D}{k_3\,\mathrm{m}}\right)$ $N_{Ar}>16.5$: $N_{Re,p}=k_4[f(D)]^{k_5}N_{Ar}^{k_6}$ $0.45\le N_{Ar}\le 16.5$: $N_{Re,p}=k_7[f(D)]^{k_8}$ $N_{Ar}<0.45$: $N_{Re,p}=k_9[f(D)]^{k_{10}}N_{Ar}^{k_{11}}$	12
19	Hayden et al.[1]	$v=\frac{2.62\left(\frac{\mu}{\rho_f}\right)^{13/21}D^{3/21}}{\mu^{8/21}}\times\left[\frac{\pi}{6}g(\rho_S-\rho_f)+\frac{1.302\times10^{-6}\,\mathrm{N/m}}{d_p^2}\right]^{8/21}$	$N_{Re,p}=\left(\frac{D}{d_p}\right)^{3/21}\times\left\{\frac{2.62^{21/8}\pi}{6}N_{Ar}^1+\left[2.62^{21/8}\times\frac{(1.302\times10^{-6}\,\mathrm{N/m})\rho_f d_p}{\mu^2}\right]^1\right\}^{8/21}$	$N_{Re,p}=\left(\frac{D}{d_p}\right)^{k_1}\left\{k_2N_{Ar}^{k_3}+\left[\left(k_4\,\frac{\mathrm{N}}{\mathrm{m}}\right)\frac{\rho_f d_p}{\mu^2}\right]^{k_5}\right\}^{k_6}$	13
20	Cabrejos[16](single particle)	Particles smaller than the viscous sublayer: $v=6.87\left(\frac{\mu}{\rho_f}\right)^{5/21}D^{3/21}\times\left[\frac{\pi}{6}g\left(\frac{\rho_s-\rho_f}{\rho_f}\right)+\frac{(1.302\times10^{-6}\,\mathrm{N/m})}{d_p^2\rho_f}\right]^{8/21}$ Particles larger than the viscous sublayer: $v=\left[1-\left(\frac{d_p}{D}\right)^{1.5}\right]\times\left[\frac{4}{3}\frac{f_s g d_p}{C_D}\left(\frac{\rho_s-\rho_f}{\rho_f}\right)\right]^{0.5}$	Particles smaller than the viscous sublayer: $N_{Re,p}=\left(\frac{D}{d_p}\right)^{3/21}\left\{\frac{6.87^{21/8}\pi}{6}N_{Ar}^1+\left[6.87^{21/8}\times\frac{(1.302\times10^{-6}\,\mathrm{N/m})\rho_f d_p}{\mu^2}\right]^1\right\}^{8/21}$ Particles larger than the viscous sublayer: $N_{Re,p}=\left(\frac{4}{3}\right)^{0.5}\frac{1}{C_D^{0.5}}f_S^{0.5}\times\left[1-\left(\frac{d_p}{D}\right)^{1.5}\right]^1N_{Ar}^{0.5}$	Particles smaller than the viscous sublayer: $N_{Re,p}=\left(\frac{D}{d_p}\right)^{k_1}\left\{k_2N_{Ar}^{k_3}+\left[\left(k_4\,\frac{\mathrm{N}}{\mathrm{m}}\right)\frac{\rho_f d_p}{\mu^2}\right]^{k_5}\right\}^{k_6}$ Particles larger than the viscous sublayer: $N_{Re,p}=k_7\frac{1}{C_D^{k_8}}f_S^{k_9}\times\left[1-\left(\frac{d_p}{D}\right)^{k_{10}}\right]^{k_{11}}N_{Ar}^{k_{12}}$	14

Table A1. *Continued*

Model No.	Model	Dimensional Equation	Dimensionless Equation	Dimensionless Form	Model Form No.
21	Rabinovich and Kalman[36]	N/A	$N_{Re,p,^*} \geq 5$: $n_D 0.011 N_{Re,p,m}^{2.34} + f_S 0.1 \left(\frac{d_p}{D}\right)^{0.29} \times N_{Re,p,m}^{2.02} = 0.524 f_S N_{Ar}$ According to Rabinovich and Kalman,[36] the second term on the left-hand side of the above equation is negligible for "real values of pipe and particle diameters". $n_D = 1.7009$ $N_{Re,p} = \left[1.25 - 0.5\exp\left(-\frac{D}{1.5\times 0.05\,\mathrm{m}}\right)\right] \times N_{Re,p,m}$ $N_{Re,p} = \left[1.25\left(\frac{64}{3\times 1.7009\times C_D}\right)^{1/2.34} - 0.5\left(\frac{64}{3\times 1.7009\times C_D}\right)^{1/2.34} \times \exp\left(-\frac{D}{1.5\times 0.05\,\mathrm{m}}\right)\right]^1 \times f_S^{1/2.34} N_{Ar}^{1/2.34}$ Gas/solid flow: $0.6 < N_{Re,p,^*} < 5$: $0.00181 n_D \times \left[\frac{N_{Re,p}}{1.25 - 0.5\exp\left(-\frac{D}{1.5\times 0.05\,\mathrm{m}}\right)}\right]^{2.744} + 0.76\left(\frac{d_p}{D}\right)^{0.234} \times N_{Re,p}^{1.64} = \frac{\pi}{6} N_{Ar} + \left(\frac{A_H}{12 s^2}\right)\left(\frac{\rho_f d_p}{\mu^2}\right)$ According to Rabinovich and Kalman,[36] the second term on the left-hand side of the above equation is dominant.	$N_{Re,p,^*} \geq 5$: $N_{Re,p} = \left[k_1 - k_2\exp\left(-\frac{D}{k_3\,\mathrm{m}}\right)\right]^{k_4} \times f_S^{k_5} N_{Ar}^{k_6}$	15

DOI 10.1002/aic

Published on behalf of the AIChE

January 2014 Vol. 60, No. 1

AIChE Journal

Table A1. *Continued*

Model No.	Model	Dimensional Equation	Dimensionless Equation	Dimensionless Form	Model Form No.
21	Rabinovich and Kalman[36]	N/A	$N_{Re,p}=\left[1.25-0.5\exp\left(-\frac{D}{1.5\times0.05\,\mathrm{m}}\right)\right]^{1}$ $\times\left\{\frac{\pi}{6\times0.00181\times1.7009}N_{Ar}^{1}+\left[\frac{\left(1.302\times10^{-6}\,\frac{\mathrm{N}}{\mathrm{m}}\right)}{0.00181\times1.7009}\frac{\rho_f d_p}{\mu^2}\right]^{1}\right\}^{\frac{1}{2.744}}$ $N_{Re,p,*}\le0.6$: $0.0277n_D\times\left[\frac{N_{Re,p}}{1.25-0.5\exp\left(-\frac{D}{1.5\times0.05\,\mathrm{m}}\right)}\right]^{1.96}+0.00635\left(\frac{d_p}{D}\right)^{0.375}N_{Re,p}^{2.625}=\frac{\pi}{6}N_{Ar}+\left(\frac{A_H}{12s^2}\right)\left(\frac{\rho_f d_p}{\mu^2}\right)$ According to Rabinovich and Kalman,[36] the first term of the left-hand side of the above equation is dominant. $N_{Re,p}=\left[1.25-0.5\exp\left(-\frac{D}{1.5\times0.05\,\mathrm{m}}\right)\right]^{1}\times\left\{\frac{\pi}{6\times0.0277\times1.7009}N_{Ar}^{1}+\left[\frac{(1.302\times10^{-6}\,\mathrm{N/m})}{0.0277\times1.7009}\frac{\rho_f d_p}{\mu^2}\right]^{1}\right\}^{1/1.96}$	Gas/solid flow: $0.6<N_{Re,p,*}<5$: $N_{Re,p}=\left[k_7-k_8\exp\left(-\frac{D}{k_9\,\mathrm{m}}\right)\right]^{k_{10}}\times\left\{k_{11}N_{Ar}^{k_{12}}+\left[\left(k_{13}\,\frac{\mathrm{N}}{\mathrm{m}}\right)\frac{\rho_f d_p}{\mu^2}\right]^{k_{14}}\right\}^{k_{15}}$ $N_{Re,p,*}\le0.6$: $N_{Re,p}=\left[k_{16}-k_{17}\exp\left(-\frac{D}{k_{18}\,\mathrm{m}}\right)\right]^{k_{19}}\times\left\{k_{20}N_{Ar}^{k_{21}}+\left[\left(k_{22}\,\frac{\mathrm{N}}{\mathrm{m}}\right)\frac{\rho_f d_p}{\mu^2}\right]^{k_{23}}\right\}^{k_{24}}$	15

Table A1. *Continued*

Model No.	Model	Dimensional Equation	Dimensionless Equation	Dimensionless Form	Model Form No.
21	Rabinovich and Kalman[36]	N/A	Liquid/solid flow: $0.6 < N_{Re,p,*} < 5$: $0.00181 n_D \times \left[\frac{N_{Re,p}}{1.25-0.5\exp\left(-\frac{D}{1.5\times 0.05\,\mathrm{m}}\right)}\right]^{2.744} + 0.76[\tan(\alpha)] \times \left(\frac{d_p}{D}\right)^{0.234} N_{Re,p}^{1.64} = \frac{\pi}{6}[\tan(\alpha)] N_{Ar}$ According to Rabinovich and Kalman,[36] the first term of the left-hand side of the above equation is dominant. $N_{Re,p} = \left[1.25 \times \left(\frac{\pi}{6\times 0.00181\times 1.7009}\right)^{1/2.744} - 0.5\left(\frac{\pi}{6\times 0.00181\times 1.7009}\right)^{1/2.744} \times \exp\left(-\frac{D}{1.5\times 0.05\,\mathrm{m}}\right)\right]^{1} \times [\tan(\alpha)]^{1/2.744} \times N_{Ar}^{1/2.744}$ $N_{Re,p,*} \le 0.6$: $0.0277 n_D \times \left[\frac{N_{Re,p}}{1.25-0.5\exp\left(-\frac{D}{1.5\times 0.05\,\mathrm{m}}\right)}\right]^{1.96} + 0.00635[\tan(\alpha)] \times \left(\frac{d_p}{D}\right)^{0.375} N_{Re,p}^{2.625} = \frac{\pi}{6}[\tan(\alpha)] N_{Ar}$ According to Rabinovich and Kalman,[36] the first term of the left-hand side of the above equation is dominant.	Liquid/solid flow: $0.6 < N_{Re,p,*} < 5$: $N_{Re,p} = \left[k_{25} - k_{26}\exp\left(-\frac{D}{k_{27}\,\mathrm{m}}\right)\right]^{k_{28}} \times f_S^{k_{29}} N_{Ar}^{k_{30}}$	15

DOI 10.1002/aic

Published on behalf of the AIChE

January 2014 Vol. 60, No. 1

AIChE Journal

Table A1. *Continued*

Model No.	Model	Dimensional Equation	Dimensionless Equation	Dimensionless Form	Model Form No.
21	Rabinovich and Kalman[36]		$N_{Re,p}=\left[1.25\times\left(\frac{\pi}{6\times0.0277\times1.7009}\right)^{1/1.96}-0.5\left(\frac{\pi}{6\times0.0277\times1.7009}\right)^{1/1.96}\times\exp\left(-\frac{D}{1.5\times0.05\,\mathrm{m}}\right)\right]^{1}\times[\tan(\alpha)]^{1/1.96}\times N_{Ar}^{1/1.96}$	$N_{Re,p,^*}\le 0.6$: $N_{Re,p}=\left[k_{31}-k_{32}\exp\left(-\frac{D}{k_{33}\,\mathrm{m}}\right)\right]^{k_{34}}\times f_S^{k_{35}}N_{Ar}^{k_{36}}$	15
22	Ramadan et al.[15]	$v_{\mathrm{lift}}=\left[\frac{2\tau_y}{C_L\rho_f}+\frac{4gd_p}{3C_L}\left(\frac{\rho_S}{\rho_f}-1\right)\sin(\theta_V)\right]^{0.5}$ $v_{\mathrm{roll}}=\left[\frac{6\left(\frac{\tau_y}{\rho_f}\right)\cos\varphi+4gd_p\left(\frac{\rho_S}{\rho_f}-1\right)\sin(\varphi+\theta_V)}{3(D_RC_D\sin\varphi+C_L\cos\varphi)}\right]^{0.5}$	$N_{Re,p,\mathrm{lift}}=\left(\frac{4}{3}\right)^{0.5}\frac{(\cos\theta)^{0.5}}{C_L^{0.5}}N_{Ar}^{0.5}$ $N_{Re,p,\mathrm{roll}}=\frac{\left[\sin\left(\frac{\pi}{6}+\frac{\pi}{2}-\theta\right)^{0.5}\right]}{\left[0.75\times0.85\times\sin\left(\frac{\pi}{6}\right)C_D^1+0.75\times\cos\left(\frac{\pi}{6}\right)C_L^1\right]^{0.5}}N_{Ar}^{0.5}$ $N_{Re,p}=\min\left(N_{Re,p,\mathrm{lift}},N_{Re,p,\mathrm{roll}}\right)$	$N_{Re,p,\mathrm{lift}}=k_1\frac{(\cos\theta)^{k_2}}{C_L^{k_3}}N_{Ar}^{k_4}$ $N_{Re,p,\mathrm{roll}}=\frac{\left[\sin\left(\frac{\pi}{6}+\frac{\pi}{2}-\theta\right)\right]^{k_5}}{\left(k_6C_D^{k_7}+k_8C_L^{k_9}\right)^{k_{10}}}N_{Ar}^{k_{11}}$ $N_{Re,p}=\min\left(N_{Re,p,\mathrm{lift}},N_{Re,p,\mathrm{roll}}\right)$	16
		$v_{\mathrm{lift}}=\left[\frac{2\tau_y}{C_L\rho_f}+\frac{4gd_p}{3C_L}\left(\frac{\rho_S}{\rho_f}-1\right)\cos(\theta)\right]^{0.5}$ $v_{\mathrm{roll}}=\left[6\left(\frac{\tau_y}{\rho_f}\right)\cos\varphi+4gd_p\left(\frac{\rho_S}{\rho_f}-1\right)\times\sin\left(\varphi+\frac{\pi}{2}-\theta\right)\right]^{0.5}\times\frac{1}{[3(D_RC_D\sin\varphi+C_L\cos\varphi)]^{0.5}}$ $v=\min\left(v_{\mathrm{lift}},v_{\mathrm{roll}}\right)$			
23	Cabrejos[16] (multiple particle)	$v=\left(\frac{1.27}{N_{Ar}^{1/3}}+0.036N_{Ar}^{1/3}+0.45\right)\times\left(\frac{0.70}{N_{Ar}^{1/5}}+1\right)v_0$	$N_{Re,p,0}=\frac{d_pv_0\rho_f}{\mu}$ $N_{Re,p}=\left[1.27\left(\frac{1}{N_{Ar}}\right)^{1/3}+0.036N_{Ar}^{1/3}+0.45\right]^{1}\times\left[0.70\left(\frac{1}{N_{Ar}}\right)^{1/5}+1\right]^{1}\times N_{Re,p,0}^{1}$	$N_{Re,p,0}=\frac{d_pv_0\rho_f}{\mu}$ $N_{Re,p}=\left[k_1\left(\frac{1}{N_{Ar}}\right)^{k_2}+k_3N_{Ar}^{k_4}+k_5\right]^{k_6}\times\left[k_7\left(\frac{1}{N_{Ar}}\right)^{k_8}+k_9\right]^{k_{10}}\times N_{Re,p,0}^{k_{11}}$	17

Table A1. *Continued*

Model No.	Model	Dimensional Equation	Dimensionless Equation	Dimensionless Form	Model Form No.
24	Fletcher[29]	$v_*=\left(\frac{\rho_S-\rho_f}{\rho_f}\right)^{0.5}\times\left[0.13\left(gd_p\right)^{0.5}+0.057\left(\frac{\gamma}{\rho_S}\right)^{0.25}\left(\frac{\mu}{\rho_f d_p}\right)^{0.5}\right]$	Cohesion: $\gamma=8.0+\left(\frac{9.4-8.0}{15.8-4.4}\right)\times\left(10^6 d_p-4.4\right)\frac{\mathrm{N}}{\mathrm{m}^2}$ $N_{Re,p,*}=0.13N_{Ar}^{0.5}+0.057\times\left[\left(\frac{\gamma\,\mathrm{N/m^2}}{\rho_f}\right)^{0.5}\frac{d_p\left(\rho_S-\rho_f\right)}{\mu}\right]^{0.5}$	Cohesion: $\gamma=8.0+\left(\frac{9.4-8.0}{15.8-4.4}\right)\times\left(10^6 d_p-4.4\right)\frac{\mathrm{N}}{\mathrm{m}^2}$ $N_{Re,p,*}=k_1N_{Ar}^{k_2}+k_3\left[\left(\frac{\gamma\,\mathrm{N/m^2}}{\rho_f}\right)^{0.5}\times\frac{d_p\left(\rho_S-\rho_f\right)}{\mu}\right]^{k_4}$	18
25	Turian et al.[45]	$\frac{v}{\left[2gD\left(\frac{\rho_S}{\rho_f}-1\right)\right]^{0.5}}=1.7951C^{0.1087}\times(1-C)^{0.2501}\left[\frac{D\rho_f\left[gD\left(\frac{\rho_S}{\rho_f}-1\right)\right]^{0.5}}{\mu}\right]^{0.00179}\times\left(\frac{d_p}{D}\right)^{0.06623}$	$N_{Re,p}=\left(1.7951\times2^{0.5}\right)C^{0.1087}(1-C)^{0.2501}\times\left(\frac{D}{d_p}\right)^{0.436455}N_{Ar}^{0.500895}$	$N_{Re,p}=k_1C^{k_2}\times(1-C)^{k_3}\left(\frac{D}{d_p}\right)^{k_4}N_{Ar}^{k_5}$	19
26	Almutahar[22] (new approach)	$v=5.66\left\{f_c\left[gd_p\left(\frac{\rho_S}{\rho_f}-1\right)\right]^{0.5}\right\}^{8/7}\times\left(\frac{D\rho_f}{\mu}\right)^{1/7}\left(\frac{1}{\Omega}\right)^{8/7}$ $f_c=\begin{cases}(1-C)^{0.15}, C>3\% \\ -2222C^2+66.7C+1, \text{otherwise}\end{cases}$ $\Omega=\begin{cases}\frac{1}{1+3.64C}, C>1\% \\ \frac{1}{0.5(1+3.64C)}, \text{otherwise}\end{cases}$	$N_{Re,p}=5.66f_C^{8/7}\left(\frac{1}{\Omega}\right)^{8/7}\left(\frac{D}{d_p}\right)^{1/7}N_{Ar}^{4/7}$	$N_{Re,p}=k_1f_C^{k_2}\left(\frac{1}{\Omega}\right)^{k_3}\left(\frac{D}{d_p}\right)^{k_4}N_{Ar}^{k_5}$	20

DOI 10.1002/aic Published on behalf of the AIChE January 2014 Vol. 60, No. 1 AIChE Journal

Table A1. *Continued*

Model No.	Model	Dimensional Equation	Dimensionless Equation	Dimensionless Form	Model Form No.
27	Davies[18]	$v=1.08(1+\alpha_D C)^{1.09}(1-C)^{0.55n_C}\times\left(\frac{\mu}{\rho_f}\right)^{-0.09} d_p^{0.18}\left[2g\left(\frac{\rho_S-\rho_f}{\rho_f}\right)\right]^{0.54} D^{0.46}$ $\alpha_D=3.64$ $n_C=\begin{cases}4, d_p<0.5\text{ mm}\\ 3, \text{otherwise}\end{cases}$ $v=1.08(1+3.64C)^{1.09}(1-C)^{0.55n_C}\times\left(\frac{\mu}{\rho_f}\right)^{-0.09} d_p^{0.18}\left[2g\left(\frac{\rho_S-\rho_f}{\rho_f}\right)\right]^{0.54} D^{0.46}$	$N_{Re,p}=(1.08\times 2^{0.54})\times(1+3.64C)^{1.09}\times(1-C)^{0.55n_C}\times\left(\frac{D}{d_p}\right)^{0.46} N_{Ar}^{0.54}$	$N_{Re,p}=k_1(k_2+k_3C)^{k_4}\times(1-C)^{k_5 n_C}\times\left(\frac{D}{d_p}\right)^{k_6} N_{Ar}^{k_7}$	21
28	Spells[40]	$v^{1.225}=0.0251 g d_p\left(\frac{D\rho_m}{\mu}\right)^{0.775}\left(\frac{\rho_S-\rho_f}{\rho_f}\right)$ $v=\left[0.0251 g d_p\left(\frac{D\rho_m}{\mu}\right)^{0.775}\left(\frac{\rho_S}{\rho_f}-1\right)\right]^{\frac{1}{1.225}}$	$N_{Re,p}=0.0251^{1/1.225}\times\left[1+C\left(\frac{\rho_S}{\rho_f}-1\right)\right]^{0.775/1.225}\times\left(\frac{D}{d_p}\right)^{0.775/1.225} N_{Ar}^{1/1.225}$	$N_{Re,p}=k_1\times\left[1+C\left(\frac{\rho_S}{\rho_f}-1\right)\right]^{k_2}\times\left(\frac{D}{d_p}\right)^{k_3} N_{Ar}^{k_4}$	22
29	Rose and Duckworth[38]	$\frac{v}{v_S}=3.2C_W^{0.2}\left(\frac{D}{d_p}\right)^{0.6}\left(\frac{\rho_S}{\rho_f}\right)^{-0.7}\times\left(\frac{v^2}{gD}\right)^{0.25}$ $v=10.24 v_S^2 C_W^{0.4}\left(\frac{D}{d_p}\right)^{1.2}\left(\frac{\rho_S}{\rho_f}\right)^{-1.4}(gD)^{-0.5}$	$N_{Re,p}=\frac{10.24}{18^2}\frac{C^{0.4}}{\left[1+C\left(\frac{\rho_S}{\rho_f}-1\right)\right]^{0.4}}\left(\frac{\rho_f}{\rho_S}\right)^{1}\times\left(\frac{\rho_S-\rho_f}{\rho_f}\right)^{0.5}\times\left(\frac{D}{d_p}\right)^{0.7} N_{Ar}^{1.5}$	$N_{Re,p}=k_1\frac{C^{k_2}}{\left[1+C\left(\frac{\rho_S}{\rho_f}-1\right)\right]^{k_3}}\left(\frac{\rho_f}{\rho_S}\right)^{k_4}\times\left(\frac{\rho_S-\rho_f}{\rho_f}\right)^{k_5}\times\left(\frac{D}{d_p}\right)^{k_6} N_{Ar}^{k_7}$	23
30	Gruesbeck et al.[21]	$v=15 v_S\left(\frac{D v_S\rho_f}{\mu}\right)^{0.39}\left(\frac{d_p v_S\rho_f}{\mu}\right)^{-0.73}\times\left(\frac{\rho_S-\rho_f}{\rho_f}\right)^{0.17} C^{0.14}$	$N_{Re,p}=\frac{15}{18^{0.66}} C^{0.14}\left(\frac{\rho_S-\rho_f}{\rho_f}\right)^{0.17}\times\left(\frac{D}{d_p}\right)^{0.39} N_{Ar}^{0.66}$	$N_{Re,p}=k_1 C^{k_2}\left(\frac{\rho_S-\rho_f}{\rho_f}\right)^{k_3}\left(\frac{D}{d_p}\right)^{k_4}\times N_{Ar}^{k_5}$	24

Table A1. *Continued*

Model No.	Model	Dimensional Equation	Dimensionless Equation	Dimensionless Form	Model Form No.
31	Thomas[154]	$\frac{v_S}{v_{0,*}}=4.90\left(\frac{d_p v_{0,*}\rho_f}{\mu}\right)\left(\frac{\mu}{D v_{0,*}\rho_f}\right)^{0.60}\times\left(\frac{\rho_S-\rho_f}{\rho_f}\right)^{0.23}$ $\frac{v_*}{v_{0,*}}=1+2.8\left(\frac{v_S}{v_{0,*}}\right)^{1/3}C^{1/2}$	$N_{Re,p,*}=\frac{1}{88.2^{\frac{1}{1.4}}}\left(\frac{\rho_f}{\rho_S-\rho_f}\right)^{\frac{0.23}{1.4}}\times\left(\frac{D}{d_p}\right)^{\frac{0.60}{1.4}}N_{Ar}^{\frac{1}{1.4}}+\frac{2.8}{\left(4.90^{\frac{10}{21}}\right)\left(18^{\frac{17}{21}}\right)}C^{\frac{1}{2}}\times\left(\frac{\rho_f}{\rho_S-\rho_f}\right)^{\frac{23}{210}}\left(\frac{D}{d_p}\right)^{\frac{2}{7}}N_{Ar}^{\frac{17}{21}}$	$N_{Re,p,*}=k_1\left(\frac{\rho_f}{\rho_S-\rho_f}\right)^{k_2}\left(\frac{D}{d_p}\right)^{k_3}N_{Ar}^{k_4}+k_5C^{k_6}\left(\frac{\rho_f}{\rho_S-\rho_f}\right)^{k_7}\left(\frac{D}{d_p}\right)^{k_8}\times N_{Ar}^{k_9}$	25
32	Zandi and Govatos[46]	$\frac{v^2C_D^{0.5}}{CgD\left(\frac{\rho_S}{\rho_f}-1\right)}=N_I$ $N_I=40$ $v=\left[\frac{40CgD\left(\frac{\rho_S}{\rho_f}-1\right)}{C_D^{0.5}}\right]^{0.5}$	$N_{Re,p}=\frac{40^{0.5}C^{0.5}}{C_D^{0.25}}\left(\frac{D}{d_p}\right)^{0.5}N_{Ar}^{0.5}$	$N_{Re,p}=\frac{k_1C^{k_2}}{C_D^{k_3}}\left(\frac{D}{d_p}\right)^{k_4}N_{Ar}^{k_5}$	26
33	Babcock[25]	$\frac{v^2C_D^{0.5}}{CgD\left(\frac{\rho_S}{\rho_f}-1\right)}=10$ $v=\left[\frac{10CgD\left(\frac{\rho_S}{\rho_f}-1\right)}{C_D^{0.5}}\right]^{0.5}$	$N_{Re,p}=\frac{10^{0.5}C^{0.5}}{C_D^{0.25}}\left(\frac{D}{d_p}\right)^{0.5}N_{Ar}^{0.5}$		
34	Shook[39]	$v=\frac{2.43C^{1/3}}{C_D^{1/4}}\left[2gD\left(\frac{\rho_S}{\rho_f}-1\right)\right]^{0.5}$	$N_{Re,p}=\frac{\left(2.43\times2^{0.5}\right)C^{1/3}}{C_D^{1/4}}\left(\frac{D}{d_p}\right)^{0.5}N_{Ar}^{0.5}$		
35	Bain and Bonnington[26]	$v=3.48C^{1/3}\left[\frac{gD\left(\frac{\rho_S}{\rho_f}-1\right)}{C_D^{0.5}}\right]^{0.5}$	$N_{Re,p}=\frac{3.48C^{1/3}}{C_D^{0.25}}\left(\frac{D}{d_p}\right)^{0.5}N_{Ar}^{0.5}$		

DOI 10.1002/aic

Published on behalf of the AIChE

January 2014 Vol. 60, No. 1

AIChE Journal

Table A1. *Continued*

Model No.	Model	Dimensional Equation	Dimensionless Equation	Dimensionless Form	Model Form No.
36	Kökpınar and Göğüş[31]	$v=0.055\left(\frac{d_p}{D}\right)^{-0.60} C^{0.27}\left(\frac{\rho_S}{\rho_f}-1\right)^{0.07} \times\left(\frac{\rho_f v_S d_p}{\mu}\right)^{0.30}(gD)^{0.5}$	$d'_*=\left\{\frac{(1-C)(2-3C)^2}{4\left[1+C\left(\frac{\rho_S}{\rho_f}-1\right)\right]}N_{Ar}\right\}^{1/3}$ $N_{Re,p,S}=\left(\frac{2-2C}{2-3C}\right)\times\left[\sqrt{25+1.2(d'_*)^2}-5\right]^{1.5}$ $N_{Re,p}=0.055C^{0.27}N_{Re,p,S}^{0.30}\times\left(\frac{\rho_f}{\rho_S-\rho_f}\right)^{0.43}\left(\frac{D}{d_p}\right)^{1.1}N_{Ar}^{0.5}$	$d'_*=\left\{\frac{(1-C)(2-3C)^2}{4\left[1+C\left(\frac{\rho_S}{\rho_f}-1\right)\right]}N_{Ar}\right\}^{1/3}$ $N_{Re,p,S}=\left(\frac{2-2C}{2-3C}\right)\times\left[\sqrt{25+1.2(d'_*)^2}-5\right]^{1.5}$ $N_{Re,p}=k_1C^{k_2}N_{Re,p,S}^{k_3}\left(\frac{\rho_f}{\rho_S-\rho_f}\right)^{k_4}\times\left(\frac{D}{d_p}\right)^{k_5}N_{Ar}^{k_6}$	27
37	Ponagandla[34]	$v=\frac{5.04}{C_1^{1.143}(1.39N_{St}+0.62)^{0.571}}\times(1-C)^{0.571\times n_C}\times d_p^{0.571}g^{0.571}\left(\frac{\rho_S-\rho_f}{\rho_f}\right)^{0.571}\times D^{0.143}\left(\frac{\mu}{\rho_f}\right)^{-0.143}(1+3.64C)^{1.143}$ $l_t=0.035D$ $N_{St}=\frac{\rho_S d_p^2}{18\mu\left(\frac{l_t}{v'}\right)}$ $C_{D,L}=1.39N_{St}+0.62$ $C_1=0.7$ $n_C=4$ $v=\frac{5.04}{0.7^{1.143}C_{D,L}^{0.571}}(1-C)^{0.571\times4}\times d_p^{0.571}g^{0.571}\times\left(\frac{\rho_S-\rho_f}{\rho_f}\right)^{0.571}\times D^{0.143}\left(\frac{\mu}{\rho_f}\right)^{-0.143}\times(1+3.64C)^{1.143}$	$N_{Re,p}=\frac{5.04}{0.7^{1.143}}\times(1-C)^{0.571\times4}\times\frac{(1+3.64C)^{1.143}}{C_{D,L}^{0.571}}\times\left(\frac{D}{d_p}\right)^{0.143}N_{Ar}^{0.571}$	$N_{Re,p}=k_1\times\frac{(1-C)^{k_2}(k_3+k_4C)^{k_5}}{C_{D,L}^{k_6}}\times\left(\frac{D}{d_p}\right)^{k_7}N_{Ar}^{k_8}$	28

Table A1. *Continued*

Model No.	Model	Dimensional Equation	Dimensionless Equation	Dimensionless Form	Model Form No.
38	Oroskar and Turian[17]	$N_{Re,OT}=\dfrac{D\rho_f\left[gd_p\left(\frac{\rho_S}{\rho_f}-1\right)\right]^{0.5}}{\mu}$ $v=1.85C^{0.1536}(1-C)^{0.3564}\left(\frac{d_p}{D}\right)^{-0.378}\times N_{Re,OT}^{0.09}x^{0.30}\times\left[gd_p\left(\frac{\rho_S}{\rho_f}-1\right)\right]^{0.5}$	Iterative: $N_{Re,p}=1.85C^{0.1536}\times(1-C)^{0.3564}x^{0.30}\times\left(\frac{D}{d_p}\right)^{0.468}N_{Ar}^{0.545}$ Non-iterative: $N_{Re,p}=\left(1.85\times0.9360^{0.30}\right)C^{0.1536}\times(1-C)^{0.3564}\times\left(\frac{D}{d_p}\right)^{0.468}N_{Ar}^{0.545}$	Iterative: $N_{Re,p}=k_1C^{k_2}\times(1-C)^{k_3}x^{k_4}\left(\frac{D}{d_p}\right)^{k_5}N_{Ar}^{k_6}$ Non-iterative: $N_{Re,p}=k_7C^{k_8}\times(1-C)^{k_9}\left(\frac{D}{d_p}\right)^{k_{10}}N_{Ar}^{k_{11}}$	29
39	Almutahar[22] (initial approach)	$v=\left\{5\left(\frac{D}{d_p}\right)\times\left[\frac{D\rho_f}{\mu}\sqrt{gd_p\left(\frac{\rho_S}{\rho_f}-1\right)\sin(\theta_V)}\right]^{1/8}\times\left(\frac{1}{x}\right)\right\}^{8/15}C^{0.31}\left(\frac{d_p}{360\times10^{-6}\,\mathrm{m}}\right)^{0.60}\times\sqrt{gd_p\left(\frac{\rho_S}{\rho_f}-1\right)\sin(\theta_V)}$ $v=\left\{5\left(\frac{D}{d_p}\right)\times\left[\frac{D\rho_f}{\mu}\sqrt{gd_p\left(\frac{\rho_S}{\rho_f}-1\right)\cos(\theta)}\right]^{1/8}\times\left(\frac{1}{x}\right)\right\}^{8/15}C^{0.31}\left(\frac{d_p}{360\times10^{-6}\,\mathrm{m}}\right)^{0.60}\times\sqrt{gd_p\left(\frac{\rho_S}{\rho_f}-1\right)\cos(\theta)}$	$N_{Re,p}=5^{8/15}C^{0.31}(\cos\theta)^{8/15}\left(\frac{d_p}{360\times10^{-6}\,\mathrm{m}}\right)^{0.60}\times\left(\frac{D}{d_p}\right)^{0.6}N_{Ar}^{8/15}$	$N_{Re,p}=k_1C^{k_2}(\cos\theta)^{k_3}\times\left(\frac{d_p}{k_4\,\mathrm{m}}\right)^{k_5}\left(\frac{D}{d_p}\right)^{k_6}N_{Ar}^{k_7}$	30
40	Han and Hunt[47]	$v=\frac{2}{9\mu}\left(\frac{d_p}{2}\right)(3.60\times10^{-6}\,\mathrm{m})\times(\rho_S-\rho_f)g\times\left(\frac{0.696+0.18}{1-0.696\times0.18}\right)$ $v=\frac{1}{9}(3.60\times10^{-6}\,\mathrm{m})\left(\frac{0.696+0.18}{1-0.696\times0.18}\right)\times\frac{gd_p(\rho_S-\rho_f)}{\mu}$	$N_{Re,p}=\frac{1}{9}\left(\frac{0.696+0.18}{1-0.696\times0.18}\right)\times\left[\frac{g(3.60\times10^{-6}\,\mathrm{m})d_p^2\rho_f(\rho_S-\rho_f)}{\mu^2}\right]^1$	$N_{Re,p}=k_1\times\left[\frac{g(k_2\,\mathrm{m})d_p^2\rho_f(\rho_S-\rho_f)}{\mu^2}\right]^{k_3}$	31

DOI 10.1002/aic Published on behalf of the AIChE January 2014 Vol. 60, No. 1 AIChE Journal

Table A1. *Continued*

Model No.	Model	Dimensional Equation	Dimensionless Equation	Dimensionless Form	Model Form No.
41	Wu and Chou[48]	$v_{\text{roll}} = \sqrt{\frac{2L_w}{C_D L_D + C_L L_L} \times \frac{\pi d_p^3}{6\left(\frac{\pi d_p^2}{4}\right)} \frac{g\left(\rho_S - \rho_f\right)}{\rho_f}}$	$N_{Re,p,\text{roll}} = \left(\frac{4}{3}\right)^{0.5} \left(\frac{L_W}{C_D L_D + C_L L_L}\right)^{0.5} N_{Ar}^{0.5}$	$N_{Re,p,\text{roll}} = k_1 \left(\frac{L_W}{C_D L_D + C_L L_L}\right)^{k_2} N_{Ar}^{k_3}$	32
		$v_{\text{lift}} = \sqrt{\frac{2}{C_L} \times \frac{\pi d_p^3}{6\left(\frac{\pi d_p^2}{4}\right)} \frac{g\left(\rho_S - \rho_f\right)}{\rho_f}}$	$N_{Re,p,\text{lift}} = \left(\frac{4}{3}\right)^{0.5} \left(\frac{1}{C_L}\right)^{0.5} N_{Ar}^{0.5}$	$N_{Re,p,\text{lift}} = k_4 \left(\frac{1}{C_L}\right)^{k_5} N_{Ar}^{k_6}$	
		$v = \min\left(v_{\text{lift}}, v_{\text{roll}}\right)$	$N_{Re,p} = \min\left(N_{Re,p,\text{lift}}, N_{Re,p,\text{roll}}\right)$	$N_{Re,p} = \min\left(N_{Re,p,\text{lift}}, N_{Re,p,\text{roll}}\right)$	
		$L_D = y_b - 0.125 d_p - 0.5\delta$			
		$y_b = \frac{d_p}{15} \exp\left(0.4 \frac{v}{v_*}\right)$			
		$L_L = L_W = 0.5 d_p \sqrt{1 - \left(0.75 + \frac{\delta}{d_p}\right)^2}$			
42	Dey[49]	N/A	$\frac{\tau_W}{g\left(\rho_S - \rho_f\right) d_p} = \frac{8\pi \times 0.433}{\left\{\begin{array}{l} \sqrt{3}\pi C_D \left(\frac{v}{v^*}\right)^2 \sqrt{8} + 24 \times 0.433 C_L \\ \times \left(\frac{v}{v^*}\right) \left(\frac{\partial\left(\frac{v}{v^*}\right)}{\partial\left(\frac{y}{d_p}\right)}\right) \\ \times \left[\begin{array}{l} 2\left(N_{Re,p,^*} \frac{\partial\left(\frac{v}{v^*}\right)}{\partial\left(\frac{y}{d_p}\right)}\right)^{-0.5} \\ + \text{sgn}\left(N_{Re,p,^*}\right) \end{array}\right] \end{array}\right\}}$	$\frac{\tau_W}{g\left(\rho_S - \rho_f\right) d_p} = \frac{k_1}{\left\{\begin{array}{l} k_2 C_D \left(\frac{v}{v^*}\right)^2 + k_3 C_L \\ \times \left(\frac{v}{v^*}\right) \left(\frac{\partial\left(\frac{v}{v^*}\right)}{\partial\left(\frac{y}{d_p}\right)}\right) \\ \times \left[\begin{array}{l} k_4\left(N_{Re,p,^*} \frac{\partial\left(\frac{v}{v^*}\right)}{\partial\left(\frac{y}{d_p}\right)}\right)^{-0.5} \\ + \text{sgn}\left(N_{Re,p,^*}\right) \end{array}\right] \end{array}\right\}}$	33
			$\text{sgn}\left(N_{Re,p,^*}\right) = \left\{\begin{array}{l} 1, \text{if } N_{Re,p,^*} > 1 \\ 0, \text{otherwise} \end{array}\right.$		

Table A1. *Continued*

Model No.	Model	Dimensional Equation	Dimensionless Equation	Dimensionless Form	Model Form No.
43	Ibrahim et al.[50]	Note: Ibrahim et al.[50] presented the force balances, and the equations for the forces. The equations for the solids transport velocity from the Ibrahim et al.[50] model are presented in Rabinovich and Kalman.[60]			34
		$v_{\text{lift}} = \left(\frac{2}{0.0375}\right)\left\{\left(\frac{\mu}{d_p\rho_f}\right)\left[\left(\frac{1}{56.9}\right)\times\left(\frac{3}{4}\pi\times 0.1\,\frac{\text{J}}{\text{m}^2}\right)\left(\frac{d_p\rho_f}{\mu}\right)+\frac{\pi}{6\times 56.9}\left(\frac{gd_p^3\rho_f\rho_S}{\mu^2}\right)\right]^{1/1.87}-\left(\frac{0.0387\,\text{m/s}}{2}\right)\right\}$	$N_{Re,p,\text{lift}} = \left(\frac{2}{0.0375}\right)\left\{\left[\left(\left(\frac{1}{56.9}\right)\times\left(\frac{3}{4}\pi\times 0.1\,\frac{\text{J}}{\text{m}^2}\right)\left(\frac{d_p\rho_f}{\mu}\right)\right)^1+\frac{\pi}{6\times 56.9}\left(\frac{gd_p^3\rho_f\rho_S}{\mu^2}\right)^1\right]^{1/1.87}-\left(\frac{0.0387\,\text{m/s}}{2}\right)\left(\frac{d_p\rho_f}{\mu}\right)\right\}$	$N_{Re,p,\text{lift}} = k_6\left\{\left[\left(\left(k_1\,\frac{\text{J}}{\text{m}^2}\right)\left(\frac{d_p\rho_f}{\mu}\right)\right)^{k_2}+k_3\left(\frac{gd_p^3\rho_f\rho_S}{\mu^2}\right)^{k_4}\right]^{k_5}-\left(k_7\,\frac{\text{m}}{\text{s}}\right)\left(\frac{d_p\rho_f}{\mu}\right)\right\}$	
		$v_{\text{drag}} = \left(\frac{\mu}{d_p\rho_f}\right)\left(\frac{1}{1.7009\times 3\pi}\right)f_S\times\left\{\left(\frac{3}{4}\pi\times 0.1\,\frac{\text{J}}{\text{m}^2}\right)\left(\frac{d_p\rho_f}{\mu^2}\right)+\frac{\pi}{6}\left(\frac{gd_p^3\rho_f\rho_S}{\mu^2}\right)-56.9\left[\frac{0.0375}{2}N_{Re,p,\text{drag}}+\frac{0.0387\,\text{m/s}}{2}\left(\frac{d_p\rho_f}{\mu}\right)\right]^{1.87}\right\}$	$N_{Re,p,\text{drag}} = \left(\frac{1}{1.7009\times 3\pi}\right)f_S^1\times\left\{\left[\left(\frac{3}{4}\pi\times 0.1\,\frac{\text{J}}{\text{m}^2}\right)\left(\frac{d_p\rho_f}{\mu^2}\right)\right]^1+\frac{\pi}{6}\left(\frac{gd_p^3\rho_f\rho_S}{\mu^2}\right)^1-56.9\left[\frac{0.0375}{2}N_{Re,p,\text{drag}}^1+\left(\frac{0.0387\,\text{m/s}}{2}\left(\frac{d_p\rho_f}{\mu}\right)\right)^1\right]^{1.87}\right\}$	$N_{Re,p,\text{drag}} = k_8 f_S^{k_9}\left\{\left[\left(k_{10}\,\frac{\text{J}}{\text{m}^2}\right)\times\left(\frac{d_p\rho_f}{\mu^2}\right)\right]^{k_{11}}+k_{12}\left(\frac{gd_p^3\rho_f\rho_S}{\mu^2}\right)^{k_{13}}-k_{14}\left[k_{15}N_{Re,p,\text{drag}}^{k_{16}}+\left((k_{17}\,\text{m/s})\times\left(\frac{d_p\rho_f}{\mu}\right)\right)^{k_{18}}\right]^{k_{19}}\right\}$	
		$v_{\text{roll}} = -\left(\frac{56.9}{2.1\times 1.7009\pi}\right)\left(\frac{\mu}{d_p\rho_f}\right)\times\left(\frac{0.15\,\pi\,\text{m}}{65\times 10^9}\times\frac{1}{d_p}\right)^{1/3}\left[\frac{0.0375}{2}N_{Re,p,\text{roll}}+\frac{0.0387\,\text{m/s}}{2}\left(\frac{d_p\rho_f}{\mu}\right)\right]^{1.87}+\left(\frac{\mu}{d_p\rho_f}\right)\left(\frac{0.15\,\pi\,\text{m}}{65\times 10^9}\times\frac{1}{d_p}\right)^{1/3}\times\left[\left(\frac{3}{4\times 2.1\times 1.7009}\times 0.1\,\frac{\text{J}}{\text{m}^2}\right)\left(\frac{d_p\rho_f}{\mu^2}\right)+\frac{1}{6\times 2.1\times 1.7009}\left(\frac{gd_p^3\rho_f\rho_S}{\mu^2}\right)\right]$	$N_{Re,p,\text{roll}} = -\left(\frac{56.9}{2.1\times 1.7009\pi}\right)\times\left(\frac{0.15\,\pi\,\text{m}}{65\times 10^9}\times\frac{1}{d_p}\right)^{1/3}\times\left\{\frac{0.0375}{2}N_{Re,p,\text{roll}}^1+\left[\frac{0.0387\,\text{m/s}}{2}\times\left(\frac{d_p\rho_f}{\mu}\right)\right]^1\right\}^{1.87}+\left(\frac{0.15\,\pi\,\text{m}}{65\times 10^9}\times\frac{1}{d_p}\right)^{1/3}\times\left\{\left[\left(\frac{3}{4\times 2.1\times 1.7009}\times 0.1\,\frac{\text{J}}{\text{m}^2}\right)\times\left(\frac{d_p\rho_f}{\mu^2}\right)\right]^1+\frac{1}{6\times 2.1\times 1.7009}\times\left(\frac{gd_p^3\rho_f\rho_S}{\mu^2}\right)^1\right\}$	$N_{Re,p,\text{roll}} = -k_{20}\left(\frac{k_{21}\,\text{m}}{d_p}\right)^{k_{22}}\times\left\{k_{23}N_{Re,p,\text{roll}}^{k_{24}}+\left[(k_{25}\,\text{m/s})\times\left(\frac{d_p\rho_f}{\mu}\right)\right]^{k_{26}}\right\}^{k_{27}}+\left(\frac{k_{28}\,\text{m}}{d_p}\right)^{k_{29}}\times\left\{\left[\left(k_{30}\,\frac{\text{J}}{\text{m}^2}\right)\times\left(\frac{d_p\rho_f}{\mu^2}\right)\right]^{k_{31}}+k_{32}\left(\frac{gd_p^3\rho_f\rho_S}{\mu^2}\right)^{k_{33}}\right\}$	
		$v = \min\left(v_{\text{lift}}, v_{\text{drag}}, v_{\text{roll}}\right)$	$N_{Re,p} = \min\left(N_{Re,p,\text{lift}}, N_{Re,p,\text{drag}}, N_{Re,p,\text{roll}}\right)$	$N_{Re,p} = \min\left(N_{Re,p,\text{lift}}, N_{Re,p,\text{drag}}, N_{Re,p,\text{roll}}\right)$	

DOI 10.1002/aic

Published on behalf of the AIChE

January 2014 Vol. 60, No. 1

AIChE Journal

Table A1. *Continued*

Model No.	Model	Dimensional Equation	Dimensionless Equation	Dimensionless Form	Model Form No.
44	Ling[51]	N/A	$\frac{\tau_{W,\mathrm{roll}}}{g(\rho_S-\rho_f)d_p}=\frac{\left(\frac{\pi}{6}\right)}{\left(\frac{1.615}{2}\right)N_{Re,p,*,\mathrm{roll}}+\left(\frac{6\pi}{\sqrt{2}}\right)}$ $\frac{\tau_{W,\mathrm{lift}}}{g(\rho_S-\rho_f)d_p}=\frac{\left(\frac{\pi}{6}\right)}{BF_1+B(1-B)F_2+(1-B)^2F_3}$ $H_1=0.5N_{Re,p,*}\times[1+2\times(1-0.8164)]$ $H_2=N_{Re,p,*}$ $B=1-\frac{H_2}{4H_1}$ $F_1=1.615H_1H_2^{0.5}N_{Re,p,*}^{0.5}$ $F_2=\frac{\pi}{4}H_1^2$ $F_3=\frac{\pi}{6}H_1^2$ $N_{Re,p,*,\mathrm{roll}}=\frac{\left(\frac{\pi}{6}\right)^{0.5}}{\left[\left(\frac{1.615}{2}\right)N_{Re,p,*,\mathrm{roll}}^1+\left(\frac{6\pi}{\sqrt{2}}\right)\right]^{0.5}}N_{Ar}^{0.5}$ $N_{Re,p,*,\mathrm{lift}}=\frac{\left(\frac{\pi}{6}\right)^{0.5}}{\left[B^1F_1^1+B^1(1-B)^1F_2^1+(1-B)^2F_3^1\right]^{0.5}}N_{Ar}^{0.5}$ $N_{Re,p}=\min\left(N_{Re,p,\mathrm{lift}},N_{Re,p,\mathrm{roll}}\right)$	$N_{Re,p,*,\mathrm{roll}}=\frac{k_1}{\left[k_2N_{Re,p,*,\mathrm{roll}}^{k_3}+k_4\right]^{k_5}}N_{Ar}^{k_6}$ $N_{Re,p,*,\mathrm{lift}}=\frac{k_7}{\left[B^{k_8}F_1^{k_9}+B^{k_{10}}(1-B)^{k_{11}}F_2^{k_{12}}+(1-B)^{k_{13}}F_3^{k_{14}}\right]^{k_{15}}}N_{Ar}^{k_{16}}$ $N_{Re,p}=\min\left(N_{Re,p,\mathrm{lift}},N_{Re,p,\mathrm{roll}}\right)$	35

Table A2. Parameter Values after Fine-Tuning

Model Form No.	Liquid/Solid Flow—Pick-Up Velocity	Gas/Solid Flow—Pick-Up Velocity	Gas/Solid Flow—Incipient Motion Velocity
1	$k_1 = 0.45$, $k_2 = 0.41$	$k_1 = 0.54$, $k_2 = 0.36$	$k_1 = 0.38$, $k_2 = 0.34$
2	$k_1 = 7.90$, $k_2 = 0.41$	$k_1 = 9.02$, $k_2 = 0.37$	$k_1 = 6.82$, $k_2 = 0.34$
3	$k_1 = 7.90$, $k_2 = 0$, $k_3 = 0.41$	$k_1 = 9.02$, $k_2 = 0$, $k_3 = 0.37$	$k_1 = 6.82$, $k_2 = 0$, $k_3 = 0.34$
4	$k_1 = 8.28$, $k_2 = 0.11$, $k_3 = 0$, $k_4 = 0.41$	$k_1 = 37.77$, $k_2 = 0.25$, $k_3 = 0.074$, $k_4 = 0.39$	$k_1 = 14.48$, $k_2 = 0.14$, $k_3 = 0.036$, $k_4 = 0.35$
5	$k_1 = 9.35$, $k_2 = 0$, $k_3 = 0.39$	$k_1 = 102.4$, $k_2 = 0.079$, $k_3 = 0.38$	$k_1 = 52.41$, $k_2 = 0.091$, $k_3 = 0.37$
6	$k_1 = 5.52$, $k_2 = 0.56$, $k_3 = 0$, $k_4 = 0.41$	$k_1 = 37.74$, $k_2 = 0.14$, $k_3 = 0.074$, $k_4 = 0.39$	$k_1 = 14.47$, $k_2 = 0.21$, $k_3 = 0.036$, $k_4 = 0.35$
7	$k_1 = 0.40$, $k_2 = 0.36$, $k_3 = 0.46$, $k_4 = 0.40$	$k_1 = 1.02$, $k_2 = 0.35$, $k_3 = 0.40$, $k_4 = 0.39$	$k_1 = 0.42$, $k_2 = 0.45$, $k_3 = 0.45$, $k_4 = 0.32$
8	$k_1 = 7.78$, $k_2 = 0$, $k_3 = 0.42$, $k_4 = 8.96$, $k_5 = 0$, $k_6 = 0.39$, $k_7 = 12.00$, $k_8 = 0.16$, $k_9 = 0.35$	$k_1 = 11.52$, $k_2 = 0.0045$, $k_3 = 0.21$, $k_4 = 4.14$, $k_5 = 1.3 \times 10^{-5}$, $k_6 = 0.45$, $k_7 = 6.01$, $k_8 = 0$, $k_9 = 0.42$	$k_1 = 6.34$, $k_2 = 6.8 \times 10^{-7}$, $k_3 = 0.40$, $k_4 = 8.51$, $k_5 = 0$, $k_6 = 0.32$, $k_7 = 0.42$, $k_8 = 0.12$, $k_9 = 0.50$
9	$k_1 = 7.90$, $k_2 = 0$, $k_3 = 0$, $k_4 = 0.41$	$k_1 = 9.02$, $k_2 = 0$, $k_3 = 0$, $k_4 = 0.37$	$k_1 = 7.56$, $k_2 = 0.030$, $k_3 = 0$, $k_4 = 0.33$
10	$k_1 = 3.95$, $k_2 = 0$, $k_3 = 0.41$, $k_4 = 1.50$, $k_5 = 0.41$	$k_1 = 0.81$, $k_2 = 0.42$, $k_3 = 0.58$, $k_4 = 0$, $k_5 = 0.55$	$k_1 = 0.87$, $k_2 = 0.38$, $k_3 = 0.57$, $k_4 = 0$, $k_5 = 0.47$
11	$k_1 = 2.19$, $k_2 = 0$, $k_3 = 0.66$, $k_4 = 1.65$, $k_5 = 1.46$, $k_6 = 0.44$, $k_7 = 3.74$, $k_8 = 0.96$, $k_9 = 0.41$	$k_1 = 3.69$, $k_2 = 0$, $k_3 = 0.76$, $k_4 = 3.17$, $k_5 = 0.25$, $k_6 = 0.44$, $k_7 = 0.88$, $k_8 = 2.03$, $k_9 = 0.28$	$k_1 = 1.07$, $k_2 = 0$, $k_3 = 0.15$, $k_4 = 8.10$, $k_5 = 1.30$, $k_6 = 0.32$, $k_7 = 5.66$, $k_8 = 1.44$, $k_9 = 0.36$
12	$k_1 = 0.56$, $k_2 = 0$, $k_3 = 0.61$, $k_4 = 8.04$, $k_5 = 0$, $k_6 = 0.41$, $k_7 = 16.62$, $k_8 = 0.93$, $k_9 = 21.71$, $k_{10} = 2.05$, $k_{11} = 0.38$	$k_1 = 2.74$, $k_2 = 0$, $k_3 = 0.75$, $k_4 = 1.71$, $k_5 = 0.99$, $k_6 = 0.44$, $k_7 = 12.15$, $k_8 = 0$, $k_9 = 1.81$, $k_{10} = 2.27$, $k_{11} = 0.33$	$k_1 = 0.35$, $k_2 = 0$, $k_3 = 0.40$, $k_4 = 7.95$, $k_5 = 0$, $k_6 = 0.32$, $k_7 = 16.80$, $k_8 = 0.45$, $k_9 = 21.41$, $k_{10} = 1.11$, $k_{11} = 0.42$
13	$k_1 = 0.17$, $k_2 = 3.23$, $k_3 = 0.97$, $k_4 = 9.5 \times 10^{-7}$, $k_5 = 0.47$, $k_6 = 0.51$	$k_1 = 0$, $k_2 = 6647$, $k_3 = 2.71$, $k_4 = 6.4 \times 10^{-4}$, $k_5 = 3.91$, $k_6 = 0.16$	$k_1 = 0$, $k_2 = 1.7 \times 10^{7}$, $k_3 = 2.90$, $k_4 = 0.15$, $k_5 = 0$, $k_6 = 0.12$
14	$k_1 = 0.045$, $k_2 = 82.42$, $k_3 = 0.97$, $k_4 = 0$, $k_5 = 1.00$, $k_6 = 0.42$, $k_7 = 1.26$, $k_8 = 0.43$, $k_9 = 0.35$, $k_{10} = 1.50$, $k_{11} = 1.00$, $k_{12} = 0.55$	$k_1 = 0.12$, $k_2 = 82.42$, $k_3 = 0.99$, $k_4 = 1.1 \times 10^{-4}$, $k_5 = 1.04$, $k_6 = 0.34$, $k_7 = 1.17$, $k_8 = 0.52$, $k_9 = 0.47$, $k_{10} = 1.50$, $k_{11} = 0.99$, $k_{12} = 0.51$	$k_1 = 0$, $k_2 = 4.5 \times 10^{7}$, $k_3 = 3.05$, $k_4 = 0.50$, $k_5 = 0$, $k_6 = 0.11$, $k_7 = 0.23$, $k_8 = 0.70$, $k_9 = 0.98$, $k_{10} = 0.24$, $k_{11} = 0.53$, $k_{12} = 0.14$
15	$k_1 = 0.56$, $k_2 = 0.058$, $k_3 = 0.76$, $k_4 = 0.37$, $k_5 = 0.40$, $k_6 = 0.58$, $k_7 = 0.21$, $k_8 = 0.33$, $k_9 = 0.10$, $k_{10} = 0.59$, $k_{11} = 0.17$, $k_{12} = 0.93$, $k_{13} = 0.10$, $k_{14} = 0.44$, $k_{15} = 0.27$, $k_{16} = 0.87$, $k_{17} = 0.75$, $k_{18} = 0.27$, $k_{19} = 0.67$, $k_{20} = 0.26$, $k_{21} = 0.090$, $k_{22} = 0.031$, $k_{23} = 0.32$, $k_{24} = 0.79$, $k_{25} = 0.30$, $k_{26} = 0.23$, $k_{27} = 0.48$, $k_{28} = 0.25$, $k_{29} = 0.36$, $k_{30} = 0.053$, $k_{31} = 0.48$, $k_{32} = 0.16$, $k_{33} = 0.88$, $k_{34} = 0.59$, $k_{35} = 0.33$, $k_{36} = 0.81$	$k_1 = 3.17$, $k_2 = 0$, $k_3 = 0.14$, $k_4 = 0.33$, $k_5 = 0.80$, $k_6 = 0.56$, $k_7 = 0.90$, $k_8 = 0.24$, $k_9 = 0.70$, $k_{10} = 0.83$, $k_{11} = 0.087$, $k_{12} = 0.82$, $k_{13} = 0.81$, $k_{14} = 0.20$, $k_{15} = 0.10$, $k_{16} = 0.25$, $k_{17} = 0$, $k_{18} = 0.62$, $k_{19} = 0.22$, $k_{20} = 1.03$, $k_{21} = 1.09$, $k_{22} = 0.085$, $k_{23} = 0.40$, $k_{24} = 0.71$, $k_{25} = 0.31$, $k_{26} = 0.093$, $k_{27} = 0.0033$, $k_{28} = 0.96$, $k_{29} = 0.73$, $k_{30} = 0.43$, $k_{31} = 0.46$, $k_{32} = 0.46$, $k_{33} = 0.86$, $k_{34} = 0.41$, $k_{35} = 0.71$, $k_{36} = 0.38$	$k_1 = 0.33$, $k_2 = 0.41$, $k_3 = 0.15$, $k_4 = 0.62$, $k_5 = 0.10$, $k_6 = 0.21$, $k_7 = 0.62$, $k_8 = 0.55$, $k_9 = 0.24$, $k_{10} = 1.02$, $k_{11} = 0.47$, $k_{12} = 0.0023$, $k_{13} = 0.41$, $k_{14} = 0$, $k_{15} = 0.64$, $k_{16} = 0.042$, $k_{17} = 0$, $k_{18} = 1.59$, $k_{19} = 3.38$, $k_{20} = 60.09$, $k_{21} = 0.11$, $k_{22} = 0.18$, $k_{23} = 0$, $k_{24} = 3.08$, $k_{25} = 0.87$, $k_{26} = 0.58$, $k_{27} = 0.73$, $k_{28} = 0.15$, $k_{29} = 0.26$, $k_{30} = 0.028$, $k_{31} = 0.83$, $k_{32} = 0.78$, $k_{33} = 0.79$, $k_{34} = 0.33$, $k_{35} = 0.45$, $k_{36} = 0.61$
16	$k_1 = 1.16$, $k_2 = 0.50$, $k_3 = 0.50$, $k_4 = 0.50$, $k_5 = 0.50$, $k_6 = 0.32$, $k_7 = 1.00$, $k_8 = 0.65$, $k_9 = 1.00$, $k_{10} = 0.50$, $k_{11} = 0.50$	$k_1 = 1.16$, $k_2 = 0.50$, $k_3 = 0.50$, $k_4 = 0.50$, $k_5 = 0.50$, $k_6 = 0.31$, $k_7 = 0.99$, $k_8 = 0.65$, $k_9 = 1.00$, $k_{10} = 0.48$, $k_{11} = 0.49$	$k_1 = 1.13$, $k_2 = 0.50$, $k_3 = 0.28$, $k_4 = 0.39$, $k_5 = 0.47$, $k_6 = 0$, $k_7 = 0.92$, $k_8 = 0.64$, $k_9 = 0.96$, $k_{10} = 0.44$, $k_{11} = 0.42$
17	$k_1 = 0$, $k_2 = 0$, $k_3 = 2.08$, $k_4 = 0.23$, $k_5 = 0$, $k_6 = 1.56$, $k_7 = 0.77$, $k_8 = 0$, $k_9 = 1.31$, $k_{10} = 0.92$, $k_{11} = 0.12$	$k_1 = 1.08$, $k_2 = 0$, $k_3 = 1.32$, $k_4 = 0.22$, $k_5 = 0.51$, $k_6 = 2.22$, $k_7 = 0.37$, $k_8 = 0$, $k_9 = 0.65$, $k_{10} = 0.52$, $k_{11} = 0$	$k_1 = 0.93$, $k_2 = 0$, $k_3 = 0$, $k_4 = 0.24$, $k_5 = 0.021$, $k_6 = 1.26$, $k_7 = 0.30$, $k_8 = 0$, $k_9 = 0.73$, $k_{10} = 0.87$, $k_{11} = 1.01$
18	$k_1 = 0.45$, $k_2 = 0.41$, $k_3 = 0$, $k_4 = 0.75$	$k_1 = 0.24$, $k_2 = 0.43$, $k_3 = 0.044$, $k_4 = 0.23$	$k_1 = 0.38$, $k_2 = 0.34$, $k_3 = 0$, $k_4 = 0.46$
19	$k_1 = 7.90$, $k_2 = 0$, $k_3 = 0.25$, $k_4 = 0$, $k_5 = 0.41$	$k_1 = 10.22$, $k_2 = 0.0090$, $k_3 = 0.15$, $k_4 = 0$, $k_5 = 0.37$	$k_1 = 7.51$, $k_2 = 0.0069$, $k_3 = 0.20$, $k_4 = 0$, $k_5 = 0.34$
20	$k_1 = 7.90$, $k_2 = 1.14$, $k_3 = 0$, $k_4 = 0$, $k_5 = 0.41$	$k_1 = 9.02$, $k_2 = 1.17$, $k_3 = 3.3 \times 10^{-4}$, $k_4 = 0$, $k_5 = 0.37$	$k_1 = 6.82$, $k_2 = 1.14$, $k_3 = 0$, $k_4 = 0$, $k_5 = 0.34$
21	$k_1 = 2.37$, $k_2 = 2.12$, $k_3 = 3.64$, $k_4 = 1.60$, $k_5 = 0.55$, $k_6 = 0$, $k_7 = 0.41$	$k_1 = 2.77$, $k_2 = 1.63$, $k_3 = 3.64$, $k_4 = 2.41$, $k_5 = 0.56$, $k_6 = 0$, $k_7 = 0.37$	$k_1 = 2.50$, $k_2 = 1.88$, $k_3 = 3.64$, $k_4 = 1.60$, $k_5 = 0.55$, $k_6 = 0$, $k_7 = 0.34$
22	$k_1 = 7.90$, $k_2 = 0.63$, $k_3 = 0$, $k_4 = 0.41$	$k_1 = 9.02$, $k_2 = 0$, $k_3 = 0$, $k_4 = 0.37$	$k_1 = 6.71$, $k_2 = 0$, $k_3 = 1.5 \times 10^{-4}$, $k_4 = 0.34$
23	$k_1 = 1.7 \times 10^{-4}$, $k_2 = 0.41$, $k_3 = 0.40$, $k_4 = 1.00$, $k_5 = 0.50$, $k_6 = 0.70$, $k_7 = 1.49$	$k_1 = 1.19$, $k_2 = 0$, $k_3 = 51.75$, $k_4 = 4.0 \times 10^{-4}$, $k_5 = 0$, $k_6 = 0.29$, $k_7 = 0.46$	$k_1 = 4.33$, $k_2 = 0$, $k_3 = 51.74$, $k_4 = 2.8 \times 10^{-6}$, $k_5 = 0.0012$, $k_6 = 0.065$, $k_7 = 0.36$

Table A2. *Continued*

Model Form No.	Liquid/Solid Flow—Pick-Up Velocity	Gas/Solid Flow—Pick-Up Velocity	Gas/Solid Flow—Incipient Motion Velocity
24	$k_1 = 7.90$, $k_2 = 0$, $k_3 = 0$, $k_4 = 0$, $k_5 = 0.41$	$k_1 = 9.02$, $k_2 = 0$, $k_3 = 0$, $k_4 = 0$, $k_5 = 0.37$	$k_1 = 6.82$, $k_2 = 0$, $k_3 = 0$, $k_4 = 0$, $k_5 = 0.34$
25	$k_1 = 0.51$, $k_2 = 0.24$, $k_3 = 0$, $k_4 = 0.40$, $k_5 = 0$, $k_6 = 0.87$, $k_7 = 0.65$, $k_8 = 0.19$, $k_9 = 0.55$	$k_1 = 1.15$, $k_2 = 0.13$, $k_3 = 0$, $k_4 = 0.14$, $k_5 = 0.33$, $k_6 = 1.8 \times 10^{-5}$, $k_7 = 0.072$, $k_8 = 0$, $k_9 = 0.45$	$k_1 = 1.84$, $k_2 = 0.21$, $k_3 = 0$, $k_4 = 0.33$, $k_5 = 0.096$, $k_6 = 1.43$, $k_7 = 0$, $k_8 = 0.53$, $k_9 = 1.44$
26	$k_1 = 8.06$, $k_2 = 2.6 \times 10^{-5}$, $k_3 = 0.0035$, $k_4 = 0$, $k_5 = 0.41$	$k_1 = 8.39$, $k_2 = 0$, $k_3 = 0$, $k_4 = 0.0092$, $k_5 = 0.37$	$k_1 = 10.62$, $k_2 = 0$, $k_3 = 0.087$, $k_4 = 0$, $k_5 = 0.29$
27	$k_1 = 8.28$, $k_2 = 0$, $k_3 = 0$, $k_4 = 0.11$, $k_5 = 0$, $k_6 = 0.41$	$k_1 = 20.97$, $k_2 = 0$, $k_3 = 0$, $k_4 = 0.22$, $k_5 = 0.12$, $k_6 = 0.40$	$k_1 = 16.04$, $k_2 = 0$, $k_3 = 0.089$, $k_4 = 0.13$, $k_5 = 0.037$, $k_6 = 0.29$
28	$k_1 = 7.94$, $k_2 = 2.28$, $k_3 = 1.00$, $k_4 = 3.64$, $k_5 = 1.40$, $k_6 = 0$, $k_7 = 0$, $k_8 = 0.41$	$k_1 = 7.58$, $k_2 = 2.28$, $k_3 = 1.20$, $k_4 = 3.64$, $k_5 = 0.96$, $k_6 = 0$, $k_7 = 0$, $k_8 = 0.37$	$k_1 = 7.56$, $k_2 = 2.28$, $k_3 = 0.99$, $k_4 = 3.64$, $k_5 = 1.03$, $k_6 = 0.18$, $k_7 = 0$, $k_8 = 0.43$
29	$k_1 = 2.58$, $k_2 = 0$, $k_3 = 0.36$, $k_4 = 0.13$, $k_5 = 0.13$, $k_6 = 0.43$, $k_7 = 3.33$, $k_8 = 0$, $k_9 = 0.36$, $k_{10} = 0.089$, $k_{11} = 0.45$	$k_1 = 0$, $k_2 = 1.49$, $k_3 = 0.89$, $k_4 = 0.42$, $k_5 = 0.52$, $k_6 = 0.69$, $k_7 = 12.36$, $k_8 = 0.023$, $k_9 = 0.16$, $k_{10} = 0$, $k_{11} = 0.37$	$k_1 = 1.90$, $k_2 = 0.020$, $k_3 = 0.34$, $k_4 = 0.29$, $k_5 = 0.18$, $k_6 = 0.48$, $k_7 = 2.17$, $k_8 = 0$, $k_9 = 0.36$, $k_{10} = 0.15$, $k_{11} = 0.38$
30	$k_1 = 12.85$, $k_2 = 3.7 \times 10^{-6}$, $k_3 = 0$, $k_4 = 0.028$, $k_5 = 0.084$, $k_6 = 0$, $k_7 = 0.38$	$k_1 = 8.98$, $k_2 = 0$, $k_3 = 0.66$, $k_4 = 0.95$, $k_5 = 3.9 \times 10^{-5}$, $k_6 = 2.0 \times 10^{-5}$, $k_7 = 0.37$	$k_1 = 7.25$, $k_2 = 0.0044$, $k_3 = 0.20$, $k_4 = 0.0083$, $k_5 = 0$, $k_6 = 0$, $k_7 = 0.34$
31	$k_1 = 0.61$, $k_2 = 8.6 \times 10^{-4}$, $k_3 = 0.59$	$k_1 = 0.21$, $k_2 = 0.024$, $k_3 = 0.54$	$k_1 = 0.061$, $k_2 = 0.33$, $k_3 = 0.49$
32	$k_1 = 7.91$, $k_2 = 0$, $k_3 = 0.45$, $k_4 = 8.50$, $k_5 = 2.0 \times 10^{-4}$, $k_6 = 0.40$	$k_1 = 11.69$, $k_2 = 0$, $k_3 = 0.35$, $k_4 = 9.02$, $k_5 = 0$, $k_6 = 0.37$	$k_1 = 12.11$, $k_2 = 0.056$, $k_3 = 0.32$, $k_4 = 8.92$, $k_5 = 0.051$, $k_6 = 0.45$
33	$k_1 = 9.68$, $k_2 = 16.78$, $k_3 = 10.28$, $k_4 = 1.47$, $k_5 = 1.48$	$k_1 = 10.70$, $k_2 = 15.40$, $k_3 = 10.57$, $k_4 = 2.96$, $k_5 = 1.02$	$k_1 = 10.45$, $k_2 = 15.40$, $k_3 = 10.90$, $k_4 = 3.03$, $k_5 = 0.52$
34	$k_1 = 0.0041$, $k_2 = 1.00$, $k_3 = 0.0092$, $k_4 = 1.00$, $k_5 = 0.53$, $k_6 = 53.33$, $k_7 = 0.019$, $k_8 = 0.062$, $k_9 = 1.00$, $k_{10} = 0.24$, $k_{11} = 1.00$, $k_{12} = 0.52$, $k_{13} = 1.00$, $k_{14} = 56.90$, $k_{15} = 0.019$, $k_{16} = 1.00$, $k_{17} = 0.019$, $k_{18} = 1.00$, $k_{19} = 1.87$, $k_{20} = 5.07$, $k_{21} = 7.2 \times 10^{-12}$, $k_{22} = 0.33$, $k_{23} = 0.019$, $k_{24} = 1.00$, $k_{25} = 0.019$, $k_{26} = 1.00$, $k_{27} = 1.87$, $k_{28} = 7.2 \times 10^{-12}$, $k_{29} = 0.33$, $k_{30} = 0.021$, $k_{31} = 1.00$, $k_{32} = 0.047$, $k_{33} = 1.00$	$k_1 = 0.0041$, $k_2 = 1.00$, $k_3 = 0.0092$, $k_4 = 1.00$, $k_5 = 0.53$, $k_6 = 53.33$, $k_7 = 0.019$, $k_8 = 0.062$, $k_9 = 1.00$, $k_{10} = 0.24$, $k_{11} = 1.00$, $k_{12} = 0.52$, $k_{13} = 1.00$, $k_{14} = 56.90$, $k_{15} = 0.019$, $k_{16} = 1.00$, $k_{17} = 0.019$, $k_{18} = 1.00$, $k_{19} = 1.87$, $k_{20} = 5.07$, $k_{21} = 7.2 \times 10^{-12}$, $k_{22} = 0.33$, $k_{23} = 0.019$, $k_{24} = 1.00$, $k_{25} = 0.019$, $k_{26} = 1.00$, $k_{27} = 1.87$, $k_{28} = 7.2 \times 10^{-12}$, $k_{29} = 0.33$, $k_{30} = 0.021$, $k_{31} = 1.00$, $k_{32} = 0.047$, $k_{33} = 1.00$	$k_1 = 0.0041$, $k_2 = 1.00$, $k_3 = 0.0092$, $k_4 = 1.00$, $k_5 = 0.53$, $k_6 = 53.33$, $k_7 = 0.019$, $k_8 = 0.062$, $k_9 = 1.00$, $k_{10} = 0.24$, $k_{11} = 1.00$, $k_{12} = 0.52$, $k_{13} = 1.00$, $k_{14} = 56.90$, $k_{15} = 0.019$, $k_{16} = 1.00$, $k_{17} = 0.019$, $k_{18} = 1.00$, $k_{19} = 1.87$, $k_{20} = 5.07$, $k_{21} = 7.2 \times 10^{-12}$, $k_{22} = 0.33$, $k_{23} = 0.019$, $k_{24} = 1.00$, $k_{25} = 0.019$, $k_{26} = 1.00$, $k_{27} = 1.87$, $k_{28} = 7.2 \times 10^{-12}$, $k_{29} = 0.33$, $k_{30} = 0.021$, $k_{31} = 1.00$, $k_{32} = 0.047$, $k_{33} = 1.00$
35	$k_1 = 0.45$, $k_2 = 0.97$, $k_3 = 0.91$, $k_4 = 13.39$, $k_5 = 8.7 \times 10^{-4}$, $k_6 = 0.41$, $k_7 = 0.76$, $k_8 = 1.01$, $k_9 = 0.93$, $k_{10} = 1.00$, $k_{11} = 1.00$, $k_{12} = 1.00$, $k_{13} = 2.00$, $k_{14} = 1.00$, $k_{15} = 0.43$, $k_{16} = 0.65$	$k_1 = 0.54$, $k_2 = 0.84$, $k_3 = 0.95$, $k_4 = 13.34$, $k_5 = 0$, $k_6 = 0.36$, $k_7 = 0.74$, $k_8 = 1.00$, $k_9 = 0.96$, $k_{10} = 1.00$, $k_{11} = 1.00$, $k_{12} = 1.00$, $k_{13} = 2.00$, $k_{14} = 1.00$, $k_{15} = 0.42$, $k_{16} = 0.67$	$k_1 = 1.30$, $k_2 = 3.52$, $k_3 = 0.86$, $k_4 = 11.70$, $k_5 = 0.49$, $k_6 = 0.41$, $k_7 = 0.31$, $k_8 = 0$, $k_9 = 1.11$, $k_{10} = 1.68$, $k_{11} = 2.50$, $k_{12} = 1.06$, $k_{13} = 2.55$, $k_{14} = 1.08$, $k_{15} = 0.24$, $k_{16} = 0.49$

Manuscript received Oct. 10, 2012, and revision received Aug. 28, 2013.